Rail Base Corrosion Detection and Prevention

TCRP
Web-Only Document 37:

Rail Base Corrosion
Detection and Prevention

Francisco C. Robles Hernandez
Kevin Koch
Transportation Technology Center, Inc.
Pueblo, CO

Gabriel Plascencia Barrera
CIITEC-IPN
Cerrada Cerati SIN
Mexico

Contractor's Final Report for TCRP Project D-7, Task 14
Submitted March 2007

Transit Cooperative Research Program
TRANSPORTATION RESEARCH BOARD

DETAILS

AUTHORS

ACKNOWLEDGMENT

COPYRIGHT PERMISSION

DISCLAIMER

THE NATIONAL ACADEMIES
Advisers to the Nation on Science, Engineering, and Medicine

The **National Academy of Sciences** is a private, nonprofit, self-perpetuating society of distinguished scholars engaged in scientific and engineering research, dedicated to the furtherance of science and technology and to their use for the general welfare. On the authority of the charter granted to it by the Congress in 1863, the Academy has a mandate that requires it to advise the federal government on scientific and technical matters. Dr. Ralph J. Cicerone is president of the National Academy of Sciences.

The **National Academy of Engineering** was established in 1964, under the charter of the National Academy of Sciences, as a parallel organization of outstanding engineers. It is autonomous in its administration and in the selection of its members, sharing with the National Academy of Sciences the responsibility for advising the federal government. The National Academy of Engineering also sponsors engineering programs aimed at meeting national needs, encourages education and research, and recognizes the superior achievements of engineers. Dr. William A. Wulf is president of the National Academy of Engineering.

The **Institute of Medicine** was established in 1970 by the National Academy of Sciences to secure the services of eminent members of appropriate professions in the examination of policy matters pertaining to the health of the public. The Institute acts under the responsibility given to the National Academy of Sciences by its congressional charter to be an adviser to the federal government and, on its own initiative, to identify issues of medical care, research, and education. Dr. Harvey V. Fineberg is president of the Institute of Medicine.

The **National Research Council** was organized by the National Academy of Sciences in 1916 to associate the broad community of science and technology with the Academy's purposes of furthering knowledge and advising the federal government. Functioning in accordance with general policies determined by the Academy, the Council has become the principal operating agency of both the National Academy of Sciences and the National Academy of Engineering in providing services to the government, the public, and the scientific and engineering communities. The Council is administered jointly by both the Academies and the Institute of Medicine. Dr. Ralph J. Cicerone and Dr. William A. Wulf are chair and vice chair, respectively, of the National Research Council.

The **Transportation Research Board** is a division of the National Research Council, which serves the National Academy of Sciences and the National Academy of Engineering. The Board's mission is to promote innovation and progress in transportation through research. In an objective and interdisciplinary setting, the Board facilitates the sharing of information on transportation practice and policy by researchers and practitioners; stimulates research and offers research management services that promote technical excellence; provides expert advice on transportation policy and programs; and disseminates research results broadly and encourages their implementation. The Board's varied activities annually engage more than 5,000 engineers, scientists, and other transportation researchers and practitioners from the public and private sectors and academia, all of whom contribute their expertise in the public interest. The program is supported by state transportation departments, federal agencies including the component administrations of the U.S. Department of Transportation, and other organizations and individuals interested in the development of transportation. **www.TRB.org**

www.national-academies.org

TABLE OF CONTENTS

TCRP D-7/Task 14

Rail Base Corrosion Study

SUMMARY

Under Transit Cooperative Research Program (TCRP) Project D-7, the Transportation Technology Center, Inc., (TTCI) studied the effects and prevention of rail base corrosion.

The following tasks were accomplished:

- Distributed questionnaire to various transit agencies in order to identify the major problems associated with rail base corrosion and actions taken by them.
- Completed a metallurgical examination of rails with corrosion present, including an electrochemical study of the rails under different corrosive environments (i.e., chlorines (KCl), sulfates ($NaSO_4$)) and direct current (DC) conditions.
- Created a Finite Element Analysis (FEA) model using ANSYS® to determine the state of stresses created by the localized corrosion and assess the risk of failure.
- Developed a draft recommended industry practice for rail base corrosion detection and prevention.

A 7-page survey was developed and sent to 28 rail transit agencies and commuter rail systems in North America. The survey concentrated on rail base corrosion and several environments under which corrosion occurs. Of the 28 agencies, 16 responded to the survey. The remaining agencies had minimal rail base corrosion in their systems. Therefore, they believed they had little to contribute to the project. In addition to the survey, site visits to 7 of the 16 responding transit systems were conducted.

The survey responses showed that 12 of the 16 respondents incurred serious rail base corrosion problems. Of the 12 respondents with corrosion problems, the research team determined that the most severe indication of corrosion was seen in systems with underground (tunnel) sections, in locations with significant history of humidity. Conversely, transit systems located above ground in the open air exhibited only minimal corrosion.

There are two main reasons for humidity in transit systems: (1) leakage from drainage systems and (2) water sources such as a river, lake, or sea. Underground systems present a situation where the corrosion rate is increased by the presence of chlorines and sulfates from chemicals being disposed into the drain systems and from underground organic matter. More important, during the winter season, salts used to melt ice and snow within a city dissolve and are carried underground leaking into the tunnels providing a major contribution to corrosion.

1

The following transit systems were visited and provided several examples of rail base corrosion:

- Philadelphia: Southeastern Pennsylvania Transportation Authority (SEPTA)
- New York: Metropolitan Transportation Authority (MTA) New York City Transit
- New Jersey: Port Authority Transit-Hudson (PATH)
- New York: Amtrak - South tunnel
- Baltimore: Amtrak - Baltimore station
- Toronto, Canada: Toronto Transit Commission (TTC)
- Mexico City: Systema de Transporte Collectivo and Tren Ligero

All of the transit systems visited use nondestructive evaluation (NDE) techniques to detect the flaws and cracks that can compromise the integrity of the rails and overall safety. Some of the NDE practices include visual inspection. In several cases, visual inspection is enough to identify rail base corrosion because corrosion occurs mainly in the tie area and can be easily observed. Unfortunately, some of the rail base corrosion is hidden between the base of the rail and the tie plate, making visual inspection vulnerable to error.

In addition to the site visits, the research team performed a metallurgical evaluation on the corroded rail samples. The evaluation included NDE methods (dye penetrant and magnetic particles inspection methods) and destructive methods (metallographic analysis) of the rail. The results of the NDE showed that there is no further damage to the parent rail materials by the corroded area. The NDE findings were confirmed by means of light optical stereoscopy. The light optical microscopy detected two regions: (1) the corroded section and (2) the parent rail. These findings are significant because it indicates that the parent rail microstructure did not present traceable changes, which means the microstructure is fully pearlitic, free of detectable crack or micro-cracks and clearly different from the oxide layer.

Two typical corrosion conditions were used as cases for the FEA model:

- Significant erosion at the rail base, which removes the majority of the rail base on top of the tie plate
- Inward corrosion growth into the base of the rail

The first case is easy to detect visually because it extends along the entire tie plate. This type of corrosion has a major contribution to stress concentrations in the vicinity of the ties because sharp corners form along the base of the rail and behave as stress risers. To decrease the risk of a derailment, a standard practice followed by some transit authorities is to remove the rail when 1/8 in. to 1/4 in. of the rail base is removed due to corrosion.

The second case is usually more severe and unpredictable. It is more difficult to detect inward growth by visual inspection methods. In addition to the difficulties of visual inspection, this type of corrosion is more severe because it has a tendency to grow internally in both vertical and horizontal directions forming irregular cavities that act as stress concentrators. In the majority of the cases, the internal cavities are not exposed to the exterior, and if they are not detected in a timely manner, they can represent a major risk for catastrophic failure that can result in rail breaks and potential derailment(s).

2

The FEA showed that areas of high stress concentration occur more often near sharp edges. In addition, sharp edges are sometimes hidden at the base of the rail making detection difficult. This can result in an unexpected rail failure.

The research team conducted a laboratory corrosion test as supporting evidence of a hypothesis that arose over the course of this project. In this hypothesis, it is proposed that insulation of the track helps to avoid any leak of direct current from the tracks to the ground via clips, spikes, bolts, and tie plates. The research team also proposes a remedy to reduce and ideally eliminate rail corrosion.

Chapter 7 details some recommended practices that could be used to reduce or minimize corrosion. These practices can be reduced to the following points:

- Conduct proper track maintenance and cleaning practices
- Install suitable insulation to prevent stray currents
- Redirect water present along the tracks
- Identify potential locations for corrosion and prevent the presence of stray currents
- Avoid direct contact between rail and track components (fastening system, ballast, ties)
- Recognize that timber ties are marginal insulators particularly when chemically treated
- Use continuously welded rail where possible; where joint bars are present, use bonding wires for proper connections
- Use coated and/or encased insulator materials for embedded tracks

3

CHAPTER 1: INTRODUCTION

Rail corrosion, particularly at the base of the rail, is a serious problem in some North American transit systems. Rail base corrosion compromises the integrity of the rail and could result in catastrophic failures. In most cases, it is difficult to detect rail corrosion in the base because it is usually hidden between the tie plate and rail base. Ultrasonic detection systems are used for corrosion detection in many transit systems. However, ultrasonic testing is limited to the determination of the height of the rail, which limits considerably its implementation as a rail base corrosion detection method. Which is one of the main reasons why even the most modern and sophisticated rail flaw detection vehicles are limited in their ability to inspect the rail base for defects.

Transit systems have also reported a susceptibility to metal loss at the rail base due to corrosion. The metal loss directly causes the rail to become more susceptible to failure. If undetected, the metal loss will result in a loss in structural strength due to a reduction in cross sectional area.

This project was designed to conduct an industry survey to identify and document adverse effects currently experienced by the transit systems, to build an FEA and flaw growth model, and to create recommended guidelines for inspection, prevention, and monitoring of rail base corrosion based on the findings of the survey and FEA. An industry survey was performed to review current practices and problems associated with rail base corrosion. Currently, there are no available standards for rail base corrosion detection or prevention.

Throughout this project, other alternative methods used by other industries, such as petrochemical and nuclear, were studied to identify technologies and standards (i.e., National Association of Corrosion Engineers, American Society of Mechanical Engineers, American Society for Testing and Materials) that can be easily implemented as recommended practices for rail base corrosion detection.

Appendix A shows the questionnaire distributed for the survey. The survey focused on the prevention, maintenance, and practices followed by transit authorities to reduce the risk of failure due to rail base corrosion. Appendices B and C summarize the responses to the survey.

This report provides recommended minimum guidelines to assist transit systems in detecting, monitoring, and preventing corrosion and metal loss at the base of the rail.

CHAPTER 2: ANALYSIS OF RAIL CORROSION

2.1   Definition

Corrosion is defined as the deterioration of a material due to its interaction with its environment (*1*). Corrosion is affected by several factors, including electrochemical, metallurgical, physicochemical, and thermodynamics (see Figure 1). The presence of hydrochloric acid (HCl) in the reactions shown in Figure 1 is due to the electrolytic decomposition of sodium chlorine (NaCl), potassium chlorine (KCl), and other chlorines present in the salts deposited on the rail. Sulfates, such as sodium sulfate (Na_2SO_4) or ammonium sulfate (($NH_4)_2SO_4$), are also decomposed and form sulfuric acid (H_2SO_4). The decomposition of the chlorines and sulfates is due to the presence of the direct current (DC) that breaks the molecules. The resultant hydrochloric and sulfuric acids form electrolytes that induce electrolysis and increase the corrosion rates. Most environments can be corrosive, but, generally, inorganic materials are more corrosive than organic materials. For example, in the oil industry, sodium chlorine, sulfur, hydrochloric, and sulfuric acids are the major factors that accelerate corrosion instead of the petroleum.

$$Fe \Leftrightarrow Fe^{2+} + 2e \qquad EMF = -0.44V \ at \ 25 \ ^0C$$
$$Fe + 2HCl \rightleftarrows FeCl_2 + H_2$$
$$O_2 + H_2O + 4e \rightleftarrows 4OH^-$$
$$2Fe + 2H_2O + O_2 + 2Fe^{2+} + 4OH^- \rightleftarrows 2Fe(OH)_2 \downarrow$$
$$2Fe(OH)_2 + H_2O + \frac{1}{2}O_2 \rightleftarrows 2Fe(OH)_3$$
$$4Fe(OH)_2 + O_2 \rightleftarrows 2(Fe_2O_3 \cdot xH_2O) + 2H_2O$$

$Fe_2O_3 \cdot xH_2O$ is the typical Rust and x vary depending of the hydration level. $\downarrow$ indicates precipitation.
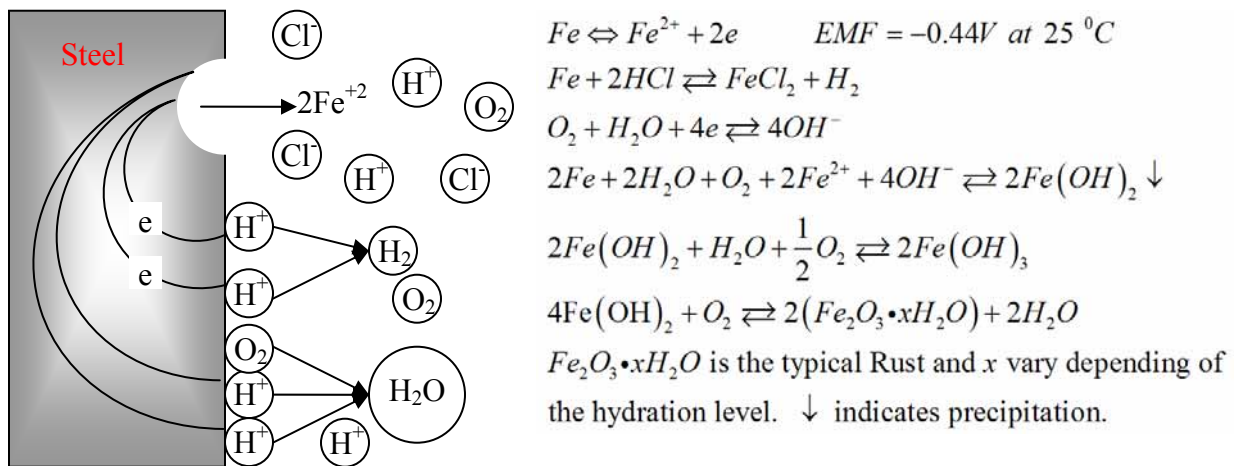
Figure 1. Electrochemical effects and reactions occurring during corrosion of Fe present in steel in aerated systems containing water (H_2O) and chlorine ions. HCl is a byproduct of dissolved chlorines + DC.

Rust is the substance formed when iron compounds corrode in the presence of oxygen and water. Rust is a mixture of iron oxides and hydroxides and is a common form of corrosion on steel. This corrosion is the result of the oxidation reaction when iron metal returns to a more stable state. The rust forming process is summarized in three stages: (1) formation of Fe^{2+}, (2) formation of hydroxide ions, and (3) the chemical reaction with oxygen to create rust. Hence, rust is Fe^{3+} oxide that is formed by the dehydration of Fe^{2+} and hydroxide. The concentration of chlorine ions accelerates corrosion by making the solution (water + salts) more conductive. A magnetic hydrous ferrite, $Fe_3O_4xH_2O$, often forms a black intermediate layer between hydrous Fe_2O_3 and FeO. Hence, rust films normally consist of three layers of iron oxides in different states of oxidation (*2,3*).

5

2.2   Corrosion Principles

Rail base corrosion is a combination of corrosion environments; for example, humidity (seawater and highly polluted water) and soil. The corrosion problems of systems with the presence of water have been well studied over many years, but despite published information on material behavior, corrosion is in some cases unpredictable. Most of the elements that can be found on earth are present in seawater, at least in trace amounts, with chloride ions being by far the largest constituent. On the other hand, soils are formed by the combined weathering action of wind and water, and also organic decay. Corrosion in soils is a major concern, especially because much of the buried infrastructure is aging. Rails are expected to function reliably and continuously over several decades. However, corrosion in soils is very complex due to the presence of several elements as well as variations in properties or characteristics across three dimensions resulting in a major impact on corrosion. Chemical reactions involving almost all of the existing elements are known to take place in soils, and many of these are not yet fully understood (2,4).

Polluted water in liquid form represents the essential electrolyte required for electrochemical corrosion reactions. A distinction is made between saturated and unsaturated water flow in soils. The latter represents movement of water from wet areas to dry soil areas. Water is usually directed against gravity, and its flow is dependent on pore size and distribution, texture, structure, and organic matter. Figure 2 shows a detailed diagram with the parameters affecting the corrosion rate (2).
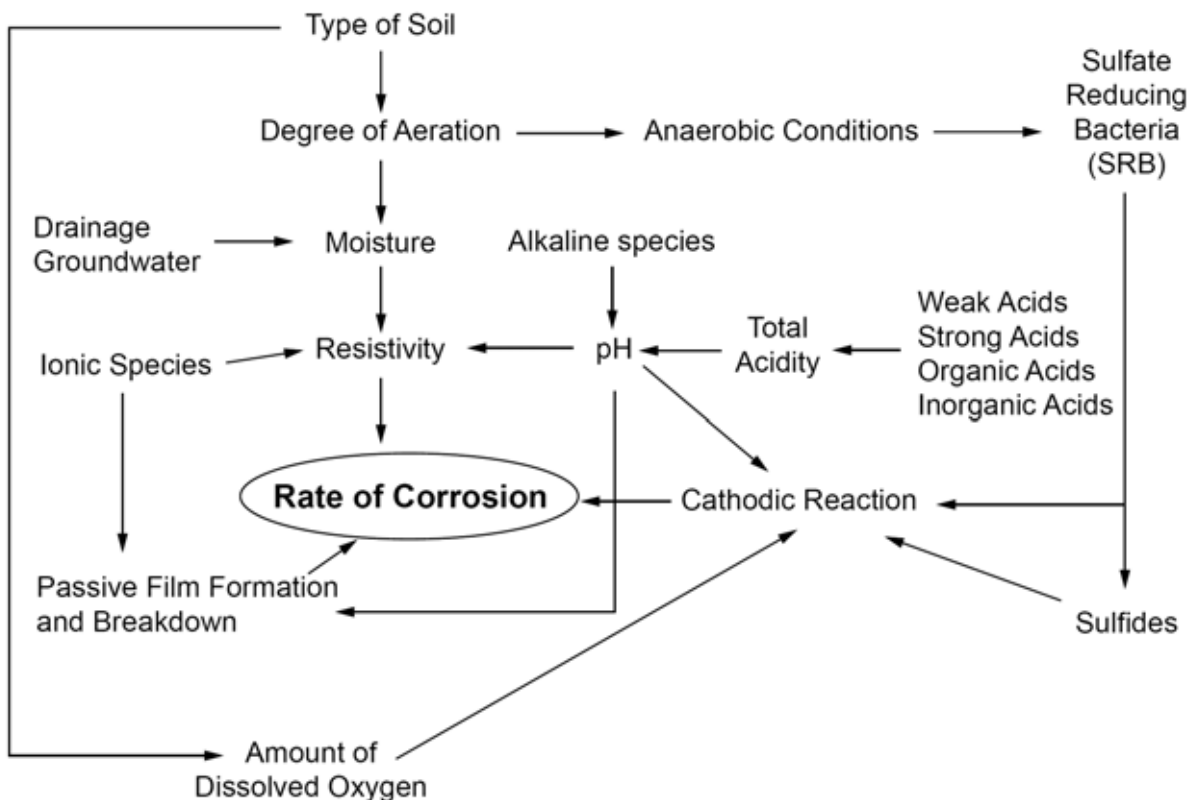

Figure 2. Relationship of variables affecting the rate of corrosion in soil (2).

6

In addition to water and soil, rail on the transit systems carries electric current that further increases the rail corrosion rate. Stray currents have promoted corrosion damage on North American rail transit systems for more than a century. In the United States alone, there are more than 20 transit systems operating electrified rail systems in major urban centers. The transit systems that show the most severe rail base corrosion effects are the ones located in high-density urban areas with high humidity or underground cables and piping (water and gas) systems, which are susceptible to this form of corrosion damage (*2,5*). In such transit systems, rails are used to close the electric circuit resulting in a system where corrosion rate can potentially be accelerated in the presence of return DC currents on the rails that transport the return current.

Oxygen transport is more rapid in coarse-textured dry soils than in fine waterlogged textures. Excavation can obviously increase the degree of aeration in soil, as compared with the undisturbed state. It is generally accepted that corrosion rates in disturbed soil with greater oxygen availability are significantly higher than in undisturbed soil. Soils usually have a pH range of 5 to 8. In this range, pH is generally not considered to be the dominant variable affecting corrosion rates. More acidic soils obviously represent a serious corrosion risk to common construction materials such as steel, cast iron, and zinc coatings. Soil acidity is produced by mineral leaching, industrial wastes, and city drain leaks. Alkaline soils tend to have high sodium, potassium, magnesium, and calcium contents (*2*). The effects of chlorines and sulfates on soils are of particular interest to the transit lines because the salt deposits found along the tracks have a high content of a white substance with high concentrations of chlorines and sulfates (*6–9*). (See Table 1 for corrosivity ratings particular to chlorine and sulfates.)

TABLE 1. Corrosivity Ratings Based on Soil Resistivity

Soil Resistivity, ohm cm	Corrosivity Rating
> 20,000	Essentially noncorrosive
10,000–20,000	Mildly corrosive
5000–10,000	Moderately corrosive
3000–5000	Corrosive
1000–3000	Highly corrosive
< 1000	Extremely corrosive

Chloride ions are generally harmful, as they participate directly in anodic dissolution reactions of metals. Pure water and oxides (e.g., SiO_2, Al_2O_3, and $CaCO_3$), usually present in soils, are nonconductors. However, the presence of salt decreases the soil resistivity allowing the transfer of DC resulting in an electrolyte. In some cases, the level of chloride ions in soils is comparable to those of seawater. The main sources of chlorine are leaks from drain systems and de-icing salts applied to roadways. The chloride ion concentration and activity in the corrosive aqueous

7

soil electrolyte will vary as soil conditions alternate between wet and dry (*6,9*). On the other hand, sulfates have a less corrosion effect than chlorides and are generally considered to be more benign in their corrosive action toward metallic materials. The presence of sulfates poses a major risk for metallic materials in the sense that sulfates can be converted to highly corrosive sulfides by anaerobic sulfate reduction (*6*). Table 2 shows the corrosion based on soil resistivity and the respective corrosion level according to the AWWA C-105 Standard.

TABLE 2. Point System for Predicting Soil Corrosivity According to the AWWA C-105 Standard

Soil Parameter Assigned Points	Soil Parameter Assigned Points
Resistivity, Ω cm	
< 700	10
700–1000	8
1000–1200	5
1200–1500	2
1500–2000	1
> 2000	0
pH	
0 - 2	5
2 – 4	3
4 – 6.5	0
6.5 – 7.5	0
7.5 – 8.5	0
> 8.5	3
Redox potential, mV	
> 100	0
50 – 100	3.5
0 – 50	4
< 0	5
Sulfides	
Positive	3.5
Trace	2
Negative	0
Moisture	
Poor drainage, continuously wet	2
Fair drainage, generally moist	1
Good drainage, generally dry	0

CHAPTER 3: MICROSTRUCTURAL ANALYSIS

The research team investigated rail from various transit authorities using nondestructive and light optical stereoscopy and microscopy. The following sections summarize microstructural analysis and provide detailed descriptions of each method used.

3.1   Rail Used in Transit Service

According to the survey and several personal communications with various transit systems, most transit systems use 115-lb RE rail and to a lesser extent 100-lb ARA. Several transit agencies are in the process of upgrading their tracks from 110-lb ARA to 115-RE rail. The MTA-NYCT uses different types of standard carbon rail of 100 lb (ARA-B, OH, FT, HH). The site visit showed that only Amtrak (New York South tunnel and Baltimore station tunnel) uses 136-lb RE rail.

3.2   Description of Test Samples

Nine samples of 115-lb rail and 10 sections of 136-lb rail showing corrosion were donated by different transit authorities. Some of these samples had experienced failures due to corrosion. Random samples of 115- and 136-lb rail were selected, as indicated in Figure 3, for the metallographic analysis. These samples were obtained from the base of the rail close to the corrosion region as well as from the head of the rail in order to compare the microstructures of corroded and noncorroded areas. NDE was performed on two sections of the 115-lb rail, which were selected based on the severity of the corrosion. The two most corroded samples were used to identify the effects of corrosion in the microstructure of the sample.

The metallographic samples were prepared using standard grinding and polishing procedures. The phases present in the microstructure were revealed using 2% Mital as the etching agent. The surfaces of the NDE samples were mechanically ground. Figure 3 shows a series of macro-images of a sample containing corrosion at the base of the rail.
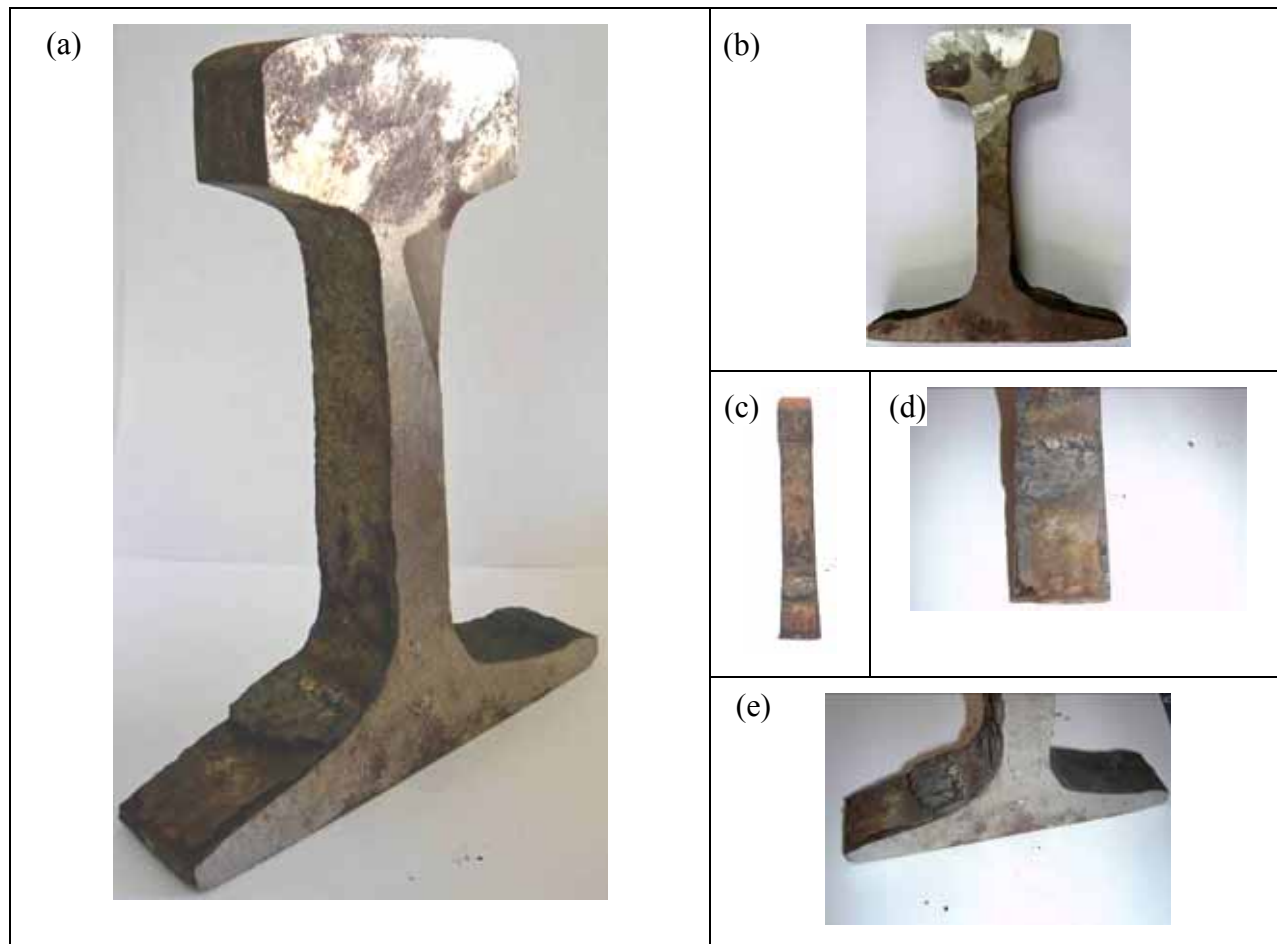
Figure 3. Macro pictures of a 115-lb rail showing corrosion at the base of the rail. Different views of a section of rail donated by the St. Louis, Missouri, Metro System: (a) 3-D image,(b) front (c) side views, (d) and (e) corroded section of the rail.
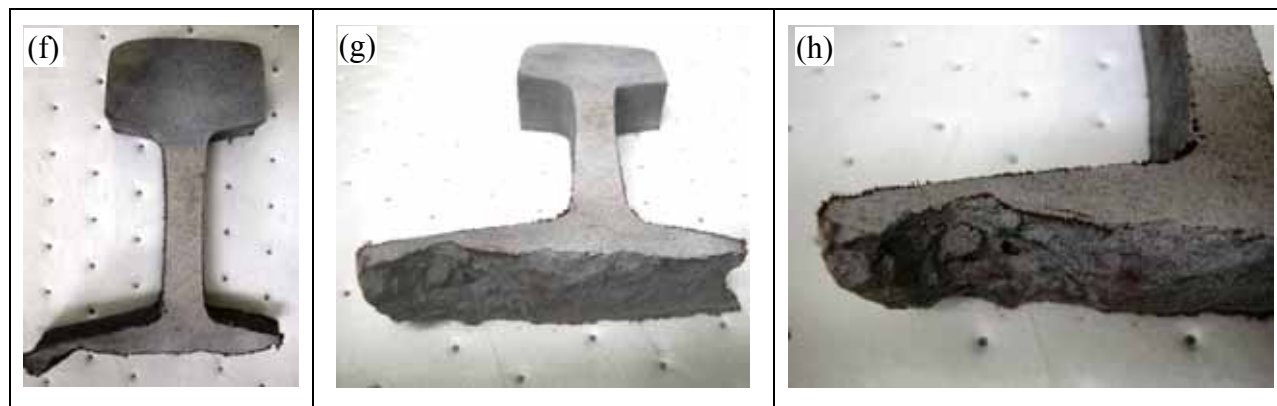
Figure 3 (continued). Different views of a section of 100-lb rail showing severe corrosion at the base of the rail. The rail was donated by Port Authority Trans-Hudson, New Jersey. This rail was used for the magnetic particle evaluation.

10

Figure 3 (continued). Sections of 136-lb rail showing different types of corrosion at the base of the rail. The presented macro-images of the rails show the rail donated by Amtrak. All of these rails failed due to corrosion in various locations along the east coast. The samples were used in the following way: (i) metallographic analysis,(j,k) numerical FEA simulations,(l,m,n) other examples. Note, view (i) shows one of the most severe corrosion conditions.

11

Other sections of rail donated by the Toronto Transit Commission will be presented in the FEA subsection 3.5 of this report. For this project, all rails used were donated by the following transportation systems:

- Amtrak
- St. Louis, Missouri, Metro System
- Port Authority Trans-Hudson (PATH), New Jersey
- Toronto Transit Commission
- Light Rail, Sistema de Transporte Colectivo Metro, México City

3.3   Nondestructive Evaluation

Two sections of rail were selected for the magnetic particle evaluation. One sample was a 115-lb rail section donated by the St. Louis, Missouri, Metro System and the other sample was a 100-lb rail section donated by PATH, New Jersey. These samples were selected because they exhibited two different types of significant damage at the rail base. Figure 4 shows pictures of the rail samples used for the NDE. The magnetic particle technique was used on both samples to determine if any cracks were present.

After applying the particles and magnetic field to the samples, there was no evidence of cracks growing into the parent material from the rail base. Under these circumstances, micro-cracking cannot be detected using magnetic particle inspection. Therefore, a more sensitive analysis, using an optical microscope, was performed to inspect for micro-cracking from the rail base into the parent material. It was found that rail base corrosion does not accelerate the crack formation or propagation to the parent rail. Therefore, it is concluded that there is no compromise of the rail's integrity due to the presence of micro-cracks; nonetheless, corrosion, in particular, pitting is usually an accelerator of fatigue-corrosion conditions. The details of this analysis are discussed in more detail in the following section including Figures 5-8.
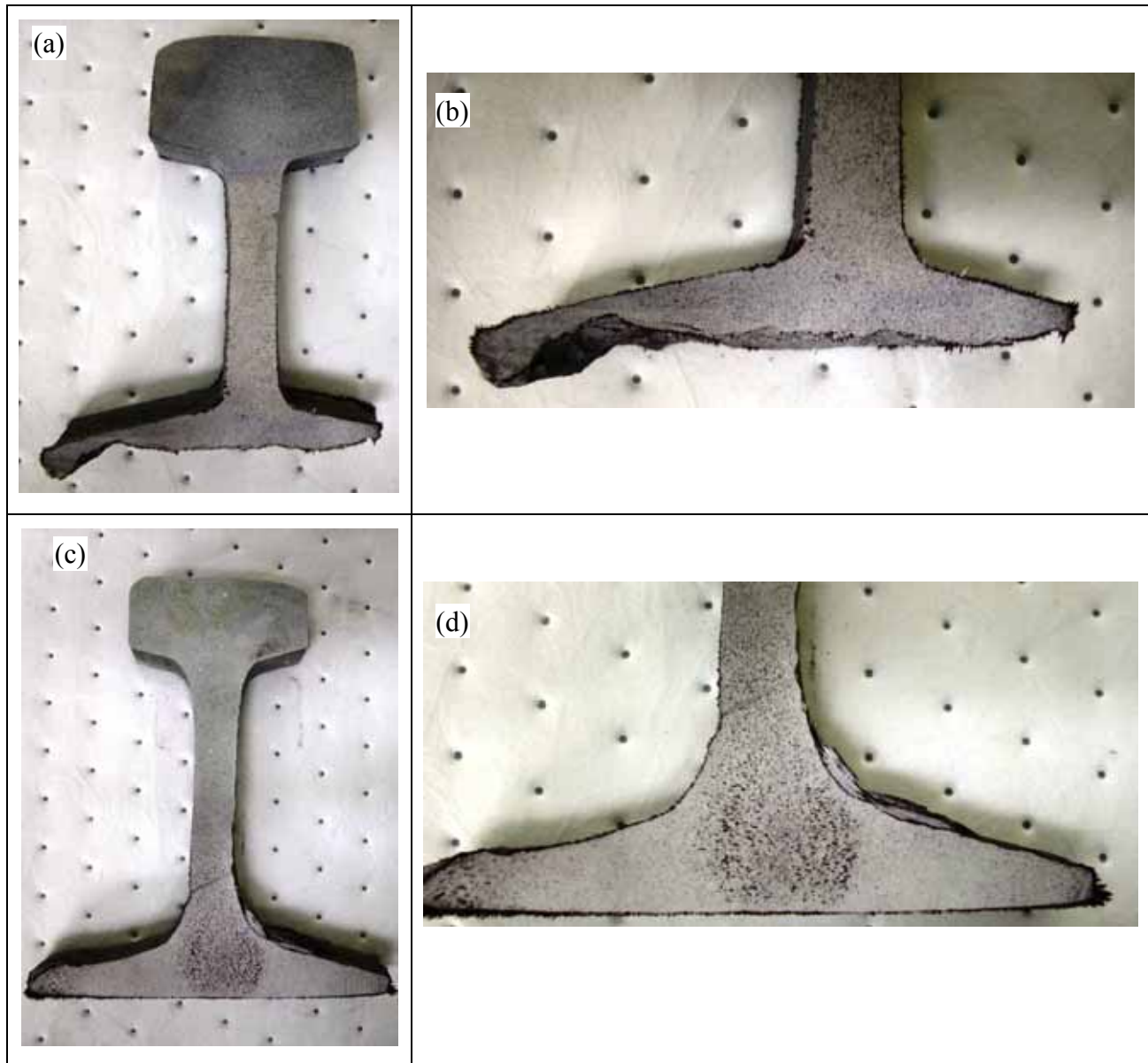
Figure 4. Pictures of the magnetic particles evaluation of the rail base for the Port Authority Trans-Hudson (a,b) and St. Louis, Missouri, Metro System (c,d). Note that there is no apparent evidence of cracks growing from the base of the rail to the parent material.

13

3.4   Metallurgical Analysis of Rails

3.4.1   100- and 115-lb Rail

The St. Louis, Missouri, Metro System donated the rail for this analysis. Figure 5 shows the microstructure of both the as-polished and as-etched conditions at different magnifications for a section of the corroded 115-lb rail. It is clear that the microstructure of both samples corresponds to the typical fully pearlitic microstructure of the standard or high strength rails. Note the amount of inclusions, coarse pearlite, interlamellar structure (typical of pearlite), and grains observed on the rail.
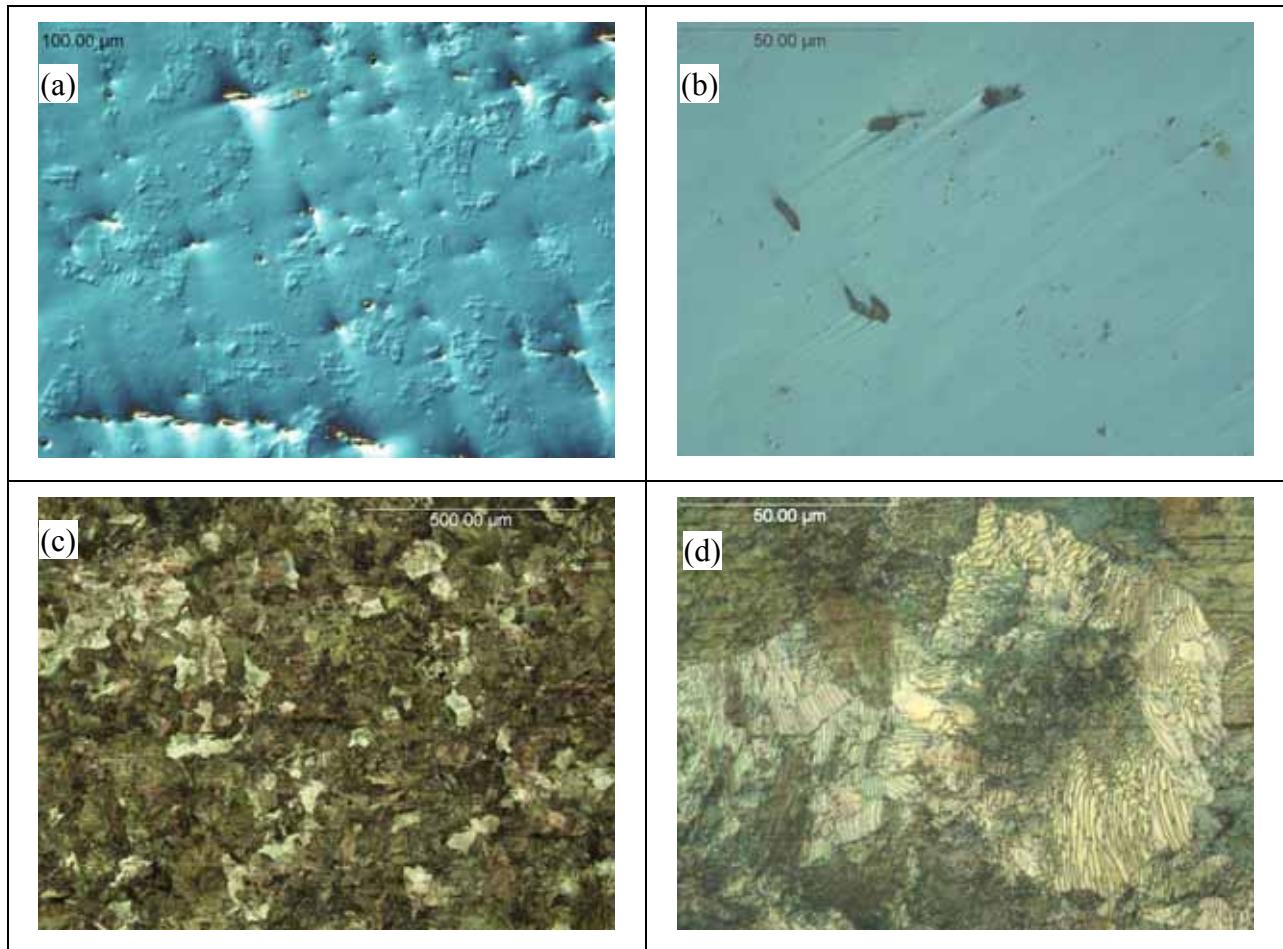
Figure 5. Microstructure of the 115-lb rail donated by the St. Louis, Missouri, Metro System. The sample in as-polished conditions at various magnifications (a) 100 X, (b) 1000 X and the sample in as-etched conditions(c) 100 X and (d) 1000 X. Note the large amount of inclusions on the as- polished (a, b) samples and the pearlitic microstructure (c, d). This sample was extracted in close vicinity of the corroded area.

14

Figure 6 shows the microstructure of both the as-polished and as-etched conditions at different magnifications for a noncorroded railhead section from the 115-lb rail. Comparing the microstructure of the rail in close vicinity to the corroded area (Figure 5) with the microstructure of a location free of corrosion (Figure 6), no significant change in the microstructure of the material is shown. This means that corrosion has no effect on the microstructure, except for the section that reacts with oxygen and water or other elements or compounds forming other phases.
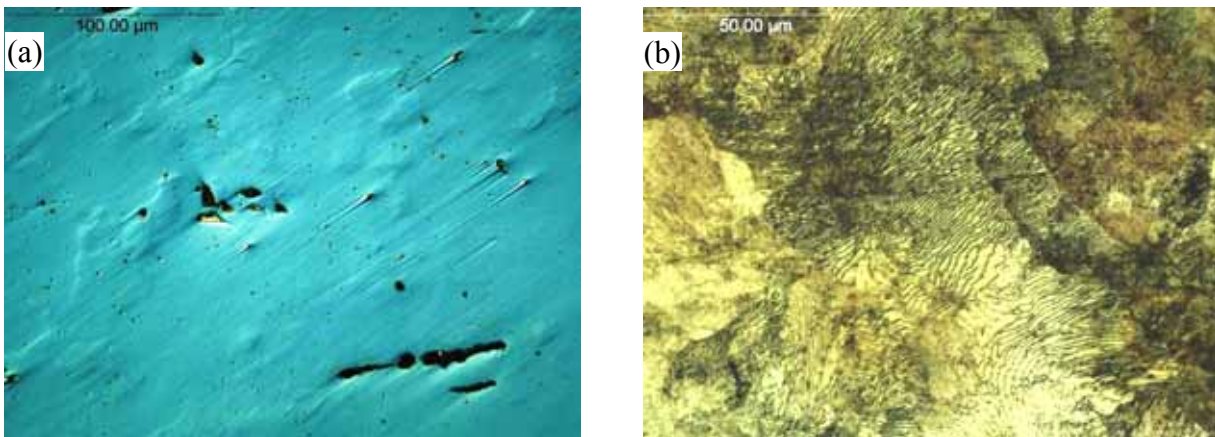

Figure 6. Microstructure of the 115-lb rail donated by the St. Louis, Missouri, Metro System. The sample in (a) as-polished, 500X and (b) as-etched conditions 1000 X, respectively.

3.4.2   136-lb Rail

The 136-lb rail was sectioned as shown in Figure 7(a) to conduct the metallographic analysis. The bottom edge of the rail shows the most severe corrosion damage. Independent of the corrosion rate in the track system (e.g., rail, tie plates, and clips), combining corrosion with cyclic stresses can considerably accelerate the risk of catastrophic failure. It is well documented that tracks with both cyclic traffic and corrosion create stress concentrators. This type of damage is usually caused by diffusion and is more commonly referred to as fatigue corrosion. The corrosion growth rate is relatively slow and uniform under these conditions, but if it is not detected in time, it can end in an abrupt catastrophic failure.

The separate sections of the rail were polished and analyzed using the stereoscope and optical microscope under polished and etched conditions. The rail section shown in Figure 7a was used to identify the effect of corrosion (i.e., micro-cracks) on the parent rail. As discussed earlier, micro-cracking can cause catastrophic failures, so a more in-depth study was completed during the metallographic analysis. Figure 7b confirms the magnetic particle inspection results, which determined that there is no evidence of micro-cracking in the sample. Figure 7c-e displays the microstructure of the 136-lb rail. These images do not show significant differences in microstructure when compared with the images of the 115-lb rail in Figures 6 and 7.

15
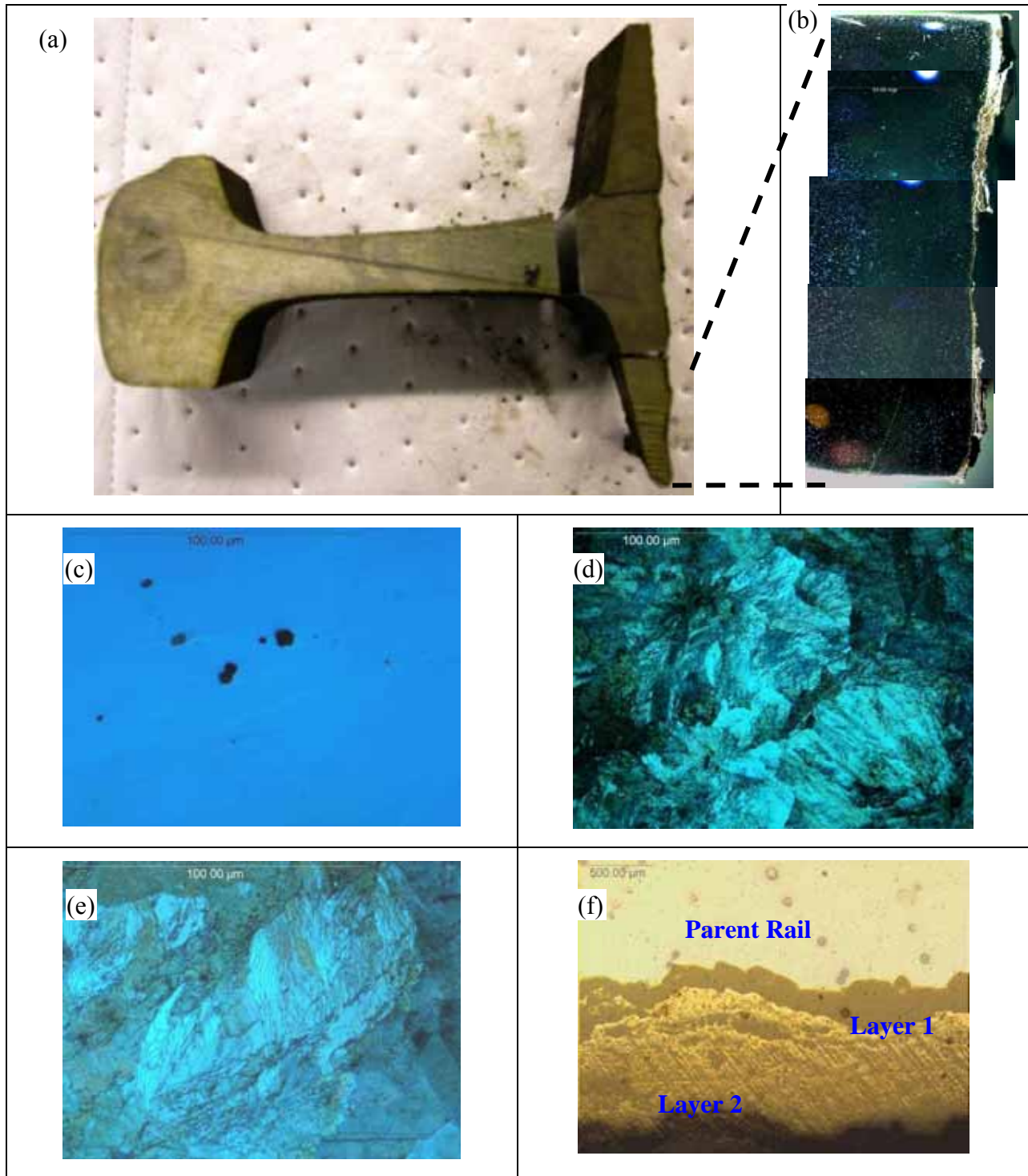
Figure 7. Macro- (a,b) and micro- (c-f) pictures of the 136-lb rail donated by Amtrak. (a) Cross section of the rail showing how the samples were extracted for analysis, (b) magnified section of the base of the rail showing no micro-cracks, microstructure (a) as-polished (1000 X) and as-etched (d) 500 X,(e) 1000 X and(f) difference between parent rail and corroded sections typical of rust.

16

CHAPTER 4: NUMERICAL SIMULATIONS

4.1   Finite Element Analysis Simulations

Based on the survey results, 100- and 115-lb rails are the most common rails used in transit systems. The first numerical simulation was conducted using a 115-lb rail provided by the Toronto Transit Commission (TTC). Figure 8 shows a section of the rail sample with severe corrosion. These images make it obvious that the structural integrity of the corroded rail is drastically compromised. The images also help to define the challenges associated with the detection of the corrosion because it occurs at the base, most likely over the tie, hiding the corrosion from visual detection. Several of the transit authorities reported that rail corrosion was not detected sometimes until the rail was removed from the tracks because the corrosion was hidden at the base of the rail (*7,9*).
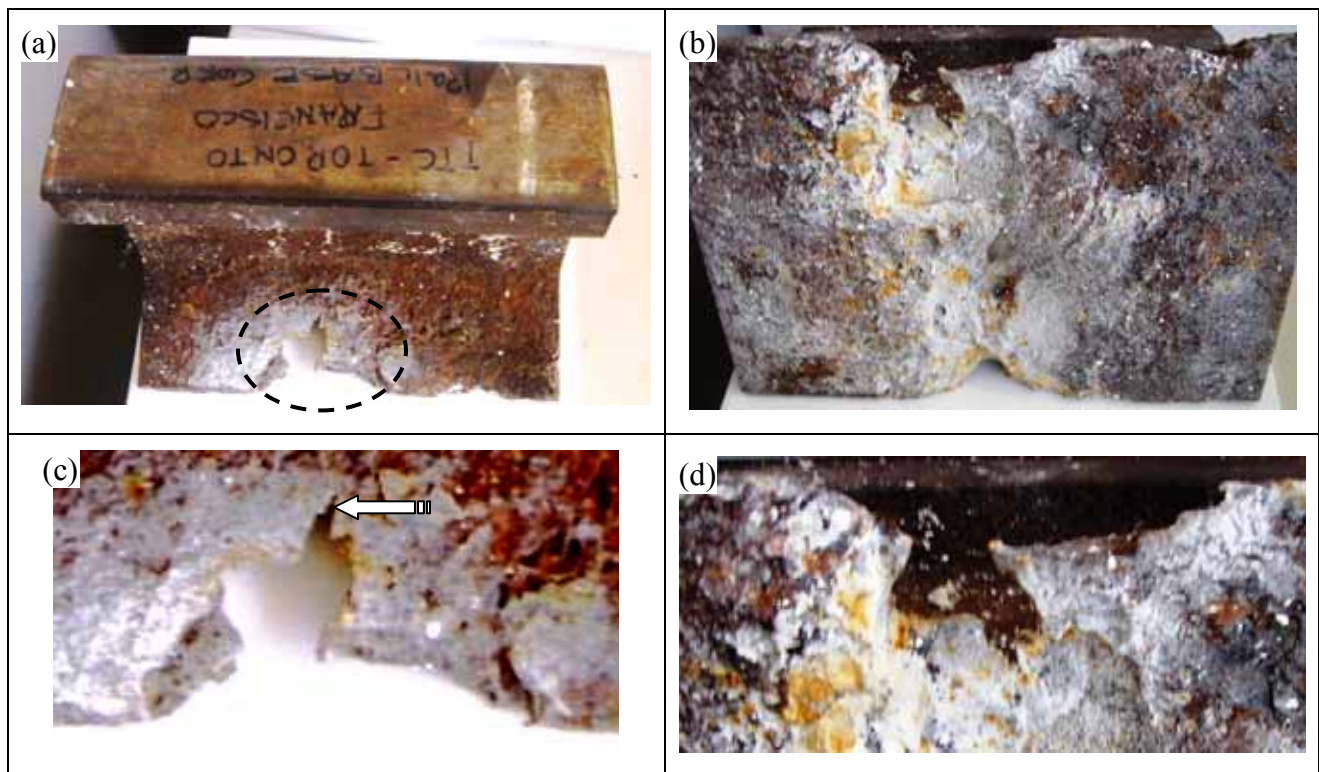
Figure 8. Pictures of the 115-lb rail used for the simulation. Pictures a-d show different angles and details of the effects of corrosion on the base of the rail. This rail was provided by TTC-Toronto, Canada. The arrow shows the location with the sharpest edge (stress concentrator).

The other simulation was conducted on a 136-lb rail donated by Amtrak. This rail sample was chosen for the second simulation because it contained common corrosion characteristics produced by the contact of the tie plate with the rail in the presence of stray currents. In this particular case, the rail base eroded leaving behind only a thin section of rail, which, in some cases, was as thin as a razor blade (*9*). Figure 9 shows several images of the rail base and

17

detailed images of the thin section. Contrary to the previously mentioned corrosion, this type of corrosion is easily detected by visual inspection. Each transit system has specific safety standards to prevent break failure for this corrosion condition, but most of them agree that the rail needs immediate replacement when 1/8 in. to 1/4 in. of the base has been removed (*8-10*).
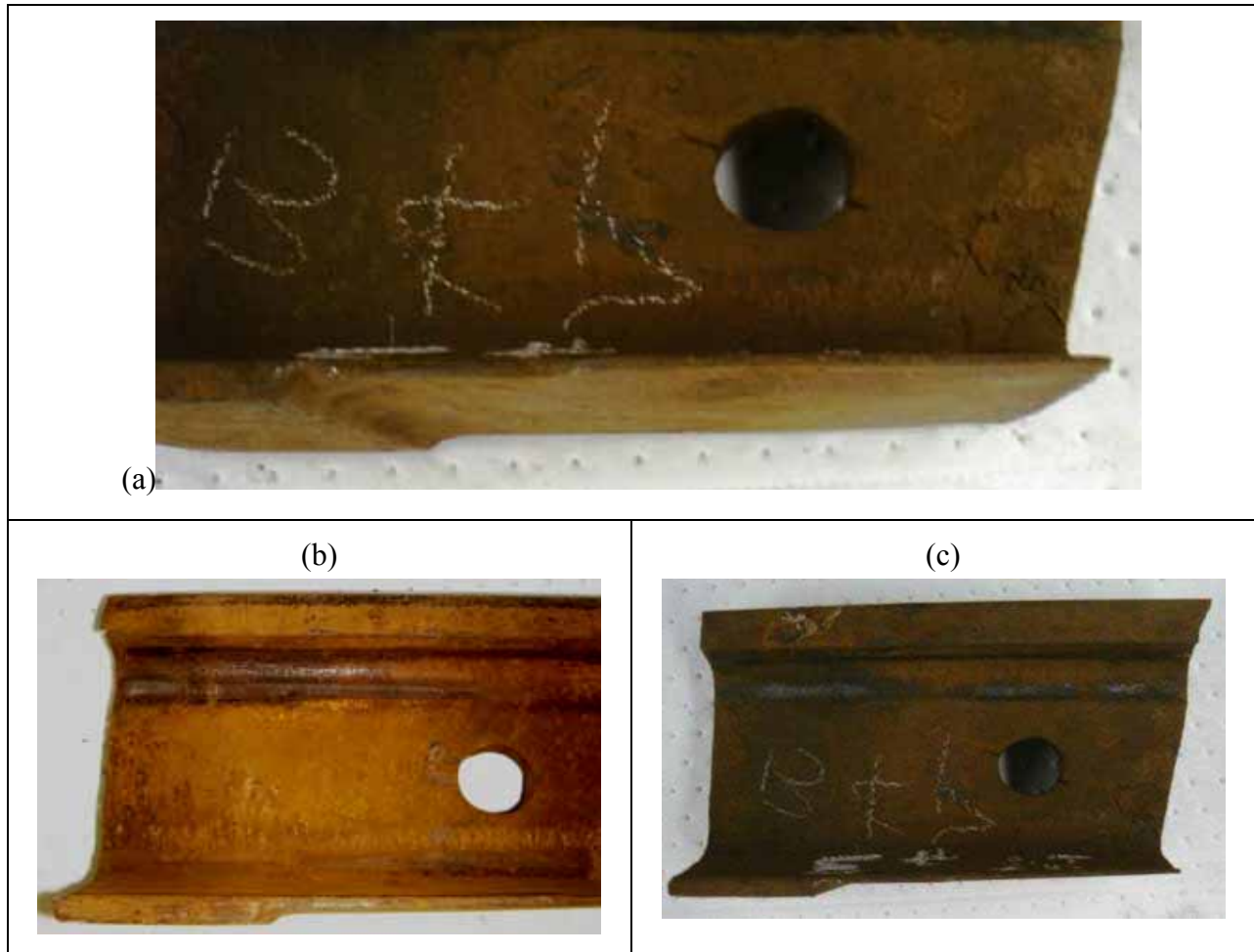
Figure 9. Pictures of the 136-lb rail donated from Amtrak for the rail base corrosion project showing a clear reduction from the base of the rail. Note: each transit authority has its own safety standard. However, most of them agree that a reduction in rail base between 1/8" to 1/4" is the maximum permissible allowance for immediate replacement of the rail.

18

4.1.1   Two Approaches for Dimensions and Size Determination

Two procedures were used to closely approximate the effects of corrosion from the base of the 115- and 136-lb rails. The first procedure used a mold of the rail base to copy the detail and determine the rough dimensions of the corrosion effects. Figure 10 shows the mold created during the first procedure.

Figure 10. Pictures of the clay molds used to copy the detail and main features of the base of the rails for the numerical simulations. (a,b) 115-lb rail and (c,d) 136-lb rail.

19

The mold for the 136-lb rail was sufficient for defining the corrosion characteristics and effects. The mold from the 115-lb rail did not provide the necessary information, so a second approach was used.

The second approach used the FARRO-Silver ARM digitizer to make an electronic digitalization of the rail. The FARRO-Silver ARM and electronic image are shown in Figure 11. The FARRO-Silver ARM produces a precise three-dimensional digitalization of the exposed surfaces. The digital data were directly used in ANSYS® to build a highly reliable model that represents the characteristics of the corroded rail.
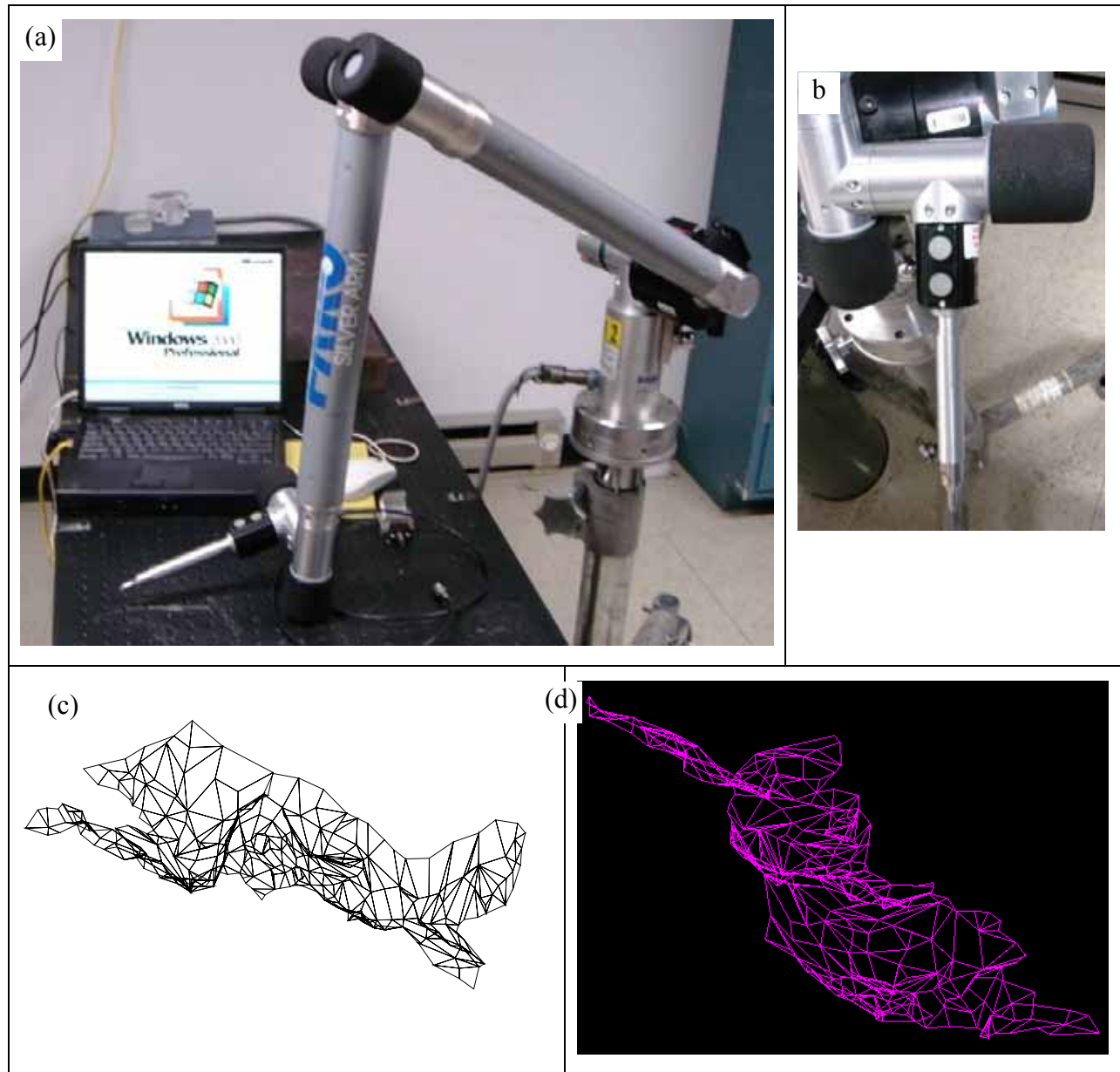
Figure 11. (a,b) Pictures of the FERRO-Silver ARM surface digitizer and (c,d) 3-D images of the corrosion effects at the base of the rail.

20

4.1.2   Finite Element Analysis 115-lb Rail

For the FEA of the 115-lb rail, the digitized image of the corroded section was imposed onto the base of a 115-lb AREMA rail profile taken from AREMA Chapter 4 (*11*). The simulation conditions for tie and tie plate dimensions and loads were provided by TTC-Toronto. The conditions used to conduct the numerical simulation are as reported by the TTC-Toronto transit system (see Appendix C).

Figure 12 shows the results of the FEA simulations. The maximum stress due to the stress concentration effects of corrosion was approximately 120 ksi, which is close to the yield strength of the steel used for this rail type. These data indicate that for this rail type, under these corrosion conditions, catastrophic failure can occur at any time. Figure 12 also shows that areas of high stress concentration occur more often near the sharp edges than the areas where extensive corrosion has occurred, which directly correlates to the stress concentration theory (*12*).
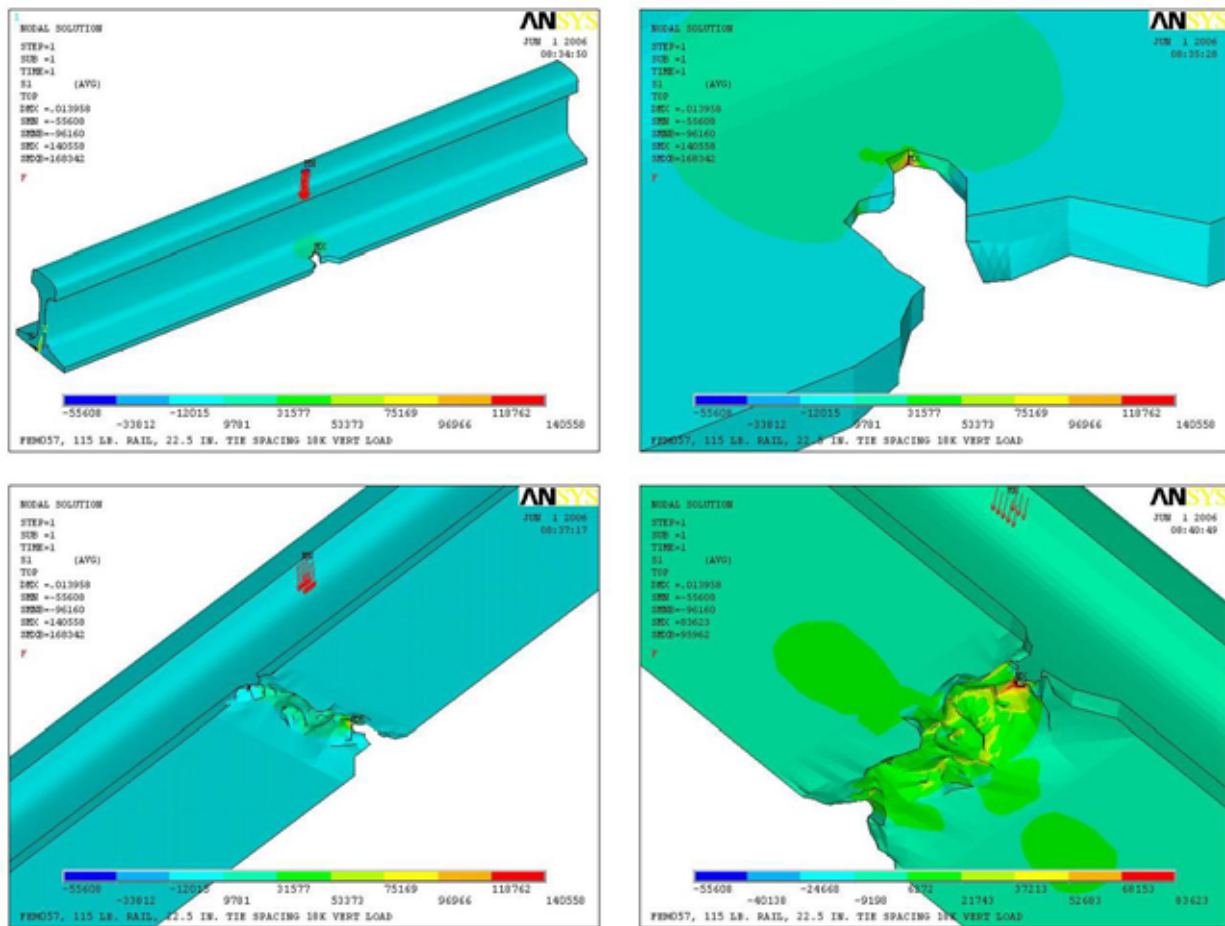
Figure 12. Results of the FEA analysis for the 115-lb rail. Notice the very high level of stresses reaching values as high as the yield strength (120 ksi) of rail steel.

21

4.1.3   Finite Element Analysis 136-lb Rail

Figure 13 shows the results of the FEA simulations for a 136-lb rail with base reduction of 1.5 mm. This simulation used a thickness value of 1.5 mm because it was the thinnest rail base found among the donated rails. The maximum stress of 22 ksi was located along the radius formed by the tie plate and perpendicular to the sharp edge and extended along the width of the rail. Comparing these results with the results of the 115-lb rail concludes that this type of corrosion provides less stress concentration than the sharp angles produced in the previous case.
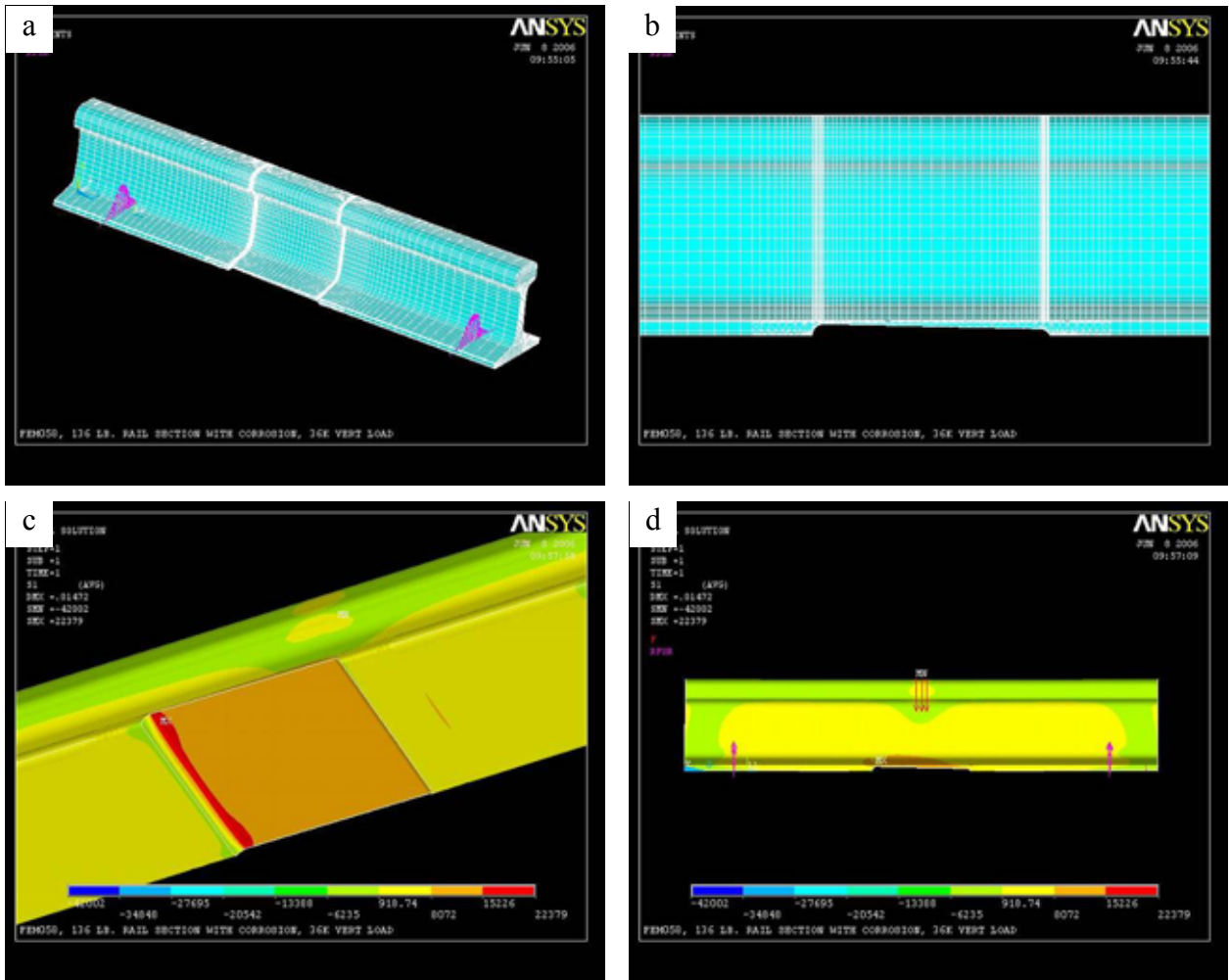
Figure 13. Results of the FEA analysis for the 136-lb rail. Notice that the highest stress is approximately 22.3 ksi and is found distributed along the sharp edge formed by the tie plate.

22

4.1.4   Conclusions of the Finite Element Analysis

The stress concentration at the base of the rail is considerably higher in the 115-lb rail than in the 136-lb rail and is dependent on the defect shape rather than the geometry of the rail and the load at which each rail is subjected by the respective transit systems. The equations shown in Figure 14 show the relationship between the size and shape of defects and their effect on stress concentration.

$$K_t = \frac{\sigma_{MAX}}{\sigma_{NOM}}$$

$$\sigma_{MAX} = \sigma\left(1 + 2\frac{a}{b}\right)$$

(1)

where: K_t is the stress concentration factor,

   a and b are the geometry parameters of cracks,

   σ_{MAX} is the maximum stress that results from the stress concentration,

   σ_{NOM} is the nominal stress or stress applied
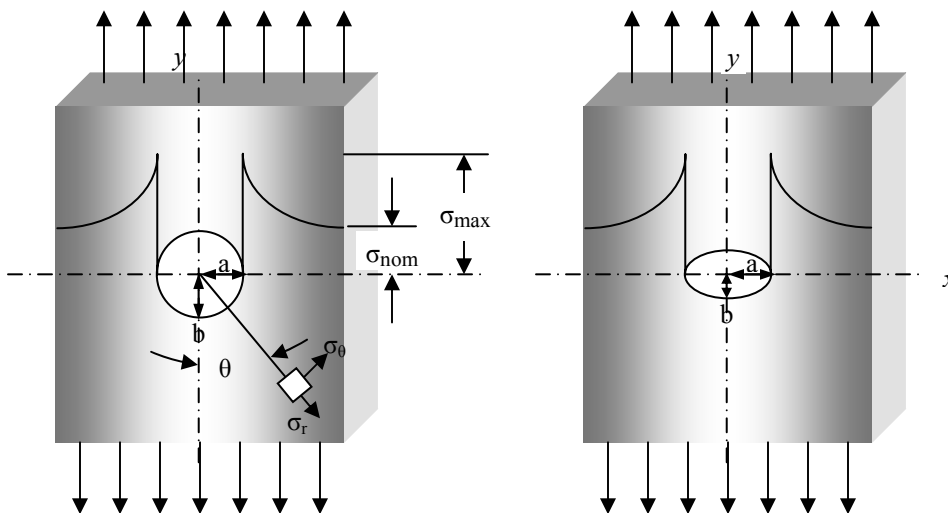
Figure 14. Stress distribution due to (a) spherical and (b) elliptical holes, respectively, along a component(12).

Equation 1 expresses the effect of geometry on stress concentration and stress distribution. Equation 1 can be used for holes of any shape along a component; the sharper the hole, the higher the concentration of stresses, which can be seen in Figure 14, where the stresses are

23

concentrated along the tips of the holes. The formula shows that as the a/b factor increases, a linear enlargement of the concentration of stresses is observed (e.g., for a circular hole Kt = 3). This confirms that locations with sharp edges correspond to the maximum stresses as confirmed by the numerical simulations shown in Figures 12(b-d) and 13(c).

The results from the FEA showed that the stress concentrations were considerably higher for the 115-lb rail than for the 136-lb rail. This is due to the shape of the corrosion induced geometry that is present in both rails, which helps to conclude that the size of defect plays an important role, even though in some cases the shape of the defect is more important. For instance, Figure 12(b) shows that at the tip of the defect, the stress levels reach intensities between 120 ksi and 140 ksi. In contrast, long defects distributed along the tie-tie plate location build up stresses of approximately 7 times lower. Therefore, the effect of evenly distributed corrosion along the base of the rail also builds up stresses, but this type of stress concentrator is not as efficient as sharp edges (see Figure 13). As a result, the stress intensity in this region is considerably lower (between 15 and 24 ksi) than the stresses observed in the 115-lb rail.

The presence of sharp edges produced by corrosion is very detrimental to the analysis of defects under the flange for two main reasons: (1) the defects are usually outside of visual inspection capabilities and (2) the corrosion typically causes very intricate defect shapes. The previous discussion directed the analysis to a numerical simulation for the determination of the effect of defects on fatigue, performance, and structural integrity of the rail.

- The analysis of the 115-lb rail proved that the level of stresses is high enough to easily cause a catastrophic failure at any time during regular traffic conditions. The cyclic stresses on this rail are equivalent to the yield strength (which is between 80 ksi and 120 ksi for standard and high strength rail steels, respectively).
- The analysis of the 136-lb rail showed that the stresses were considerably below yield. A high cycle fatigue analysis was conducted for the 136-lb rail because the stresses indicated by the numerical simulation can be detrimental under high cycle fatigue and corrosion. Section 4.2 provides the conditions and results of the fatigue simulations.

4.2   High Cycle Fatigue Analysis

The following parameters were used for the high cycle fatigue analysis. The values for the analysis were in accordance to the data provided by Amtrak (*9*), except where indicated and properly referred.

4.2.1   Load/Stress Environment

- 216 passenger trains per day
- Each train contained eight passenger cars and two locomotives
- Each locomotive weighed 146,000 lb and each car weighed 78,500 lb
- Wheel loads estimated as 12,500 lb for locomotives and 10,000 lb for cars
- FEA was used to calculate maximum stress in corroded areas due to wheel loads. Maximum stresses of 7,771 psi and 6,220 psi for locomotive and passenger car wheel loads were used, respectively. The resulting stress cycle environment used per train consisted of 12 cycles of zero to 7,771 psi and 32 cycles of zero to 6,200 psi.

4.2.2   Rail Material Properties

- A section the width of a tie corroded away on the bottom surface of the rail.
- Material is considered to be quenched and tempered Ni/Cr/Mo wrought steel with a yield of 110 ksi and a tensile strength of about 180 ksi.
- S-N curve for the material is estimated to have stress range intercept of about 94.3 ksi and a life cycle of 1.0E6 of 43.5 ksi. The S-N curve has a constant slope on a Log-Log plot, and the slope remains constant to a life cycle of 1.0E10 (Figure 15).
- The S-N curve is considered to be produced from small test samples or coupons ─ not from full-scale rail samples.
- The S-N curve used is Stress Range versus Life Curve.

4.2.3   Fatigue Analysis Parameters

- The Goodman mean stress correction factor was used to account for all cycles having only positive stress.
- A correction factor accounting for a corrosive environment was used to modify the material S-N curve.
- The Miner's constant was reduced from 1.0 to 0.90 to account for the rough surface produced by the corrosion.

4.2.4   Results of the High Cycle Fatigue Analysis

Estimated life (for 50% of the locations) until crack initiation with this type of base corrosion is approximately 1.39E7 to 1.87E7 "load blocks" or "trains." This is equivalent to 176 to 237 years, if there are 216 trains passing through the location each day. This implies that this type of situation is not as dangerous for rail's integrity as the presence of sharp edges. However, it is very important to notice that the "razor sharp" effect (9) was not found in any of the rails provided for the current research. Therefore, by introducing this effect on the numerical simulation, the rail's life can be reduced considerably.

25
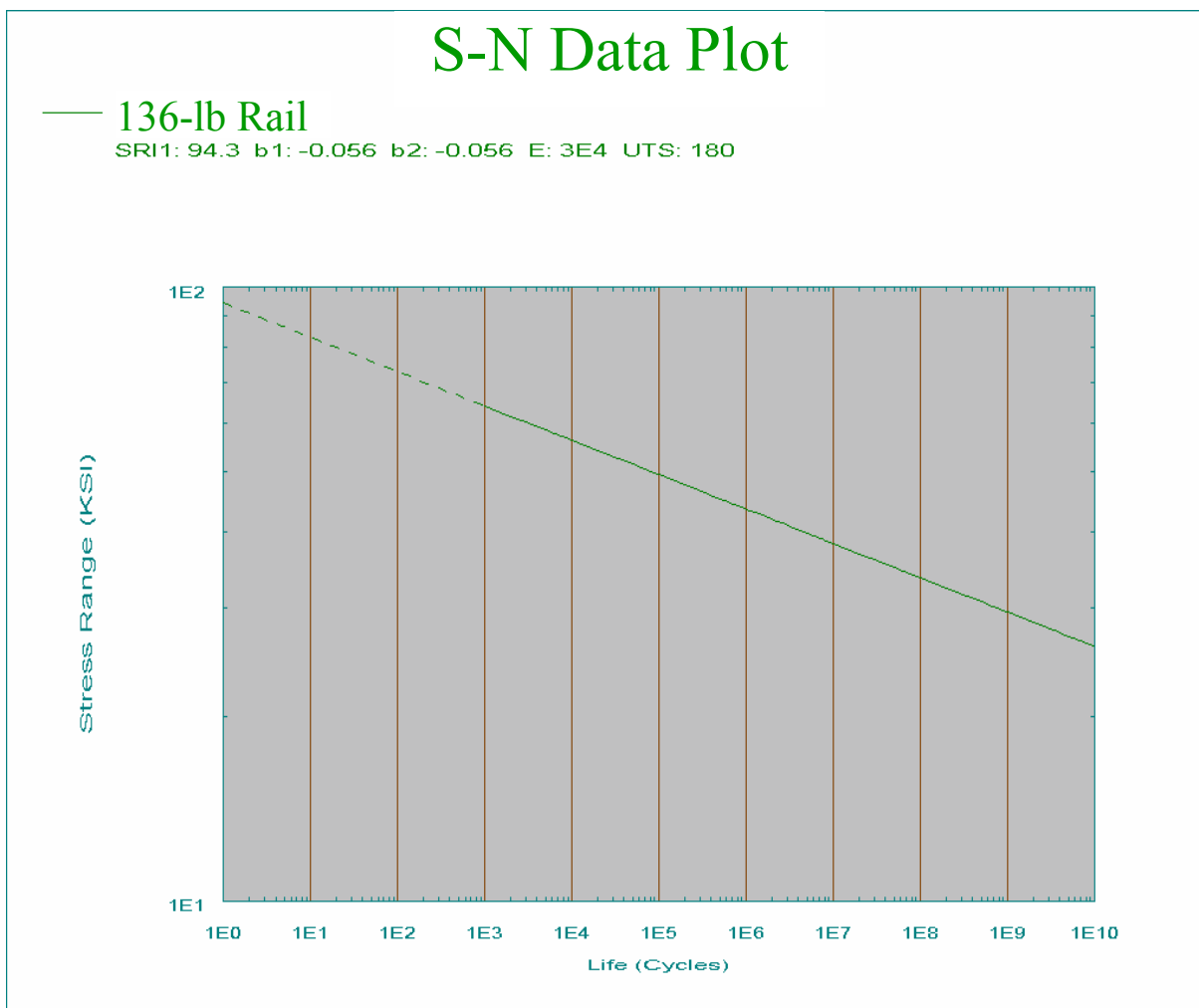
Figure 15. S-N curve for 136-lb rail steel.

CHAPTER 5: CORROSION PREVENTION METHODS

5.1   Presence of Salts on the Tracks

The presence of salt on rails creates a very detrimental effect on the integrity of the rails because the salts form electrolytes promoting oxygen to react with the rails, thereby accelerating corrosion. During site visits, salt deposits on top of the tie plates were observed at several locations. Most of the locations are usually humid so there is consistent contact between the rail/tie/clip and ground. Figure 16 shows some of the deposited salts on top of the tie plates and rail found at several different sites. Figure 17 displays the differences between a clean and well insulated tie and tie plate and a tie plate with deposited salts and corrosion.

The chemical analysis as reported by the Edmonton Transit System includes mainly alkaline salts, chorines, and sulfates (*7*). This was further confirmed by other transit authorities (*13-15*). Appendix E shows the chemical analysis conducted by the Edmonton Transit System.

(a)

Figure 16. (a) Salts deposited along the tracks at Port Authority Trans-Hudson.

27

(b)

Figure 16. (b) Salts deposited along the tracks at Southeastern Pennsylvania Transportation Authority.

a

b
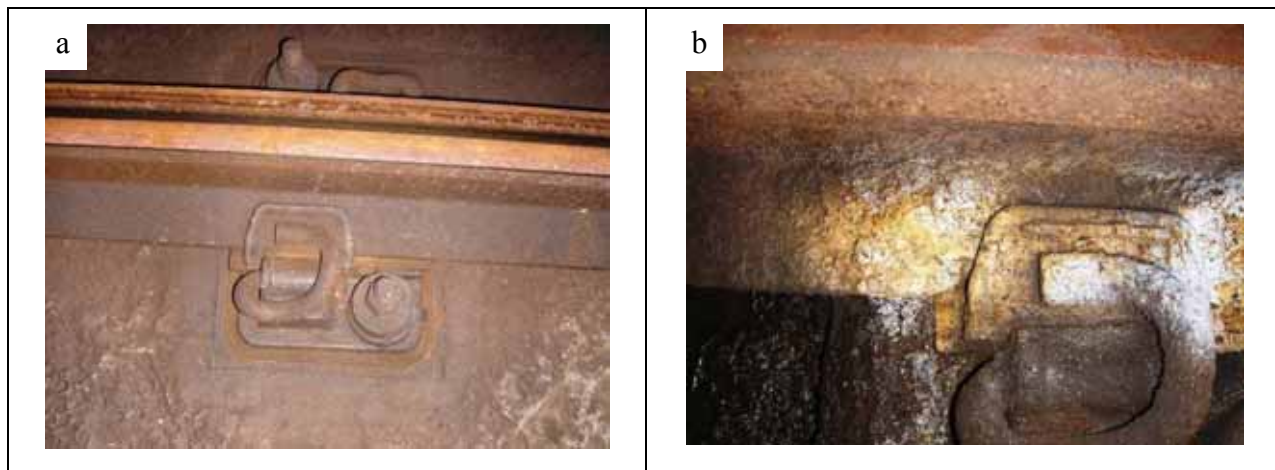
Figure 17. Examples of Pandrol clips showing (a) good condition and (b) salts deposited around the Pandrol clip. Both pictures were taken at the Toronto Transit Commission subway during the site visit.

28

5.2   Analysis of Ballast

An analysis was performed on ballast specimens from the research team to determine the effect of salt. Figure 18 shows the ballast specimens used.
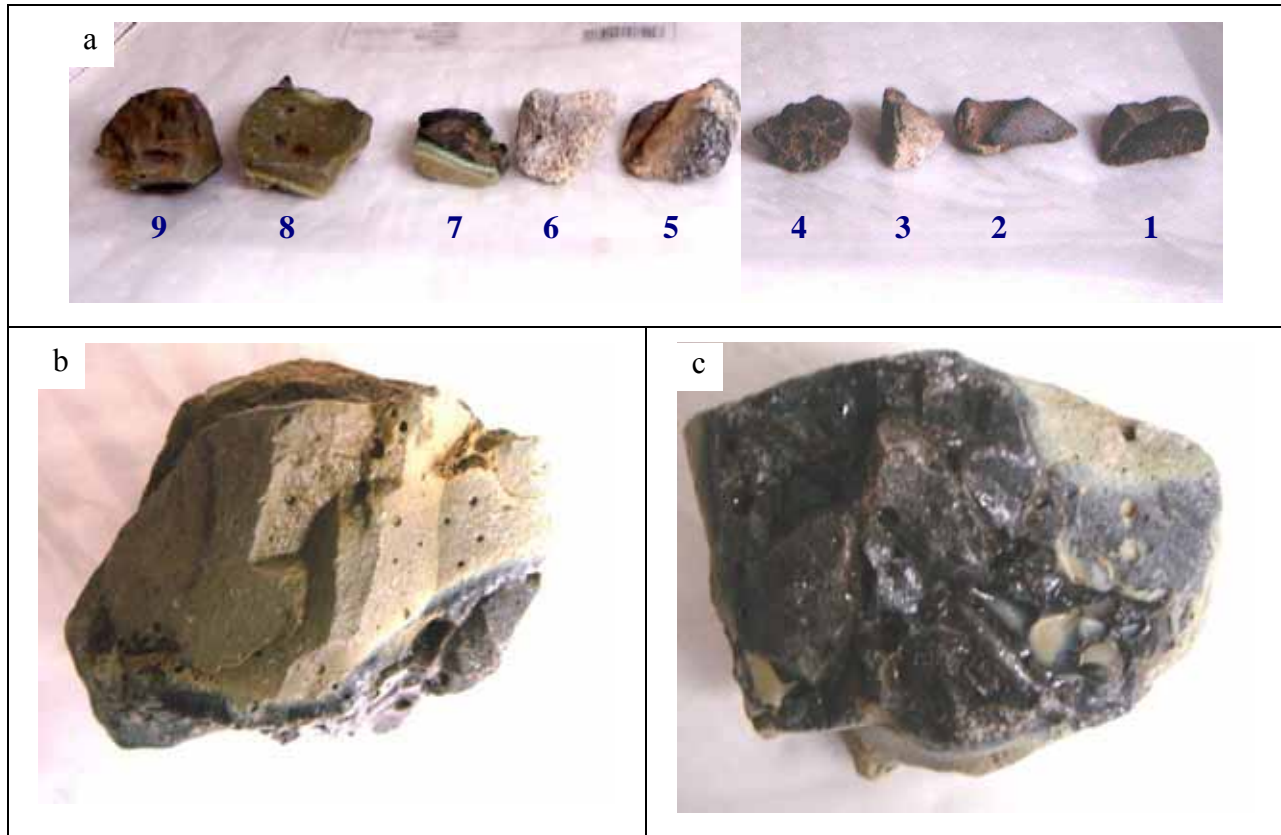
Figure 18. Ballast specimens used for the resistivity test: (a) all tested ballast and slag based ballast (b) green section, and (c) black/glassy section.

Two types of ballast were used for the test: mineral and slag based. The resistivity of the ballast was measured under dry and wet conditions. To simulate wet conditions, ballast types were immersed in water for 5 seconds and then excess water was removed. This was completed in order to measure the effects of absorbed water (humidity), rather than the surface deposited water. Table 3 shows the average resistivity results of at least 10 measurements of all ballast types under dry and wet conditions.

TABLE 3. Resistivity results on dry and wet ballast. The >> symbol is used to report the average resistivity measurements of specimens 3 and 6 and respective 7 and 9 specimens. The other measurements were OL = Overload.

Ballast	1	2	3	4	5	6	7	8	9
Dry	OL	OL	OL	OL	OL	OL	OL	OL	OL
5 seconds in water	10 MΩ	15 MΩ	5 MΩ	2 MΩ	4 MΩ	5 MΩ	>> 20 MΩ	8 MΩ	>> 11 MΩ

The results of the test indicate that both ballast types have high resistivity after excess water is removed. Observations showed that the resistivity for all dry ballast overloaded the meter showing that under dry conditions ballast is a good insulator. Comparison of the results found in Table 3 concludes that the ballast types tested have negligible effect on corrosion. Furthermore, an evaluation of the parameters extrapolated to rail base corrosion (Table 2) indicates that the severity of corrosion is 15+, of which 5 points are from resistivity, 0 points for pH, 5 points for REDOX, 3.5 points for the presence of sulfates, and 2 points from moisture. The 5 points from resistivity is a conservative number and varies from tunnel to tunnel and environmental conditions, particularly salt deposits. Therefore, the environmental conditions at which the rail is exposed can be substantially detrimental to the rail's integrity.

Some of the literature reviewed by the research team recommended avoiding slag based ballast because of its relatively high conductivity (probably due to its high metallic content) (*5*). However, in the laboratory test, slag based ballast was found to have the highest resistivity under dry conditions (see Figure 18 and Table 3 ballast specimens 7-9). Ballast specimens 3 and 9 in Table 3 were selected to undergo a second test, immersing the ballast for 5 minutes in water to see if there would be any changes in the resistivity. There was no change in specimen 6 between a 5-second and 5-minute immersion, but the resistivity of specimen 9 was reduced from 8 MΩ to 2.5 MΩ. That is still a very high resistance, indication of a good insulator, except for when the ballast is thoroughly wet.

5.3   Rail Steels

Rail steels are mainly made of iron and carbon. Iron is usually found in the form of α-Fe or ferrite (dilute solid solution of Fe and C) forming carbides, intermetallics, and inclusions (oxides and other nonmetallic compounds). However, the presence of inclusions is considerably low. Most of the iron in steel is found as pearlite, where the α-Fe lamellas are considerably more vulnerable to corrosion than any other steel component (iron carbide and Fe_3C). In fact, elements like carbon in steel have very little, if any, effect on corrosion (*1*). Rail steel is usually a low alloy steel with some C, Cr, Mn, Cu, Ni, V, Mo, Nb, etc., with minor additions of other elements. Elements such as C, Cr, V, Mo, Mn are added for hardening, corrosion resistance, and strengthening. Larger additions of strategic elements (Cr and Ni) can considerably increase the resistance to atmospheric corrosion and/or corrosion in aqueous systems (*1*). However, this would considerably increase the cost of rail and probably have limited to no corrosion reduction benefits because the main factor that accelerates the rail base corrosion is the return current.

Corrosion of carbon steel in water is controlled by the availability of oxygen to the metal surface. In rail structures, the water or humidity deposited on the rail usually has high amounts of dissolved oxygen, and the water layer is thin enough to permit an easy flow of oxygen. Under static conditions, carbon steel corrodes at rates between 100 and 200 μm/year, depending upon the oxygen level and temperature variations at different locations. As velocity causes a mass flow of oxygen to the surface, corrosion is very dependent on flow rate and can increase by a factor of 100 (*2*). This factor of 100 does not consider the presence of stray currents, a major concern for transit systems. Additionally, when the deposited salts on top of the rails become dry, very aggressive corrosion conditions are formed. This is due to the relatively good conductivity and the ability to dissolve oxygen, resulting in an increase of the rate at which corrosion erodes the rail.

5.4   Cathodic Protection

Cathodic protection is one process used to prevent steel corrosion. A zinc (Zn) coating is most commonly used. Zn is used under normal atmospheric conditions, not because it is inert to corrosion, but rather because it corrodes considerably faster than steel, resulting in a coupled system (Figure 19). Zn coatings show increased corrosion rates under nonstatic conditions, so it would only provide a limited benefit to the transit system because rails are a nonstatic system. Galvanizing is more appropriate for static systems (*1,16*).
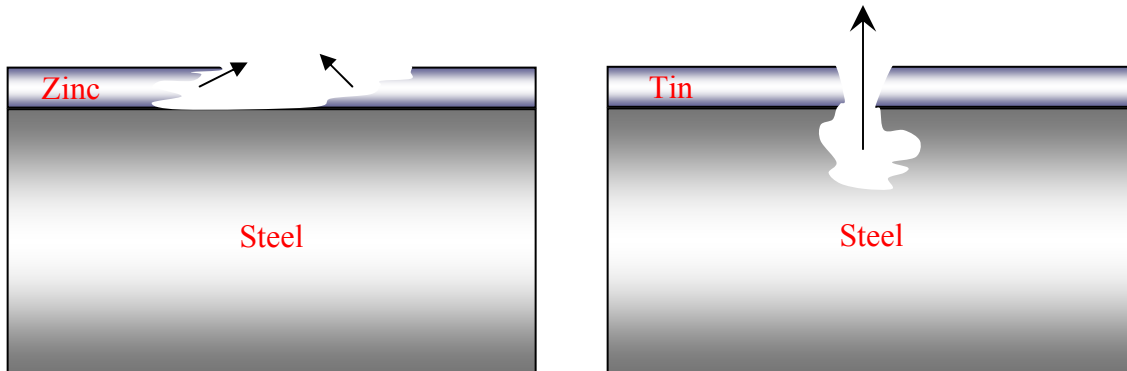
Figure 19. Examples of galvanic corrosion using zinc and tin on steels. Note that while zinc makes a protective layer preventing the corrosion of steel, tin is protected by the corrosion of steel.

5.5   Sacrifice Anodes

Figure 20 shows another typical cathodic Protection method used in the pipeline industry. This type of protection is very useful for static systems (i.e., pipelines), but in particular systems that have no introduction of external currents. This method closes an electrical circuit by introducing a more active element (Mg) that corrodes faster than the material under protection. For instance, a steel pipe in a corrosive environment with Mg cathodic protection will force the Mg to become more vulnerable to corrosion than the steel that creates a corrosion protection shield for the steel. This type of system is widely used by several industries and is a reliable method for corrosion protection. However, one of the conditions of this type of protection is that no current should be passing thorough the material under protection; otherwise, the current will alter the effectiveness of the anode. Therefore, cathodic protection will be ineffective for transit systems because there is a return current along the rails (*1,16).*

Ground Level

Earth
Environment

Coated Copper Wire

Current

Steel
Pipe

Mg
Anode

Backfill
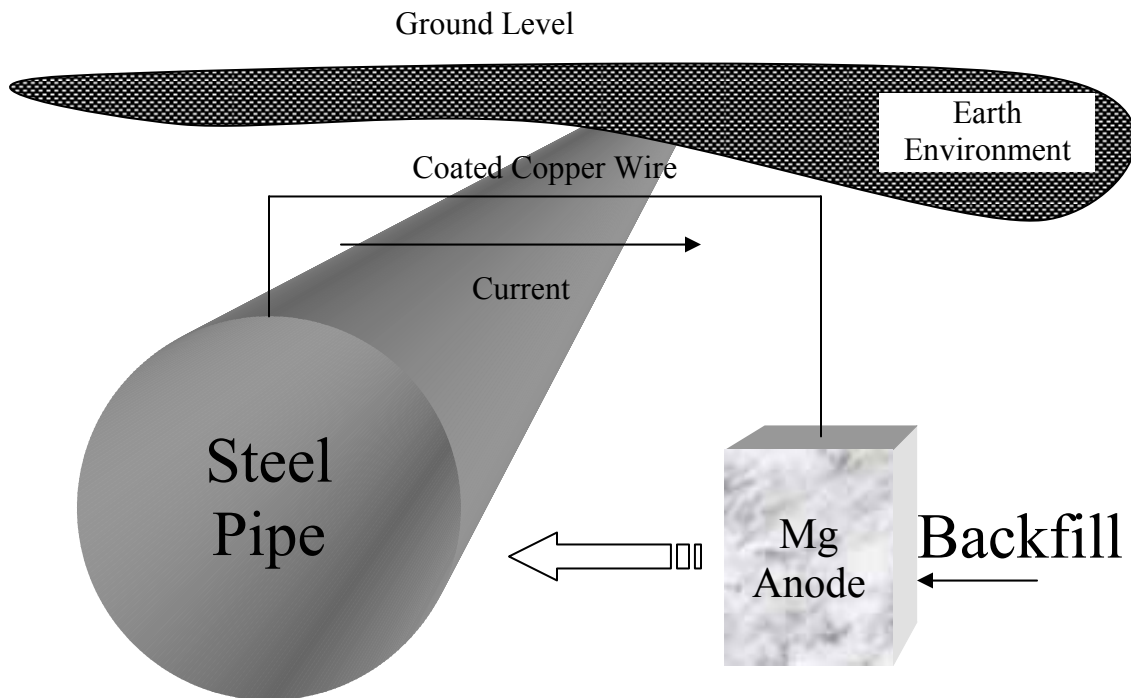
Figure 20. Protection of an underground pipeline with a magnesium anode (1).

The return current for transit systems is the byproduct of the train that closes the circuit of the overhead catenary or third rail. Ideally, the return current on well insulated rails will not have detrimental effects. However, in most cases there are stray currents caused by leaks where the current breaks the circuit through the path with less resistance (usually wet soil with high concentrations of salts, drain systems, electrical city circuits, etc). The electrical current always travels along the path of least resistance, or the current is divided along several paths in proportional amounts of current. For example, when the electrical continuity of the track structure is poor or the circuit is broken, more stray current will return through another path. The corrosion rate is directly proportional to the stray currents, limiting or eliminating the stray current occurrence will considerably reduce and probably eliminate rail base corrosion.

5.6 Recommendations for Rail Corrosion Protection

Cathodic protection has great potential to prevent corrosion; however, in most cases, it is only applicable for static systems in the absence of dynamic currents. Rails are subjected to high dynamic stresses and are a good path for return current to the ground. In addition, the presence of deposited salts on the rails and the corroded rail itself increases the corrosion rate. The presence of moisture, salts, and iron-based powder(s) amplify the corrosion effects on the rails because the salts form an electrolyte when combined with DC that promotes electrolytic reactions increasing the corrosion rate. Furthermore, salt and iron powders have a large surface

32

area promoting the formation of stray current locations that result in increasing the detrimental effects of oxygen, thus increasing corrosion rate, as Figure 1 shows.

Therefore, the best way to prevent the corrosion of the rails is by properly insulating the rails (see Chapter 7), avoiding any DC leaks from the rail to the ground, forcing the current to return properly and closing the circuit. References 1, 4, 6, 16-35 contain information on corrosion and corrosion prevention with particular interest to the transit industry.

33

CHAPTER 6: POTENTIAL FOR RAIL BASE FLAW DETECTION

6.1   Available Technologies for Rail Base Flaw Detection

Currently, there are very few nondestructive test methods that have the ability to detect flaws in the base of the rail. TTCI is currently developing an advanced ultrasonic testing technology that will be capable of monitoring the entire rail, including the base. This technology seems to be the potential solution to monitor and detect rail base corrosion. The test system uses a high powered laser to produce ultrasonic waves and air-coupled transducers to receive the signal. Conventional ultrasonic principles are applied in this system, but the noncontact nature of the system provides the ability to go far beyond the inspection capabilities of current systems. Because no contact is required between the rail and the transmitter/receiver, many inspection limitations are removed, which allows this technology to monitor the head, web, and base of the rail, unlike most of the rail flaw detection units in industry today that focus only on the inspection of the railhead (*36*). Schematics, principles, and the methodology currently under development by TTCI are presented in Figures 21 and 22. This technology is of particular interest for the transit industry because detailed monitoring of the base of the rail can be easily and efficiently conducted.
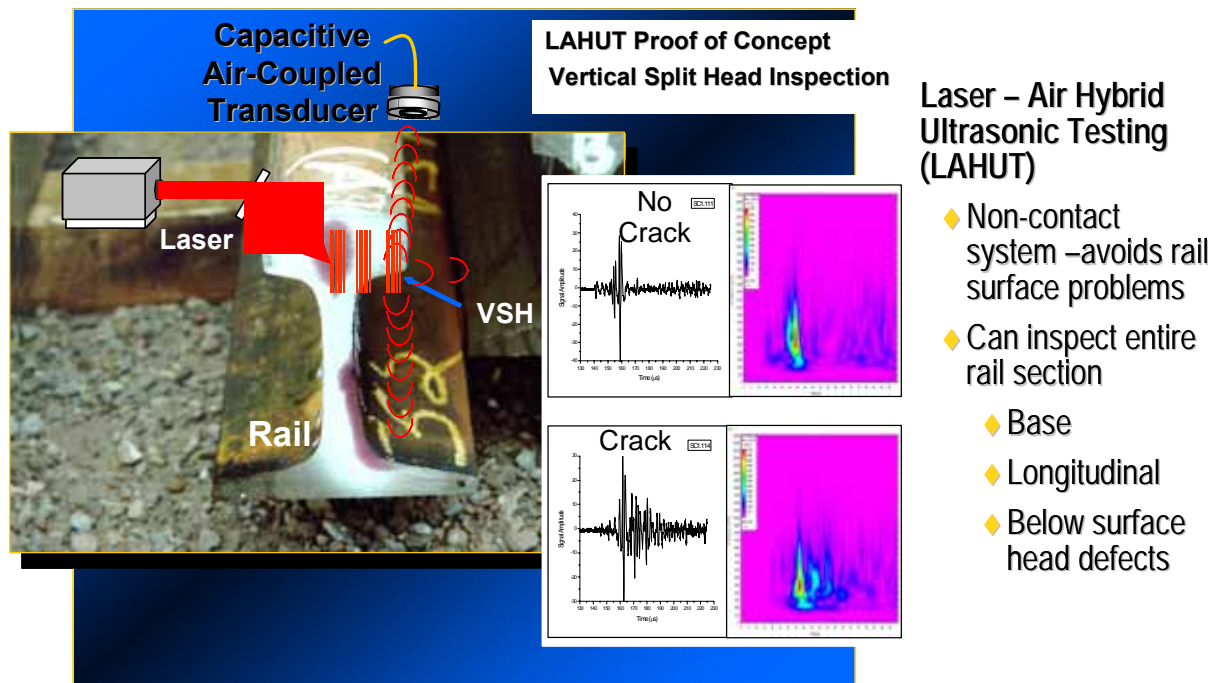
Figure 21. Principles of emerging technologies for rail flaw detection (37).
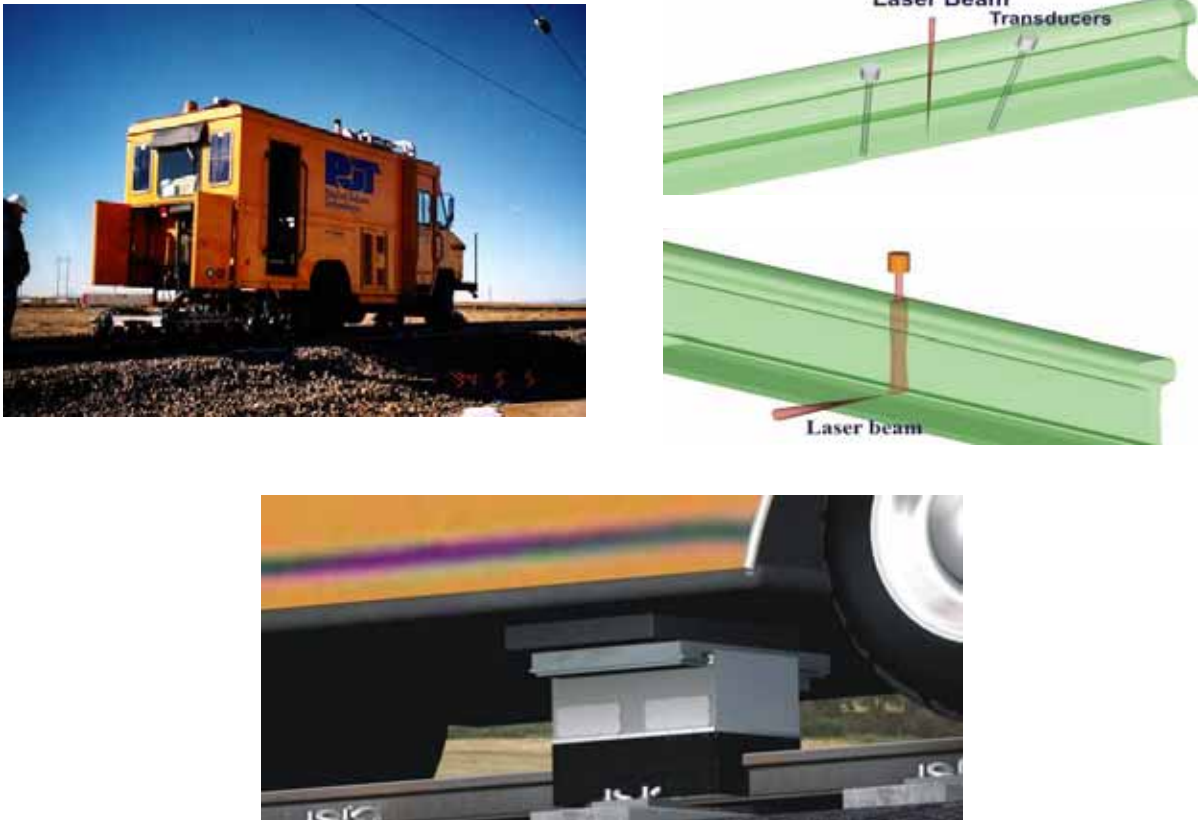
Figure 22. (a) Rail flaw detection vehicle showing (b) location of the lasers and transducer and (c) ultrasonic device monitoring a rail in service (37).

6.2 Current Technologies and Examples of Nondestructive Techniques with Potential for Implementation

A variety of NDE methods has become available that are viable candidates for the detection of corrosion. Those that will be considered here are visual, ultrasonic, radiographic, eddy current, electromagnetic acoustic transducer scanning, thermographic inspection, and ground penetrating radar.

6.2.1 Visual Inspection

Visual inspection has been and continues to be the primary method for corrosion detection. Visual inspections continue to be one of the more sensitive and reliable inspection methods because careful evaluation of the specimen by touch and sight is a very important part of the process. Visual inspection requires good vision, adequate lighting, and knowledge of what to look for, so only qualified personnel can complete a thorough inspection of the rail. Enhancement of visual inspection can be done by using low powered magnifying glasses, borescopes, or video cameras (*38*). Unfortunately, visual inspection is only applicable to corrosion that is exposed to the surface; internal and hidden corrosion can easily go unseen.

35

6.2.2 Ultrasonic Inspection

Ultrasonic testing (UT) methods can be used to measure the thickness or length of an item. Another common use of ultrasound is for flaw detection. Ultrasound also has the ability to detect liquids inside a component, measure the presence and amount of corrosion in buried anchor rods, and interrogate concrete. Automated ultrasonic inspection systems have been successfully used to detect subsurface corrosion and cracking in piping, storage tanks, and aircraft components. Ultrasonic thickness meters are also commonly used to check pipelines for corrosion. Although these meters can determine wall thickness, it is still very difficult to detect localized internal corrosion. Ultrasonic thickness mapping of specifically selected inspection points provides far more information about the condition of a piping component, tank wall, or floor (*38*).

Automated ultrasonic inspection systems, in particular phased array UT systems, can be successfully used to detect subsurface corrosion on piping, tank walls, aircraft lap-joints and micro-cracking around rivets of high speed aircraft. The use of a phased array UT system can replace several conventional UT probes, and the angle of incidence can be controlled electronically. For more information, refer to reference 39.

Phased array systems generate a beam with various probe elements pulsing at slightly different times. By precisely controlling the delays between the probe elements, beams of various angles, focal distance, and focal spot size, an optimization of the beam can be produced. It is possible to change the angle, focal distance, or focal spot size, simply by changing the timing to the various elements. The sectorial scan is a real-time side view generated from a single inspection point, without any physical motion from the probe. Phase array has the advantage that the probe has various transducers that can monitor in various directions or angles at once.

6.2.3 Radiographic Inspection

Radiographic inspection provides more information about the condition of a component than any other method; however, it also presents the highest safety risks because it requires the use of dangerous ionizing radiation. It also requires access to both sides of the component being inspected, and it is expensive. Radiographic films have been the primary method to capture images of the component under investigation, but there are several new image-recording methods now becoming available (*38*).

One of the newer image-recording devices, referred to as computed radiography, employs the use of photo-sensitive plates which are used similarly to conventional films. One of the most important differences is that the photostimuable plates are reusable and more efficient at collecting data than film. The dynamic range is far greater with the plates than the film because the latent image is digitized. Other important methods for capturing radiographic images are lens and charge coupled devices, direct imaging flat panel devices, linear arrays, and image intensifiers. All of these devices can be configured into programmable automated scanning systems. The collected image data provided by each of these image collection devices can be enhanced, stored, and retrieved (*38*). Unfortunately, this method is complicated for implementation into various transit systems.

6.2.4   Eddy Current Inspection

Eddy current inspection aids in the detection of surface (or near surface) anomalies and is used quite extensively in the aerospace industry. Eddy current technology is also an excellent, inexpensive tool used for material sorting and measuring coating or material thickness. Specialty tubing manufacturers rely on automated eddy current inspection devices to test their products. Eddy current thickness mapping is performed to detect corrosion in aluminum aircraft skins.

6.2.5   Electromagnetic Acoustic Transducer

Electromagnetic Acoustic Transducer (EMAT) induces ultrasonic waves in metals without the need for a coupling medium. The method is designed for rapid assessment of corrosion in piping, even if the piping is coated or at temperatures up to 500°F. A volumetric interrogation of the full circumference of a pipe run is accomplished with the EMAT devices astride the top of the pipe. Anomalies that have been detected in long runs of piping by this method are erosion, pitting, and cracking (*38*).

6.2.6   Thermographic Inspection

Thermographic inspection, commonly referred to as infrared inspection, locates defects using thermal characteristics of the specimen. This inspection method is being successfully used throughout the railway industry. Locating hot spot defects in electrical services has been particularly effective. Other uses include the determination of process liquid or catalyst levels in chemical towers and/or columns and boiler tube corrosion characterization with a scanning thermal line device. Thermographic images are acquired in real-time and advanced processing provides information about coating defects and/or thickness variations in the coating and subsurface corrosion spots (*38*).

Lawrence Livermore National Laboratory has developed a dual-band infrared computed tomography system that can search for defects on bridge decks and airplane fuselages. The dual-band infrared images are acquired as maps. The data is then processed, revealing corrosion damage and other surface and subsurface anomalies.

6.2.7   Ground Penetrating Radar

Ground penetrating radar systems provide three-dimensional information about reinforced concrete. Ground Penetrating Radar (GPR) requires access to only one surface and is faster, safer, and less expensive than radiography. GPR can provide information concerning rebar that is below the surface and has been found to be useful in evaluating existing structures for continued use, modification, or repair (*38*).

37

CHAPTER 7: GUIDELINES FOR CONTROLLING AND DETECTING RAIL BASE CORROSION

One of the most effective ways to control corrosion is by insulating the contact between materials or components with different chemistries that have a tendency to form galvanic pairs. However, this is close to impossible because perfect insulators do not exist. Therefore, the solution is to prevent DC leaks or stray currents from the rail to the ground. Refer to references 4 and 16 for additional information on this subject. Eliminating water leaks to the tunnels is significantly difficult; nonetheless, water should be re-directed out of the tracks in order to avoid humidity that can promote stray currents from the rail to the ground. In the following subsections recommended guidelines for corrosion prevention and corrosion detection are discussed.

7.1   Corrosion Prevention

Preventing stray currents (current leaks) and reducing humidity (particularly the salts in water leaks) minimizes corrosion. Therefore, the following guidelines are recommended to eliminate or to reduce conditions causing or contributing to corrosion (see also reference 16).

- Maintain good maintenance and good insulation. Clean and keep track roadbed water free.
- Maintain a stray current control program by conducting rail-to-earth resistance and sub-station-to-earth tests (*16*).
- Identify locations where stray currents are occurring or have a tendency to occur and create proper insulating conditions. Stray currents should be avoided when possible.
- Install welded rail in place of jointed rail because welded rail has significant traction current return. Make sure the rail is electrically bonded if jointed rail is installed. Otherwise electric arcs or leaks can be formed and produce stray currents.
- Insulate rail from fastening systems (Figure 23). For embedded tracks, it is crucial to coat and/or encase the rail with a good insulator.
    - A good insulation system can be made using as a base the insulators from the Pandrol. In addition, Figure 23 and reference 16 provide the details for insulators as well as for the encasing materials that can potentially prevent rail corrosion.
- Maintain clean and dry ballast or slabs. Any direct contact between the rail and ballast must be avoided. It is recommended to have at least 1 in. (25 mm) of clearance between the rail and the ballast (*16*).
- Include an extra line of welded conductors along the rail's web to provide an alternative low resistant path to prevent stray currents.
- Consider using plastic ties to better insulate the track from the ground (see Chapter 8).

These guidelines are of crucial importance for the design and construction of new tracks in order to prevent and/or reduce costly corrosion prevention methods in the future.

(a)

ELASTIC FASTENING

INSULATED RAIL BASE PAD

RAIL BASE INSULATORS

MOUNTING SURFACE

(b)

BOLT/LAG SCREW
SPRING LOCK WASHER
FLAT WASHER
INSULATOR COLLAR/ THIMBLE
FASTENING PLATE
INSULATED FASTENING PAD

ENLARGED VIEW

INSULATED FASTENING PAD

ANCHOR INSERT
MOUNTING SURFACE
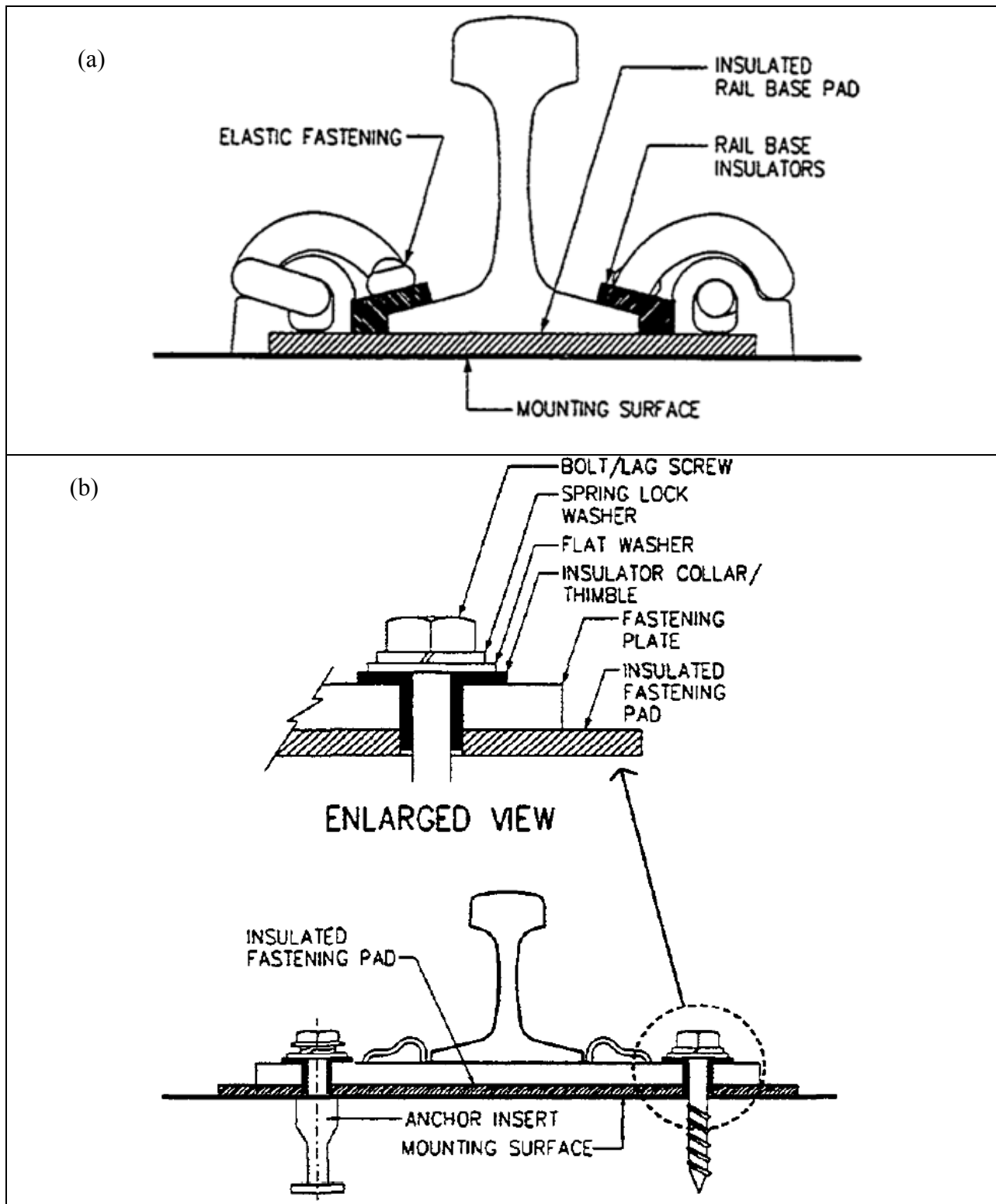
Figure 23. Examples of tracks insulating (a) insulation at the rail base and (b) isolation of the fastening or fastener base. For more information consult reference 16, Chapter 5.

39

7.1.1   Effect of Direct Current on Corrosion

A constant leak of current of one ampere (A) can corrode up to 20 pounds of iron per year (*16*). Therefore, an electric system where the return current can be as high as 750 A or higher, can result in damages of the rail of up to 15,000 lb or 7.5 tons of iron per year. Thus, it is important to prevent or eliminate stray currents by properly insulating the rails from the ground. (Proper insulation can be applied to new track when it is being built.)

In contrast, the use of sacrificial anodes can be useful, but most likely insufficient, when the return current from a train is present. Nonetheless, sacrificial anodes can help prevent natural corrosion (due to the environment) along the rails.

7.1.2   Effect of Improper Drainage on Corrosion

Maintaining good drainage is important in preventing corrosion. Most of the transit systems visited showed water leaks along their tunnels, and, in all cases, the water was pumped or directed to a channel located in the middle of the tracks. This resulted in an increase in humidity of the surroundings and in some cases caused wet tracks (including the concrete slab, ballast, ties, etc.). It is recommended to re-direct this water to an alternative path as far as possible from the electrified tracks. A good example was observed at the TTC-Toronto facilities where all ceiling leaks were re-directed by a drain-like system to a channel out of the tracks. The re-direction of the water will probably not solve the problem, but can potentially reduce the moisture on the track. Examples of wet track are shown in Figure 24.

Deposited salts on top of tracks are carried by the water leaks and the deposits are presumably formed due to water evaporation at locations where stray currents occur. This occurs because stray currents create an arc that probably evaporates the present water leaving dissolved salt deposits. This can compromise the track's insulation and lead inevitably a perfect location that sponsors corrosion due to the formation of a highly concentrated electrolyte. It is for this reason that eliminating the deposited salts from track is important; in fact, it is better to avoid them by installing welded jumper cables that can considerably reduce electrical resistance at this particular location.

40

(a)

(b)
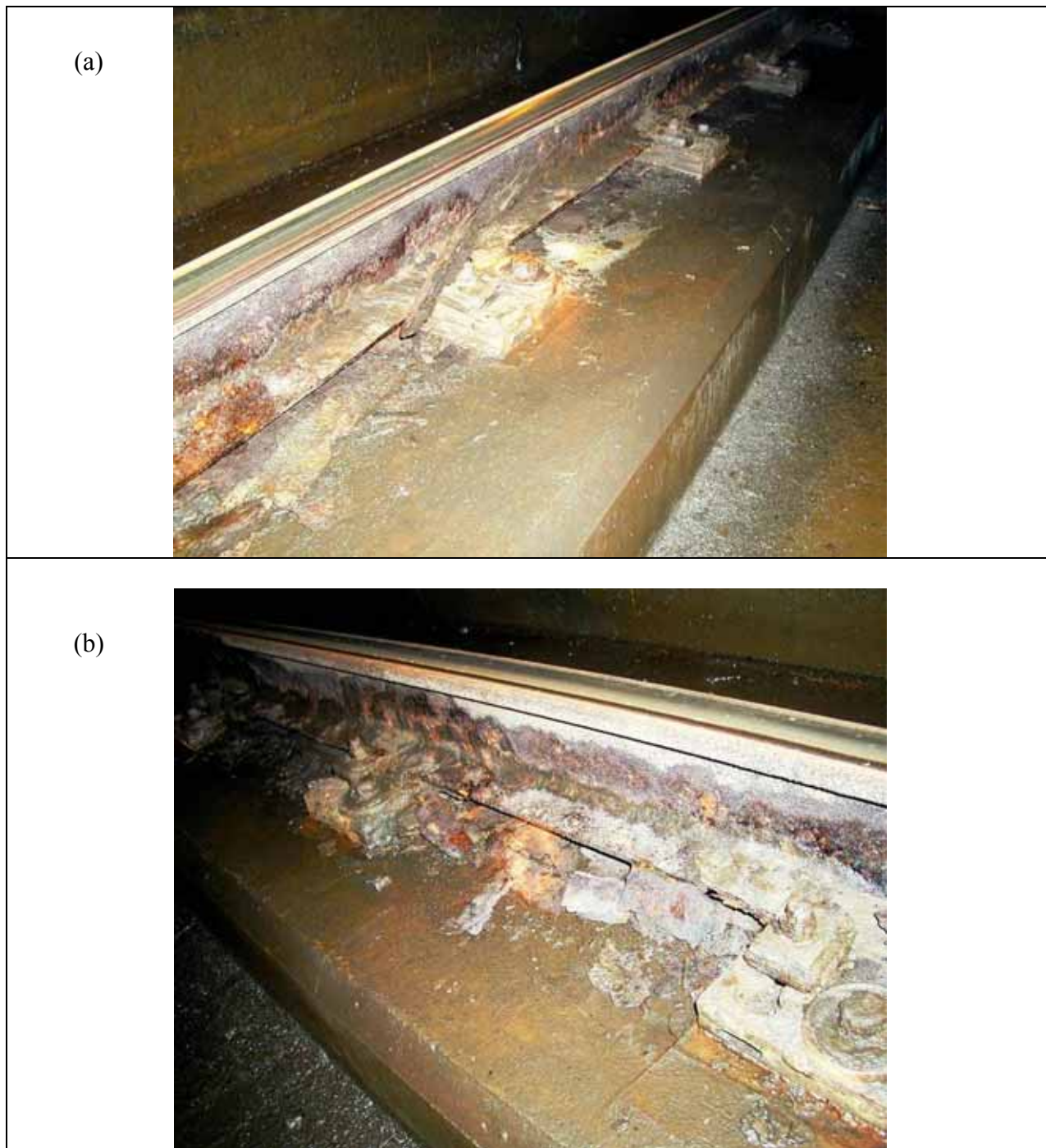
Figure 24. Wet tracks and detrimental corrosion effects on rails, fastening system, and tie plates. Notice the rust shells peeling out of the rail tracks.

41

7.2   Corrosion Detection

The best way to detect corrosion is by visual inspection. Expert track walkers can detect corrosion on exposed rail easier than on rail that is embedded. For instance, locations where there is homogeneous erosion, as Figure 8 shows, visual detection is easy. Locations where corrosion is hidden between the tie plate and the base of the rail make its detection more difficult until erosion forms on the rail flanges. However, these locations can be visually detected where salts are deposited on the track, particularly at the rails section seated above the tie plate and where iron like oxide powder is observed at the tie plate locations.

Once the presence of rail base, corrosion, salts, and/or iron like powder are detected along a track, it is suggested that the rail be scanned using non-destructive techniques. The research team scanned rails showing severe rail base corrosion using the samples presented in Figures 8 and 9. As a result, it was found that the practices to monitor rails with corrosion could be quite complicated. In contrast, it is suggested that each transit system should develop its own corrosion detection practice, which can be more precise and adequate for its own needs in accordance to the location, environment, and severity. In an effort to reliably scan rails, it was found that grease instead of couplant has some advantages. Chapter 6 provides potential techniques that can be considered to monitor rail base corrosion, particularly with a rail flaw detection vehicle.

42

CHAPTER 8: FUTURE RESEARCH

The research team suggests further research to investigate the use of plastic composite ties to insulate the rails from the ground. Plastic ties have the potential to prevent leaks of stray electric currents traveling from the rails to ground, thereby reducing rail base corrosion.

The research team has been evaluating the field performance of plastic ties from several manufacturers since 1997. The first group of ties that were installed in track has been subjected to more than 1 million MGT (million gross tons) of heavy axle load traffic at the Facility for Accelerated Service Testing. The majority of the plastic ties tested has the same dimensions and weigh about the same as typical hardwood ties. The in-track tests conducted at TTCI indicate their performance is generally comparable with wood ties although cracking and some fractures have been documented (*40, 41*).

More recently, during the summer of 2006, a laboratory test was conducted by TTCI to characterize the electrical resistance of plastic ties from three manufacturers. Figure 25 shows one of the plastic ties tested. The minimum allowable electrical impedance (resistance) of 20,000 ohms for concrete crossties, as specified in the AREMA Manual for Railway Engineering (18), was used as a baseline.

Since the plastic ties tested are almost impermeable on their exterior, the test was conducted on cross sectional slices to expose any internal porosity. The purpose of exposing the porosity was to simulate a worse case condition, where water entered the interior of the tie potentially increasing electrical conductivity. Figure 25 shows the internal porosity of one of the test samples and the seven locations where the electrical resistance was measured under dry and water-soaked conditions. Figure 26 shows that some of the measurements were taken using typical screw spikes and some were taken directly on the surface of the sample.

The electrical resistance of the tie samples was measured under dry conditions soon after they were cut from the three test ties and again after 3 weeks of total submersion in water. The results indicate that measurement location 1 (see Figure 26), screw spike to screw spike, provided the least resistance in all three tie types. The dry samples of the three tie types provided more resistance than the water soaked samples. The electrical resistance of tie type 1 at measurement location 1 was significantly lower than that of tie types 2 and 3 after being submerged in water for 3 weeks. However, at 65 k ohms, it was 3.25 times higher than the 20 k ohm minimum specified by AREMA. The remaining measurements ranged from 500 k ohms (25 times higher than the AREMA minimum) to over load indications on the ohmmeter.

The laboratory test results indicate that although the 3 tie types provided different levels of electrical resistance, those levels were well above the AREMA specification. The in-track performance of plastic composite ties under heavy axle loads has been documented. That and the result of the recent electrical resistance lab tests suggest that test plastic ties be tested on a transit system where rail base corrosion has been a problem.

Figure 25. One of the plastic composite ties used for the electrical resistance laboratory test at TTCI.
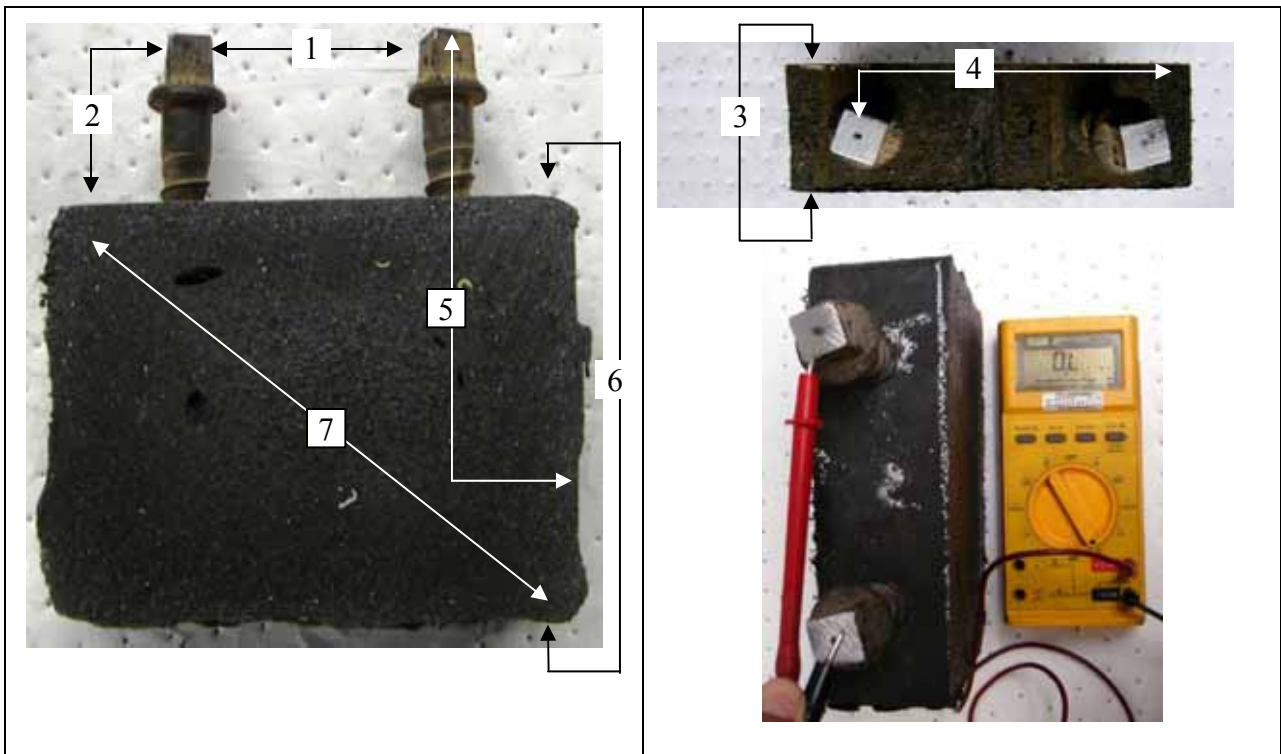
Figure 26. The electrical resistance measurements were taken at seven locations under dry and water-soaked conditions using a typical ohmmeter.

44

REFERENCES

1. Fontana, M. G and N. D. Greene. Corrosion Engineering, *Materials Science and Engineering Series*, McGraw-Hill, Second Edition, 1978, pp. 464.

2. Roberge, P.R.. *Handbook of Corrosion Engineering*, McGraw-Hill, 2000.

3. Wikipedia, The Free On-line Encyclopedia, as posted on July 24, 2006, http://en.wikipedia.org/wiki/Main_Page.

4. Stray Currents in Transit Systems, www.corrosion-doctors.org/StrayCurrent/Transit-Systems.htm, as posted on 07/21/06.

5. Parsons Brinckerhoff Quade & Douglas, Inc., *TCRP Report 57: Track Design Handbook for Light Rail Transit*, National Research Council, TRB, Washington, D.C., 2000.

6. CORPRO Canada Inc. (041212-102A), Corrosion protection Study, Edmonton Light Rail Train System, Stantec Consulting Ltd., Edmonton Alberta, 2005.

7. Personal communication with Mr. Brian Longson, Toronto Transit Commission, Toronto, ON Canada, March 3, 2006.

8. Personal communication with Mr. Antonio Cabrera, Director, Track Engineering, Metropolitan Transit Authority, New York City Transit, New York City, NY, February 28, 2006.

9. Personal communication with Mr. Glenn Pedersen, Sr. Engineer Track Cond. & Analysis, National Railroad Passenger Corp. – Amtrak New York, March 01-03, 2006.

10. Personal communication with Mr. Antony Bohara, Director, Engineering, SEPTA, Philadelphia, PA, February 27, 2006.

11. American Railway Engineering and Maintenance-of-the-Way Association (AREMA), *Manual for Railway Engineering*, Chapter 4, Rail Specifications 4-2-1, 2006.

12. G. E. Dieter, *Mechanical Metallurgy*, Second Edition, pp. 247-288, 1976.

13. Personal communication, Jim Stein, General Supervisor, Right-of-Way & Facilities, Edmonton Transit, February 13, 2006.

14. Personal communication, James D. Dwyer, Director Technical Support (Retired), Port Authority of Allegheny County, May 14, 2006.

15. Personal Communication (telephone) with Mr. Joseph Oriolo, Chief Engineer, May 15, 2006.

16. *TCRP Report 57: Track Design Handbook for Light Rail Transit*. Chapter 8: Corrosion Control, National Research Council, TRB, Washington, D.C., 1999.

17. Nestleroth, J. B. and T. A. Bunenik, "Magnetic Flux Leakage (MFL) Technology," The Gas Research Institute, United Stated National Technical Information Center, 1999.

18. AREMA, *Manual for Railway Engineering*, Volume 1, Article 1.9.1.14: Electrical Resistance Test, 2005.

19. *International Union of Railways*, UIC CODE 605 OR 2nd ed., pp. 11-81, Protection from Corrosion, Measures to Be Taken on Direct Current Catenaries to Reduce the Risk on Adjacent Piping and Cables Systems, Way and Work Committee, Paris, June 1980.

20. Baboian R. (Editor of the Section), *Corrosion Test and Standards*, Application and Interpretation, 2nd Edition, ASTM International, Section I: General Information, Edited by ASTM International, West Conshohocken, PA, 2005.

21. Hack H. P. (Editor of the Section), *Corrosion Test and Standards*, Application and Interpretation, 2nd Edition, ASTM International, Section III: Types of Test, Chapters 7, 9, 10, 12, 13 and 15, Edited by ASTM International, West Conshohocken, PA, 2005.

22. Scully, J. R. (Editor of the Section), *Corrosion Test and Standards*, Application and Interpretation, 2nd Edition, ASTM International, Section IV: Testing for Corrosion Types, Chapters 17, 18, 20, 23, 25-27, Edited by ASTM International, West Conshohocken, PA, 2005.

23. Hack H. P. (Editor of the Section), *Corrosion Test and Standards*, Application and Interpretation, 2nd Edition, ASTM International, Section V: Testing in Environments, Chapters 29-34 and 41, Edited by ASTM International, West Conshohocken, PA, 2005.

24. Hibner E. L. (Editor of the Section), *Corrosion Test and Standards*, Application and Interpretation, 2nd Edition, ASTM International, Section VI: Materials Testing, Chapters 48, 56-57, 59, Edited by ASTM International, West Conshohocken, PA, 2005.

25. Dean, S. W., Jr. (Editor of the Section), *Corrosion Test and Standards*, Application and Interpretation, 2nd Edition, ASTM International, Section VII: Testing in Industries, Chapters 64, 68, 73-74 and 78, Edited by ASTM International, West Conshohocken, PA, 2005.

26. ASTM Standards International, *Standard Guide for Estimating the Atmospheric Corrosion Resistance of Low-Alloy Steels*, Designation: G 101-04, West Conshohocken, PA.

27. ASTM Standards International, *Standard Guide for Examination and Evaluation of Pitting Corrosion*, Designation: G 46-94, (Re-approved 1999) West Conshohocken, PA.

28. ASTM Standards International, *Standard Guide for Corrosion-Related Failure Analysis*, Designation: G 161-00, West Conshohocken, PA.

29. ASTM Standards International, *Standard Guide for Conducting and Evaluating Galvanic Corrosion Tests in Electrolytes*, Designation: G 71-81 (Re-approved 2003), West Conshohocken, PA.

30. ASTM Standards International, *Standard Guide for Determining Rail-to-Earth Resistance*, Designation: G 165-99, West Conshohocken, PA.

31. NACE International, The Corrosion Society, NACE Standard, RP0193-2001, Item No. 2106, *External Cathodic Protection On-Grade Carbon Steel Storage Tank Bottoms*, Houston, TX, approved October 1993, revised 2001.

32. NACE International, The Corrosion Society, NACE Standard, RP0387-99, Item No. 21036, "Standard Recommended Practice: Metallurgical and Inspection Requirements for Cast Galvanic Anodes for Offshore Applications," Tank Bottoms, Houston, TX, approved October 1987, revised 1999.

33. NACE International, The Corrosion Society, NACE Standard, RP0285-2002, Item No. 21030, "Standard Recommended Practice: Corrosion Control of Underground Storage Tank Systems by Cathodic Protection," Tank Bottoms, Houston, TX, approved October 1987, revised 2002.

34. NACE International, The Corrosion Society, NACE Standard, RP0286-2002, Item No. 21032, "Standard Recommended Practice: Electrical Isolation of Cathodically Protected Pipelines," Tank Bottoms, Houston, TX, approved October 1987, revised 2002.

35. NACE International, The Corrosion Society, NACE Standard, RP0284-2003, Item No. 21215, "Standard Recommended Practice: Evaluation of Pipeline and Pressure Vessel Steels for Resistance to Hydrogen-Induced Cracking," Tank Bottoms, Houston, TX, approved October 1984, revised 2003.

36. http://www.trainweb.org/elso/SPERRY.HTM

37. Garcia, G. and R. Reiff, "Test and Evaluation of Rail Flaw Detection Technologies," Research Report No. R-934, Association of American Railroads, Transportation Technology Center, Pueblo, CO, August 1999.

38. Bar-Cohen, Yoseph, Emerging NDE Technologies and Challenges at the Beginning of the 3rd Millennium - Part I, Jet Propulsion Laboratory, Caltech, Vol. 1, No. 5, January 2000, available at http://www.ndt.net/article/v05n01/barcohen/barcohen.htm (08/28/06).

39. http://www.intelligendt.de/en/PortalData/1/Resources//07_Druckschriften/Dokumente/the_phased-array_principle.pdf#search=%22phase%20array%20ut%20systems%22.

40. Jimenez, Rafael and Dave Davis. "In-Track Performance of Plastic Composite Ties under Heavy Axle Loads at FAST, *Technology Digest*, No. TD-06-015, Association of American Railroads, Transportation Technology Center, Pueblo, CO, June 2006.

41. Jimenez, Rafael, Dave Davis, and Joseph LoPresti. "Progress Report: In-track Performance of Plastic Composite Ties at FAST," *Technology Digest* No. TD-02-004, Association of American Railroads, Transportation Technology Center, Pueblo, CO, 2002.

APPENDIX A

TRANSIT COOPERATIVE RESEARCH PROGRAM

RAIL BASE CORROSION STUDY

QUESTIONNAIRE

1. TRANSIT AUTHORITY

Date: _____

Transit Authority: _____

_____

Name: _____

Title: _____

Address: _____

_____

_____

Telephone: _____

Fax: _____

Email: _____

If selected, are you willing to participate for a site visit? If so, please indicate your most convenient date between the proposed dates.

O   February 6 – 10, 2006.   Specific date _____
O   February 11 – 17, 2006.   Specific date _____
O   Other, Indicate _____

A-1

1. TRACK & OPERATING DATA

Do you have rails with corrosion at the base available for this study? Are you willing to provide and ship them to TTC for the present research investigation? If so, how many pieces/sections?

_____

_____

Rail: Size, geometry, manufacturer (including chemistry and heat treatment (if available)):

_____

_____

_____

Likely location of corrosion occurrence:

O   At the tie   O   High rail   O   Low Rail

O   At the tunnels   O   On the curves   O   Tangent sections

O   Joints   O   Distance from the tie _____

O   Other (please specify) _____

What is the severity of the problem based on previous analysis of failure, statistics, laboratory analysis, field results, numerical simulations, etc. The submission of an attached or electronic copy of any of the previously mentioned studies would be beneficial for the present research.

_____

_____

_____

Occurrence of corrosion based on weather and environmental conditions particularly where failures due to corrosion have been reported:

_____

_____

_____

Approximate Number and Type of reported corrosion locations within the track/month/year:

_____

_____

_____

Maintenance & Operations:

Wheel Load:_____

Data of Strain history (i.e., S-N curves):_____

Corrosion Rate and History:_____

Type of Tie:_____

Traffic Density (Annual MGT):_____

Maximum Operating Speed:_____

Third Rail/Overhead Catenary:_____

Rail Defect Detection Frequency:_____

Track Ownership:_____

Maintenance Responsibility:_____

Light Rail/Heavy Rail Transit:_____

Electric Current (Intensity) and Type Passing through the Rail(s):_____

Joint Use:_____

A-3

3. RAIL BASE CORROSION – CONDITIONS AND DESCRIPTION

Description of current corrosion occurrence and the possible factor(s) that contribute to corrosion at the base of the rail including details such as type of fastenings and anchors and their effect on corrosion; effect of any kind of welded/bolted sections or devices to the rail, rail base surface preparation, any record of corrosion in regions that were preheat/post heat treated after welding or any other reasons, allowable temperature range (ambient/rail), characteristics of the corroded affected zone, inspection and quality control requirements:

A-4

4. RAIL BASE CORROSION – PROBLEMS & SAFETY CONCERNS

Description of rail base corrosion problems and safety concerns. If rail failures have occurred include information as to the location, position, type and number for both detected internal defects and broken rail:

_____

_____

_____

_____

_____

_____

_____

_____

_____

_____

_____

_____

_____

_____

_____

Note: Please provide information as to the availability of rail failure samples that may be used for metallurgical analysis and/or previous analysis (provide photographs if available).

_____

_____

_____

A-5

5. ALTERNATIVE RAIL BASE CORROSION PREVENTION

Description of alternative procedures now in use to detect/prevent corrosion particularly at the base of the rail, together with any problems and safety concerns. Details including corrosion type and size, position on rail, rail surface (at the base) conditions and any mechanical damage of the rail, allowable temperature range, inspection and quality control requirements (provide photographs if available):

6. ADDITIONAL COMMENTS

APPENDIX B

List of all the transit authorities and personnel contacted for the survey as well as a brief description of the responses from the various transit authorities.

	Transit Agency	Contact	Comments
1	New York City Transit	General Superintendent Maintenance	
	New York City Transit	Track Engineering	Positive response and provided all the facilities and commodities for the site-visit
	New York City Transit	Assistant Chief Electrical Officer, TRO	at the MTA New York City Transit tunnels in Manhattan and Bronx, NY.
2	Southern California Regional Rail Authority (SCRRA)	Director of Engineering & Construction	Positive response answered and submitted the survey.
3	Port Authority of New York and New Jersey	Chief Maintenance Supervisor	Positive response and provided all the facilities for the TTCI personnel to visit the New Jersey (PATH) transit.
4	Director Rail Systems	St. Louis Metro Transit	Contacted and provided the info from Mr. Paul G.
	Track Chief Engineer	St. Louis Metro Transit	Positive response and provided their facilities for the TTCI personnel site-visit. They contributed with the survey. Unfortunately, due to time constrains TTCI was not able to visit their facilities.
5	Dallas Area Rapid Transit	Sr. Manager Signal Systems	They provided the information from Mr. Darvin Kelly, Sr. Mgr. Track & Right of Way, who submitted the survey to TTCI.
	Dallas Area Rapid Transit	Signal Supervisor	
	Dallas Area Rapid Transit	Supervisor Track & Right of Way	
6	New Jersey Transit Corporation	Deputy General Manager - Infrastructure Engineering	They provided the information from Mr. Stelian Canjea, P.E.; Light Rail Program Manager, who responded the survey.
	New Jersey Transit Corporation	Engineer-Signal Design & Planning	
	New Jersey Transit Corporation	Chief Engineer Track	
7	Edmonton Transit	General Supervisor Right of Way and Facilities	Positive response and provided the survey as well as a comprehensive report of failures in the Edmonton's Transit detailing the reasons for corrosion together with the failure analysis.
	Edmonton Transit	Power & Signals Engineer	
8	Calgary Transit	Manager Light Rail & Facilities	At the time Calgary officials were contacted, they responded that they had no corrosion on their tracks.
	Calgary Transit	Coordinator LRT Signals/ Trac Pwr.	
9	Southeastern Pennsylvania Transportation Authority	Chief Railroad Operations Off	
	Southeastern Pennsylvania Transportation Authority	Manager Track Design & Engineering	Positive response and provided the opportunity to tour their facilities as well as several discussions over the phone and in person.
10	The Toronto Transit Commission	Superintendent-Subway/SRT Track Superintendent-Track Maintenance	Positive response and provided the opportunity to tour the TTC-Toronto facilities. Also sent the survey and on more than one occasion, held telephone and personal discussions.
11	Amtrak	Deputy Chief Engineer Maintenance	Provided the information from Mr. Glenn H. Pedersen; Sr. Engineer Track Cond. & Analysis, Mr. Walt Heide; Deputy Chief Engineer and Mr. John A. Pielli; Director Track Maintenance & Compliance. They permitted the TTCI personnel to tour their
	Amtrak	Manager Maintenance of Way	
	Amtrak	Director C&S	

			facilities in their tunnels in New York and Baltimore and provided 10 sections of rails showing failures due to corrosion and their survey.
12	Sistema de Transporte Colectivo Metro (STCM) and Tren Ligero Mexico City	Sub head of operations & infrastructure	Positive response and provided the opportunity to tour their facilities as well as several discussions with their maintenance and submitted the survey.

APPENDIX C

Transit Authority: Port Authority Trans-Hudson Corporation
Response Received: 01/10/06
Contact: Steven Abramopaulos, Chief Maintenance Supervisor Track
                                 (201) 216-7200

SUMMARY

The Port Authority Trans-Hudson (PATH) Corporation operates a 50-track mile, 600-V DC third rail traction, passenger transit system. Rail includes 100-lb RB Beth welded and/or bolted. The following table summarizes the operating and inspection conditions used by the PATH:

Maximum operating speed	60 mph
Wheel load	10,000 lb
Frequency of the rail breaks due to rail base corrosion	Eight annually
Rail defect detection frequency	Twice per year
Type of ties	Wood and concrete ballast
Power Source	Third rail

It has been reported that severe corrosion occurs at various locations for the PATH. The New Jersey transit location experiences a significantly high incident of corrosion because of the tunnel locations. In the tunnels, there are locations where the humidity/water has been identified. In general the corrosion locations are identified in sections with leaks. Over the last few years several locations with corrosion were found, but, on average, eight of these locations caused rail breaks. It has been determined that the major contributor to rail base corrosion is the negative return current that is grounded through the rail. The following photos show samples collected from the PATH line exhibiting severe rail base corrosion.

C-1
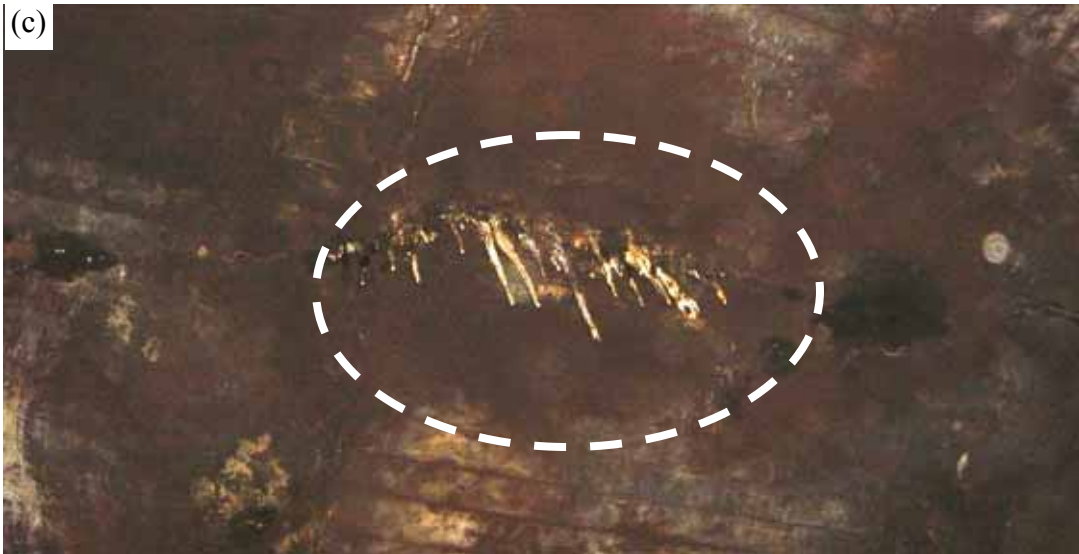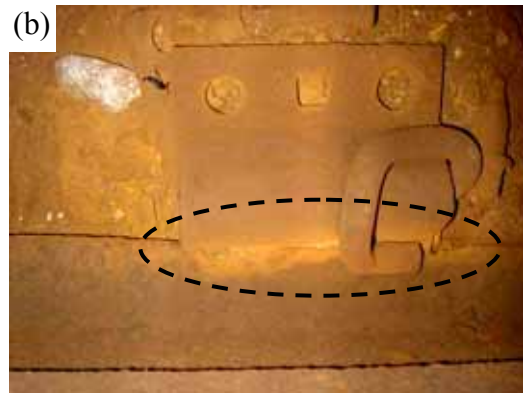
PATH Transit System showing (a, b) rail corrosion, (c) ice spikes from sealant used to prevent water leaks in the tunnel, and (d) salts deposited along the tracks. Note: The site visit was conducted during January 2006 and due to the weather conditions in New York and New Jersey, the water leaks froze forming the ice spikes shown in photo (c).

C-2

Transit Authority: Toronto Transit Commission
Response Received: 01/25/06
Contact: Brian H. Longson, Superintendent – Maintenance
                     Engineering Track & Structure Department
                     1138 Bathurst Street
                     Toronto, Ontario M5R 3H2
                     (416) 393-4419

SUMMARY

Toronto Transit Commission (TTC) operates a 42.5-track mile, 600-V DC. Negative returns carry a 500 A at a potential of no more than 30 V above ground. In addition, the other rail carries the signal circuit which is less than 1 amp current and > 10 volts. Their rail facilities are integrated by both, Sysco Standard Carbon (100 lb ARA-A) and 115-lb RE, rails, with nominal rail hardness of 300 Brinell and the tracks are usually flash welded.

TTC reported between ½ and 1 corrosion defect/mile/year or between 30 and 60 defects require removal annually with the majority of these defects being in the same location. This transit system consists of a direct fixation line with a heavy transit with a yearly traffic of 25 million gross tones (metric) per year. TTC maintenance is conducted manually in-house when the facilities are closed at night to the public.

The rail base corrosion occurs due to electrolysis caused by DC at the contact point with wet debris (mud, slime) building up under the rail base. Stress corrosion cracking is evident and is suspected to result from sulfide corrosive environments often caused by tunnel leakage. These may develop sharp, vertical fissures in the base/web region, which are very difficult to detect.

Detection is accomplished primarily by a NDT crew. In addition to declaring rail defective and requiring replacement, the NDT crew notifies the maintenance crew to clean rail base/seal leaks within a specified timeframe; otherwise rail is re-inspected and replaced. Prevention is mainly accomplished by ensuring rail fastening system insulation is functioning and via leakage sealing of tunnels. The following table summarizes the operating and inspection conditions regularly used by TTC-Toronto:

Maximum Operating Speed	50 mph
Wheel Load	7.5 ton/wheel
Frequency of the Rail Breaks due to Rail Base Corrosion	Between ½ and 1 corrosion defect/mile/year or between 30 and 60 defects requiring removal annually.
Rail Defect Detection Frequency	In-house and on daily basis.
Type of Ties	Direct fixation to invert and large block (double) concrete ties
Power Source	Third rail

The following photos show samples collected from the TTC-Toronto line and exhibiting severe rail base corrosion.

TTC-Toronto tracks showing deposited salts and resulting corrosion.

Organization: National Railroad Passenger Corporation — New York
Response Received: 02/03/06
Contact: Walt Heide, Deputy Chief Engineer – Track
                    John A. Pielli, Director Track Maintenance & Compliance
                    Glenn H. Pedersen, Sr. Engineer Track Cond. & Analysis
                    (215) 349-3139 or 1179

SUMMARY

The National Railroad Passenger Corporation (Amtrak) system carries both freight and Amtrak trains. There are two types of passenger trains: Acela and regular passenger trains. The Acela has a wheel load of 16-25½ tons per car. Both types of power are used: AC (overhead catenary) and DC (third rail).

Wood ties, direct fixation and embedded tracks are used by Amtrak. Rail life is ~4.5 years due to the excessive corrosion in the system. Although the ~4.5 year life is average, there are some sections of rail that are replaced yearly. The corrosion at the base of the rail is extended in almost all areas of the track including, tie plates, tunnels, curves, tangents, joints, and high and low rail. Yearly traffic running through the seven tunnels in New York is conservatively 200 MGT, and the maximum operating speed is 60 mph. Amtrak conducts its own maintenance and track inspection, with the following regularly performed practices:

- Internal inspection twice yearly
- Bi-annual dedicated detailed base corroded rail walking inspection
- Twice weekly walked daily track inspection

The tracks are owned by Amtrak, with dedicated routes for the Long Island Rail Road and New Jersey Transit. Amtrak-NY consists of a heavy rail transit system using 136 lb RE rail. The electric currents passing through the rail are AC traction return with a frequency of 25 Hz and 650 V. Additionally, there is a DC traction return with 91 2/3 Hz signal. The temperature in the tunnels varies between 20 and 80 degrees Fahrenheit within a 1,000-foot section, and inside the tunnel the temperature ranges from 35 to 75 degrees Fahrenheit.

There is no rail preparation prior to its installation on tracks. The typical corrosion occurs at the base and works its way up toward the web. It may cause a "hollowing-out effect" or gradually thin out the base until the edge is razor sharp. The major factors that contribute to corrosion for Amtrak are

- Moisture in a confined space,
- Competing fields of electricity, AC, DC, and uncontrolled stray currents,
- Impedance bonds and cab signal assets,
- AC power returns to substation through neutral leads in rail from impedance bond cut section, and
- Original tunnel design included a sacrificial bank of lead in the bench wall, which is no longer connected.

The following photos show corroded rail on the south tunnel in New York City.

Amtrak tracks showing flooded tracks and pumping system used to remove water from the track.

Organization:　　　National Railroad Passenger Corporation — Baltimore

Response Received:　02/03/06
Contact:　　　　　　Walt Heide, Deputy Chief Engineer – Track
　　　　　　　　　　John A. Pielli, Director Track Maintenance & Compliance
　　　　　　　　　　Glenn H. Pedersen, Sr. Engineer Track Cond. & Analysis
　　　　　　　　　　(215) 349-3139 or 1179

SUMMARY

The National Railroad Passenger Corporation (Amtrak) system carries freight, Amtrak, and commuter trains. Amtrak passenger trains have 25.6 gross tons for passengers and 37 gross tons for freight cars. Power types used are overhead catenary (AC) and DC light rail nearby. The system is composed of wood ties encased in concrete due to the excessive corrosion in the system. Rail life is ~4.5 years. The yearly traffic running through two tunnels in Baltimore is ~ 25 MGT, and the maximum operating speed is 30 mph. Amtrak conducts its own maintenance and track inspection, with the following regularly performed practices:

- Internal inspection twice yearly
- Bi-Annual dedicated detailed base corroded rail walking inspection
- Twice weekly walked daily track inspection

The Baltimore tunnel is owned by Amtrak and utilizes 136-lb RE rail. Electric currents passing through the rail are 25 Hz AC traction return and 100 Hz signal. Temperatures in the tunnels vary from 20 to 80 degrees Fahrenheit within a 1,000-foot section. Inside the tunnel, temperatures range from 35 to 75 degrees Fahrenheit.

No rail preparation is made prior to installation on tracks. The typical corrosion occurs at the base and works its way up toward the web. It may cause a "hollowing-out effect" or gradually thin out the base until the edge is razor sharp. Major factors contributing to corrosion for Amtrak are

- Moisture in a confined space.
- Competing fields of electricity, AC, DC, and uncontrolled stray currents.
- Impedance bonds and cab signal assets.
- AC power returns to substation through neutral leads in rail from impedance bond cut section.
- Disconnect of neutral through the tunnel. There is a neutral area with a ground at Weehawken and at MP 3 for the 2 North River tunnels.
- Original tunnel design included a sacrificial bank of lead in the bench wall, which is no longer connected.

The following photos are examples of corrosion occurring in the Baltimore station tunnels.

C-7

Rail donated by Amtrak (Baltimore) and a location on the tracks showing severe corrosion.

Transit Authority: Port Authority of Allegheny County
Response Received: 06/22/06
Contact: James D. Dwyer, Director Technical Support (Retired)
                      Jimdwyer@nauticom.net

SUMMARY

The Port Authority of Allegheny County (PAAC) system is a 40-track-mile system. Energy is supplied by an overhead catenary system using a 660 V DC system. The track is made of 115-lb RE standard carbon rail.

The rail used by this transit agency is embedded in the concrete roadway slab without insulation or corrosion protection. The corrosion is usually located at the railroad crossings. At this time, this transit authority has no reports of rail failure due to rail base corrosion. Average rail life is between 10 and 15 years. Track condition is not optimum. However, no safety problems have been reported.

Currently a new method for rail installation is used. This method consists of embedded rail that is cast in an elastomer (Icoset) that totally seals the rail, which means the rail is encapsulated. The Icoset is poured into a slot located in the concrete slab. No ties are used on the slabs, which are between 10 and 12 feet long. Slab and rail are installed according to procedures described in *TCRP Report 71*, "Track-Related Research, Volume 6, Direct-Fixation Track Design Specifications, Research, and Related Material, Part A: Direct-Fixation Track Design and Example Specification," which is used by different transit agencies. The track is owned by the Port Authority of Allegheny County, which is also responsible for its maintenance. The track is inspected weekly by track inspectors, and ultrasonic testing is conducted yearly.

The following table summarizes the operating and inspection conditions used by Port Authority of Allegheny County light rail cars:

Maximum Operating Speed	10 mph thru ungated rail crossings
Wheel Load	12 to 14 tones
Frequency of the Rail Breaks due to Rail Base Corrosion	None reported
Rail Defect Detection Frequency	Once yearly
Type of Ties	Concrete, direct fixation
Power Source	Overhead catenary

The following photo, donated by the Port Authority of Allegheny County, is an example of rail corrosion at the base of a rail.

Rail donated by PAAC showing severe corrosion at the base.

Transit Authority: Metropolitan Transit Authority, New York City Transit
Response Received: 07/12/06
Contact: Antonio Cabrera. P.E.; Director, Track Engineering
                       130 Livingston St, Room 8028, Brooklyn, NY 11201

SUMMARY

The Metropolitan Transit Authority-New York City Transit (MTA-NYCT) system consists of a heavy rail rapid transit system. NYCT is the largest agency in the MTA regional transportation network. It has the fourth largest subway car fleet in the world. The MTA-NYCT network has approximately 660 miles of passenger service track and 180 miles of nonrevenue service track (e.g., in subway yards). Energy is supplied by a third rail system using a 600 V DC. The track uses 100-lb ARA-B, OH, FT, HH standard carbon rail. Recently, the MTA-NYCT began changing track from 100 lb to 115-lb AREMA rail. Currently, the rail in open areas and some of the tunnels is 115 lb. However, in some locations the transition from 100-lb rail to 115-lb rail is ongoing.

The corrosion of the rail base has been observed in several locations, including tunnels, curves, tangent sections, joints, high rail, and low rail. The corrosion of the rails was identified mainly in the tunnels. This corrosion is presumably promoted by the leaks of water coming from the city's drainage system. In most cases, the corrosion starts at the base of the rail, but in some cases also affects the web of the rail. Contrary to other transit systems, the corrosion at the MTA-NYCT is independent of the weather; that is, the addition of salt to melt the snow during the winter has a negligible effect on the corrosion of the rails. The reports of corrosion indicate that several dozen locations are identified with corrosion and rail breaks per year. In 2005, 121 rail breaks were reported in the MTA-NYCT system, and 20 of them were rail base corrosion related. As of February 28, 2006, the number of rail breaks in the system was 24, and only 4 were due to corrosion.

MTA owns and maintains the track on the MTA-NYCT line. Rail defect detection is conducted up to six times per year. The return current is directed to the rail (600 V DC). There is also a superimposed AC for the signal circuits (7-10 V, 60 Hz).

The following table summarizes the operating and inspection conditions regularly used by MTA-NYCT.

Maximum Operating Speed	50 mph
Wheel Load	Max. 16,250 lbf, static
Frequency of the Rail Breaks due to Rail Base Corrosion	12% of the rail breaks in 2006 were due to corrosion
Rail Defect Detection Frequency	Up to 6 times per year
Type of Ties	Wood (oak) blocks embedded in concrete
Power Source	Third rail

MTA-NYCT tunnels showing severe water leakage from the walls, severe humidity under the tracks, and erosion of the rail base.

Transit Authority: Sistema de Transporte Colectivo Metro and Tren Ligero Mexico City

Response Received: 01/31/2006

Contact: Luis Canut Abarca, P.E., Subhead of Operations & Infrastructure
+(5255) 5627-4773

SUMMARY

The Sistema de Transporte Colectivo Metro (STCM) operates two transit systems: (1) conventional light rail and (2) the Metro with trains running on a concrete guideway. Rubber tires are guided on the concrete guideway with steel rails used for emergencies; that is, when tires fail. The tracks for light rail are composed of 115-lb RE rail. The STCM uses concrete ties in tangents and curves with curvatures of less than 6 degrees. Wood ties are used elsewhere, with direct fixation. The STCM does not report significant corrosion on the rails. In addition, the humidity in the environment is not as high as in the eastern USA, Canada, or Mexico. The 95% + of the light rail tracks are open air with just a small tunnel at the end of the system. In contrast, 70 percent of the Metro is a subway (tunnel) system. However, there is not as much water or brine leakage to the tracks (rails). The Metro operates with a third rail system; the light rail system uses an overhead catenary. The maximum speed for both systems is 56 mph. The power source consists of a DC system of 750 V. A wheel load of 8 metric tons per axle is used for both the Metro and light rail system for a combined total of 20 MGT of traffic per year (metric tones). The tracks are owned by the STCM. A monthly rail flaw inspection is conducted by STCM for the 34 miles of the tracks.

In the past, some rail base corrosion was reported that was due to small leaks throughout the subway stations. Improper disposal of cleaning materials (containing NH_4OH and/or $NaOH$), commonly used at every station, also caused corrosion. This occurrence was remedied by proper materials/waste disposal practices. Also, some electro-erosion in isolating joints was detected. This vibrating causing erosion provokes, impacts, and unstabilizes joints.

Transit Authority: Dallas Area Rapid Transit

Response Received: 12/29/05
Contact: Darvin Kelly, Sr. Mgr. Track & Right of Way
                      Dallas, TX 75266-7285
                      P.O. Box 660163
                      (214) 928-6239

SUMMARY

Dallas Area Rapid Transit (DART) operates at 750-Volt DC. Rail used is 115-lb RE, AREMA Spec from various manufacturers. The environment is dry. Therefore minimal rail base corrosion is detected, reported, or observed. DART is a light rail system, and rail defect detection is conducted twice yearly. The track is owned and maintained by DART. The electrical system consists of an overhead catenary. The following table summarizes the operating and inspection conditions regularly used by DART.

Maximum Operating Speed	65 mph
Wheel Load	20 ton/wheel
Frequency of the Rail Breaks due to Rail Base Corrosion	None
Rail Defect Detection Frequency	Twice per year
Type of Ties	Concrete ties
Power Source	Overhead catenary

Transit Authority: Tri County Metropolitan Transportation District
Response Received: 01/10/05
Contact: Kai Looijenga, Engineer III - Systems
                         710 NE Holladay St
                         Portland, OR 97232
                         (503) 962-2175

SUMMARY

Tri County Metropolitan Transportation District (TRIMET) operates a light rail system using an overhead catenary power supply that has a maximum current of 750 V DC. The rail used is open track — 115-lb RE, control cooled carbon steel rail manufactured in accordance with AREMA specifications. The tracks for TRIMET are paved track — R159 girder rail, manufactured in accordance with ASTM designation A2, Class B.

There are some locations where corrosion was detected at the web and base of the rail. These locations are at the tie and at the road crossing panels. However, the detected corrosion levels have been of an insufficient magnitude to warrant repair or replacement of the rail. To date, no failures from corrosion have been detected. The estimated traffic for the TRIMET light rail system is approximately 13.5 MGT. The tracks are owned and maintained by TRIMET. Track is inspected using ultrasonics every two years.

Corrosion of the rail occurs mostly at the transition from ballasted track to road crossing panels due to debris build-up. TRIMET also detected corrosion of the web and base of rail on a section of track through a road crossing. This corrosion was caused mostly by current exchange from rail to earth due to incorrect installation of the insulating boot. The crossing was identified as having insufficient insulation from rail to ground during regularly scheduled testing of the cathodic protection levels on a waterline under it. In ballasted track sections with wood ties, corrosion is limited to the spikes. The concrete embedded tracks have no access for corrosion inspection. Therefore, they have not been inspected. Nonetheless, a combination of rail-to-earth potential and earth gradient measurements are conducted and used as an indicator of the level of insulation for the embedded track areas.

The following table summarizes the operating and inspection conditions regularly used by TRIMET.

Maximum Operating Speed	55 mph
Wheel Load	9324 lbs/wheel
Frequency of the Rail Breaks due to Rail Base Corrosion	Insufficient data
Rail Defect Detection Frequency	Ultrasound inspection for cracks every 2 years
Type of Ties	Mix: wood, concrete, embedded track
Power Source	Overhead catenary

Transit Authority: Southeastern Pennsylvania Transportation Authority (SEPTA)
Response Received: 07/14/06
Contact: Anthony Bohara
Director of Engineering
1234 Market St.
Philadelphia, PA 90017
(215) 580-82780

SUMMARY

SEPTA is a light and heavy rail transit system. The systems run between 2 and 3 MGT per year on 100-lb RB and 115-lb RE rail. Usually, the corrosion is observed at the ties in the tunnels. One of the major issues with corrosion is the low corrosion rate, which lowers attention toward corrective actions and in one case up to 100 spots with corrosion were found in a single location. The tracks are ultrasonically inspected on a yearly basis and visual inspection is usually conducted twice a week. The power is supplied using third rail and overhead catenary and is a DC current of 600V. The tracks are owned by SEPTA and SEPTA also conducts the maintenance.

The corrosion is usually detected in the locations where water is present. Usually, the corrosion goes from the base to the web of the rail. In general the fastening system is severely affected. SEPTA has reported rail failures due to corrosion; typically, rail fastener/fixation is destroyed as well as rail. Unfortunately, most of the rail base corrosion is not easy to identify using ultrasonic rail inspection methods. SEPTA has found that insulated anchors and insulation of rails on direct fixation tracks help reduce corrosion. In addition, SEPTA tries to control water leaks to reduce the humidity, thus corrosion media.

The following table summarizes the operating and inspection conditions regularly used by SEPTA.

Maximum Operating Speed	Light rail (50 mph) and heavy rail (70 mph)
Wheel Load	15 ton
Frequency of the Rail Breaks due to Rail Base Corrosion	Non reported
Rail Defect Detection Frequency	Ultrasound inspection once a year - 2 times per week visual
Type of Ties	Wood
Power Source	Conventional DC circuit only (third rail and overhead catenary)

C-16
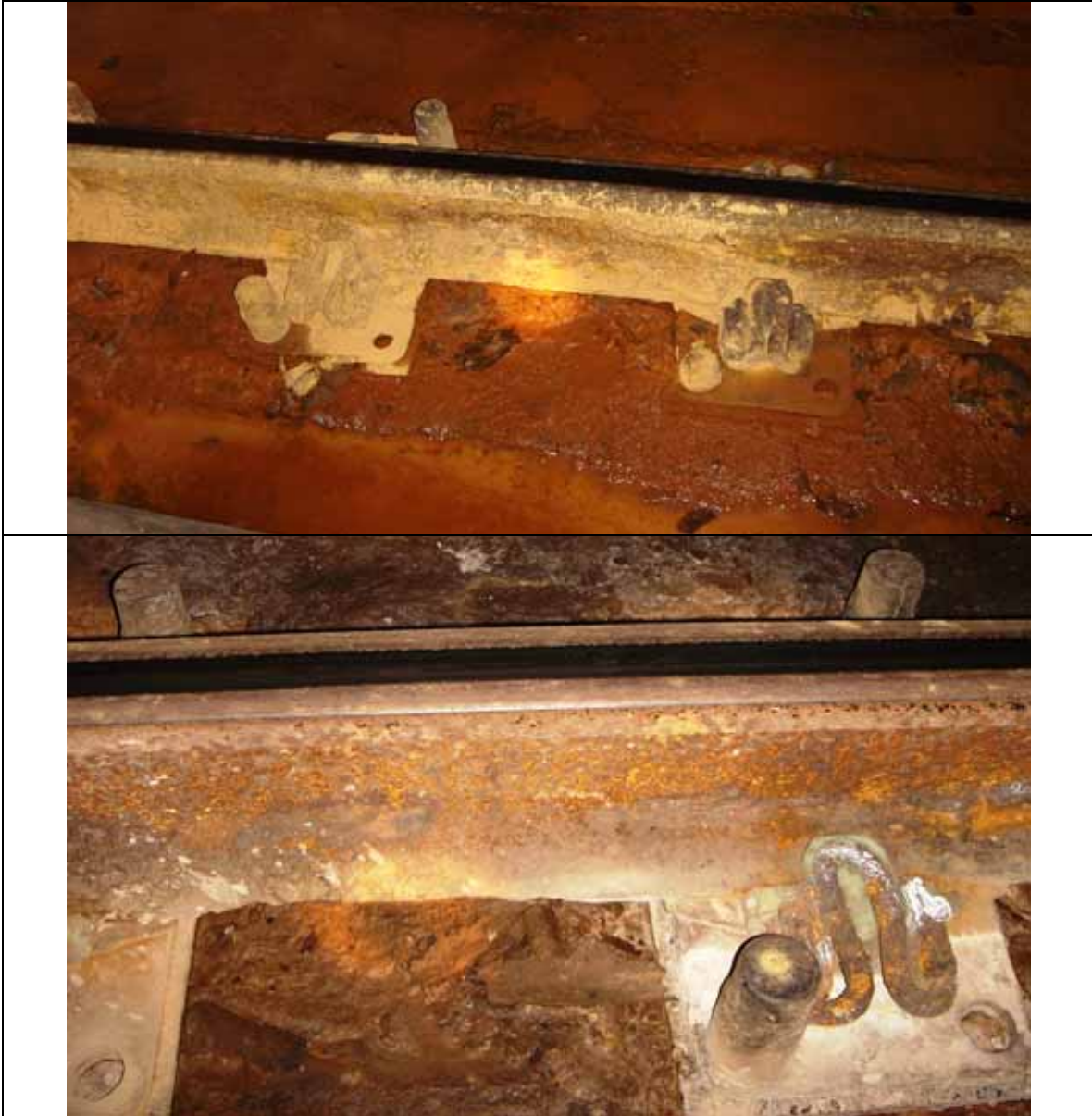
Light rail SEPTA tunnels showing severe corrosion.

Transit Authority: Southern California Regional Rail Authority
                                    Commuter rail with freight and Amtrak trains
Response Received: 12/28/06
Contact: Michael E. McGinley,
                                    Director of Engineering and Construction
                                    700 So. Flower St., Suite 2600
                                    Los Angeles, CA 90017
                                    (213) 452-0250

SUMMARY

The Southern California Regional Rail Authority (SCRRA) system carries commuter, freight, and Amtrak trains. The power supply is conventional DC track circuits only. The rail is 136-lb CF&I CC, some from 1973 and 1983. The rail is almost all tangent, placed on wood ties in crushed rock ballast on a native sandstone tunnel floor. The corrosion at the base of the rail occurs in water flooded locations; some of the rails have lost of up to 1/8"of the base. All observed corrosion has been at the rail base/tie plate interface in wet conditions. These are 14" AREA tie plates on wood ties with cut spike fasteners. Anti-creeper anchor boxes are located on every other tie. The temperature in the longest tunnels is ~50°F during the winter and ~70°F during the summer. In the shorter tunnels temperatures range between 40 and 90°F.

The estimated traffic for the SCRRA tracks is approximately 15 MGT for the light rail. The tracks are owned by SCRRA, and Herzog was hired to conduct maintenance. The tracks are inspected using ultrasonic techniques every two years. The corrosion detection operation is conducted every 120 days.

To date, no corrosion has caused rail fractures, and no defects have been detected by ultrasonic testing. Nonetheless, the base of rail is too irregular to re-use, even to the point of spotting in replacement crossties. Of 16,000 feet of tunnel, 4,000 feet have corrosion and water problems in three of the six tunnels. SCRRA installed pumps every 100 feet to keep the water drawn down below the base of the rail, which appears to help.

The following table summarizes the operating and inspection conditions regularly used by SCRRA.

Maximum Operating Speed	50 mph
Wheel Load	Vary depending on the type of car from 18 ton/car to 143 ton/car
Frequency of the Rail Breaks due to Rail Base Corrosion	None
Rail Defect Detection Frequency	Ultrasound inspection every 2 years
Type of Ties	Treated timber
Power Source	Conventional DC circuit only

C-18

Transit Authority: New Jersey Transit Corporation
Response Received: 01/12/2006
Contact: Stelian Canjea, P.E., Light Rail Program Manager
(973) 566-6704

SUMMARY

The New Jersey Transit Corporation (NJ Transit) is currently operating three light rail systems:

- Newark City Subway

- Hudson-Bergen LRT

- River Line

The Newark City Subway is the oldest and was opened in 1935. In 1982, the entire 5-mile double track system was rehabilitated. The old 100-lb rail has been replaced with 115-lb RE. The Hudson-Bergen LRT is a brand new system opened in 2000 and uses 115-lb RE rail. The River Line is also a brand new system operating diesel-electric cars from Trenton to Camden and was opened in 2004. All tracks are 115-lb RE rail. Until now, the New Jersey Transit Corporation had not reported rail base corrosion. The operation conditions of the tracks have variable wheel loads for the NCS and HBLRT LRT cars; the wheel loads vary from 8500 lb to 12,000 lb. The River Line car also has a variable wheel load from 10,000 lb to 18,000 lb. The tracks consist of wood ties (90%) and direct fixation ties embedded in track (10%). The traffic for the Newark City Subway and the Hudson-Bergen LRT is approximately 15 trains per hour 12 hours a day. For the River Line, the traffic is approximately 24 trains per day. Freight trains utilize a major part of the River Line.

The tracks are owned by New Jersey Transit. Overhead catenary is used by both the Newark City Subway and Hudson-Bergen LRT. This is a light rail system using DC of 750 V. The maintenance is conducted by the New Jersey Transit and DBOM Contractors for the Hudson-Bergen LRT and River Line. None of the above described lines present evidence or report rail base corrosion.

Transit Authority: St. Louis, Missouri, Metro
Response Received: 01/17/2006
Contact: Paul Genisio, Chief Engineer – Track
                      (314) 982-1411

SUMMARY

The St. Louis, Missouri, Metro is a light rail system. The tracks are composed of 132-lb RE rail manufactured in 1968 with heat numbers 78 T 131 D2. The corrosion is usually found at the base and web of the rail with a considerable amount of moisture with sand and dirt. The top of the head of the rail receives brine dripping rain in the tunnels. Rail was changed out at Mileposts 14.5-15.1 and 13.5-13.6, where corrosion was reported. The load per car is approximately 12 tons per axle. The tracks are owned by Metro. The tracks have direct fixation ties with a catenary power source system. The maximum speed is 55 mph.

Maintenance and track inspection are conducted by Mr. Paul Genisio and Weather Ford. The tracks are ultrasonically inspected twice a year. There is also a weekly inspection of the tracks (rails) to identify moisture and deposited sand at the e-clip location. Based on their reports, the corrosion located in the tunnels is due to brine that runs off the bridges. In addition, the tunnels themselves are damp and when dirt and sand accumulate on top of the e-clips and fasteners (MP 14.5 - 15.1), or on the spikes with anchors (MP 13.5 - 16.6). A detrimental environment results for the integrity of the rails/tracks. It is important to point out that welded sections of rail that were preheated are not an issue. The ambient temperature in the tunnels varies on average from 55–60°F.

Transit Authority: Edmonton Transit
Response Received: 04/25/06
Contact: Jim Stein; General Supervisor, Right-of-Way & Facilities
(780) 496-4364

SUMMARY

The Edmonton Transit system is a light rail system that operates on 7.7 track miles. Energy is supplied by an overhead catenary system using a 600 V DC. The entire track uses 100-lb ARA standard carbon rail.

Corrosion of the rail base has been observed at the main line grade (road) crossings. Currently, measurements conducted indicate that in some locations, the rail base thickness is approaching the condemning limit, and a number of Pandrol fasteners have failed as a result of corrosion. Corrosion appears to be related to high salt content; that is, from the salt-sand mixture used on roads during the winter and high moisture content; that is, the ground does not dry in road crossings because it is covered by crossing panels. All road crossings have some degree of rail base corrosion. The Edmonton Transit line has seven road crossings, all installed between 1991 and 2000. Corrosion is more severe where there are high salt concentrations and/or where the wheel flange does not fit tight to the running rail and crossing panels. Current leakage through the concrete crossing ties may also be a contributing factor.

The track is owned and maintained by Edmonton Transit. Ultrasonic testing is conducted yearly. Because of the corrosion that is occurring at the existing grade crossings, the Edmonton LRT Design Guidelines have been changed to require: (a) rubber flange rail covering the full width of the rail base on both the gauge side and field side and (b) use of hardwood ties.

The following table summarizes the operating and inspection conditions regularly used by Edmonton.

Maximum Operating Speed	70 kmph
Wheel Load	5.8 metric tones
Frequency of the Rail Breaks due to Rail Base Corrosion	None reported
Rail Defect Detection Frequency	N/A
Type of Ties	Concrete ties in road crossings; wood elsewhere
Power Source	Overhead catenary

APPENDIX D

"Estimation of the magnitude of the stresses formed due to corrosion cracks in railway rails"

Final Report

Submitted by

Gabriel Plascencia, PhD

&

David Jaramillo, PhD

To the Transportation Technology Center, Inc.

CIITEC – IPN

Cerrada Cecati s/n

México, D.F. C.P. 02250

México

e-mail: gplascencia@gmail.com

CONTENTS

Presentation

The scope of this project is to evaluate alternative solutions for a constant material damage problem that underground transportation systems face across North America. Such problem is the deterioration of the rails due to a severe corrosion attack.

In this report, we are presenting experimental results (metallographic characterization and corrosion tests) as well as some numerical calculations of the state of mechanical stresses that rails with and without corrosion damage present.

The samples used to evaluate the metallurgical structure, and the corrosion resistance of the materials used in subway systems, were obtained from two different sources: 1) Mexico City's subway system and 2) St. Louis, Missouri, Metro system. While the Mexican system provided two rail samples (one deformed due to its wear and a second one from a completely new rail), the second supplier only provided a sample severely corroded.

The three samples were evaluated in the same manner both for their metallographic features as well as for their corrosion resistance. On the other hand, the numerical estimation of the mechanical stresses was conducted by means of the Finite Element Method analysis, using commercial software.

It was found that in spite of the presence of non-metallic inclusions the materials showed structural features that allow them to perform as expected when a train passes on them. They also exhibited similar corrosion resistance regardless of the media in which they are tested. The numerical calculations showed that unless a sharp edge crack develops at the base of the rail, the material can withstand the loads applied to it without seriously compromising it performance under service.

Experimental

As mentioned before, metallurgical examination and corrosion tests were conducted; parallel to these experiments, the numerical modelling of the rails was carried out. Figure D1 shows a schematic of how the different experimental activities related to this project were done.


| Materials reception |
| Optical inspection |

| Sample cutting & machining |
| Metallographic preparation |
| Metallurgical |

- Grinding with sand paper grades
  80 to 1000
- Polishing with an alumina emulsion

| Sample cutting & encapsulation for corrosion testing |
| Surface cleaning for corrosion testing |
| Corrosion tests |

- Tests in different media:
  KCl (1 & 0.1 M)
  Na₂SO₄ (1 & 0.1 M)
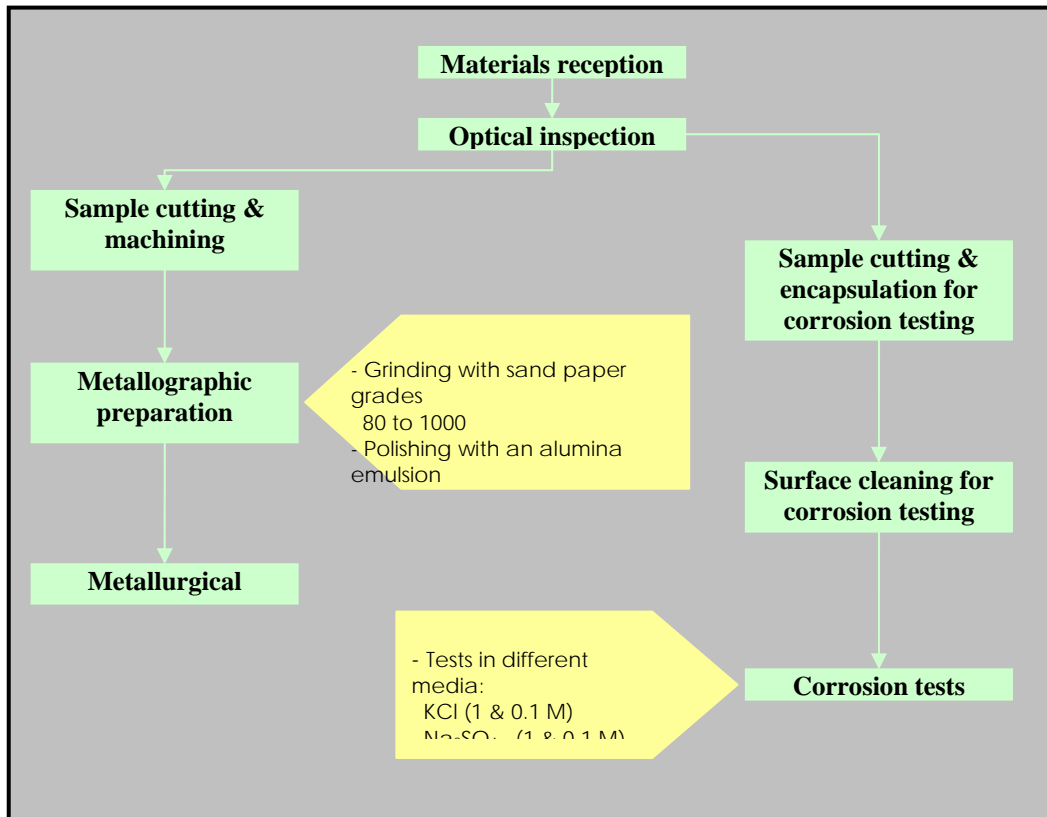
Figure D1.   Experimental sequence in the evaluation of the rails samples.

Two samples of rails were received from Mexico City's Sistema de Transporte Colectivo (STC). One of the samples (SW) is from a worn rail which exhibits severe deformation on its head, whereas the second sample (SU) was taken from a new rail. In each case, the rails exhibited some corrosion products onto their surface; the corrosion products are due to the exposure to rain in the warehouse facilities of the STC. Figure D2 shows pictures of the rails in the as received condition. After initial inspection, the rust was removed from the surface of the rails by means of a mechanical brush.
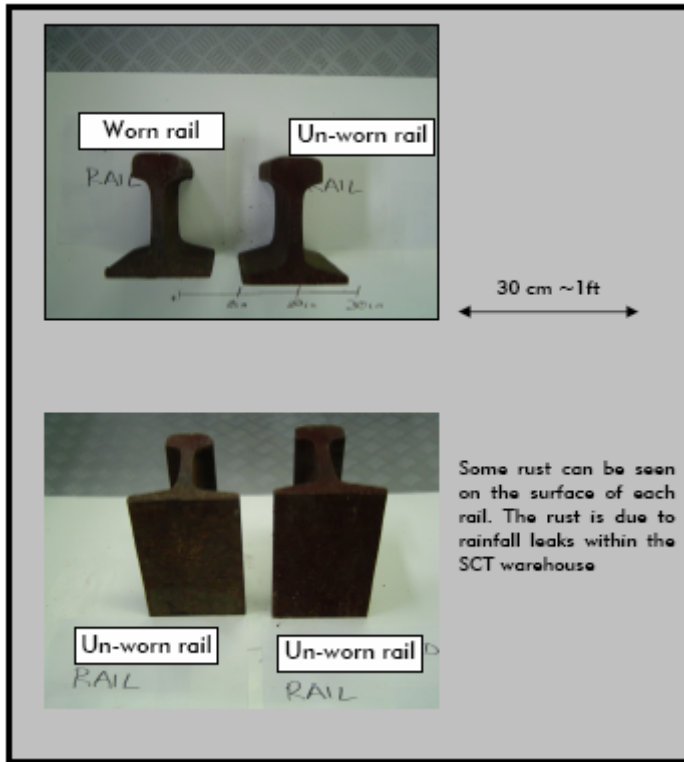
Figure D2. *Rails from STC in the as received condition.*

It was noticed after cleaning the rails, that both of them have some porosity, especially in their bottom end. The worn sample exhibited more porosity than the un-worn one. The initial inspection suggests that this porosity is due to the manufacturing of the rails (rolling operations); further examination of the rails will lead to a more conclusive evaluation of the source of such porosity. Figure D3 shows a picture of the bottom end of the SW sample.
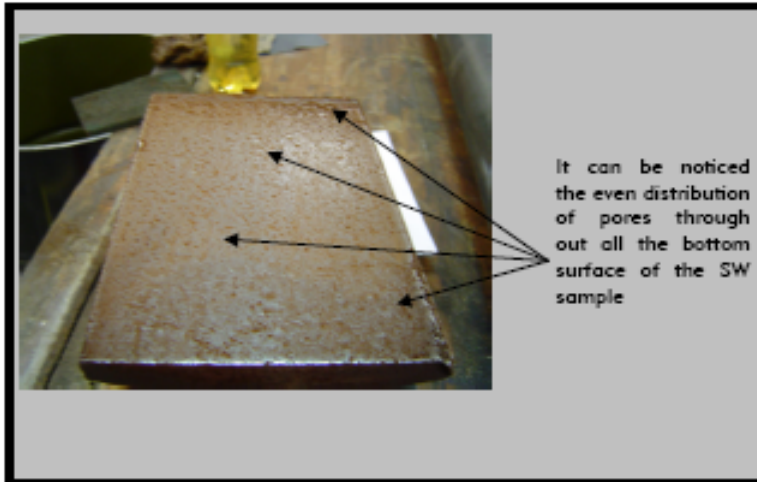
*Figure D3.   Bottom end of the SW sample, showing some porosity.*

After receiving STC's rails, we obtained a sample from St. Louis, Missouri, Metro system through representatives (Dr. Francisco C. Robles Hernández) of TTCI, Inc. This sample (USA) exhibited a severe corrosion attack on its base and web. Figure D4 shows this rail as received.
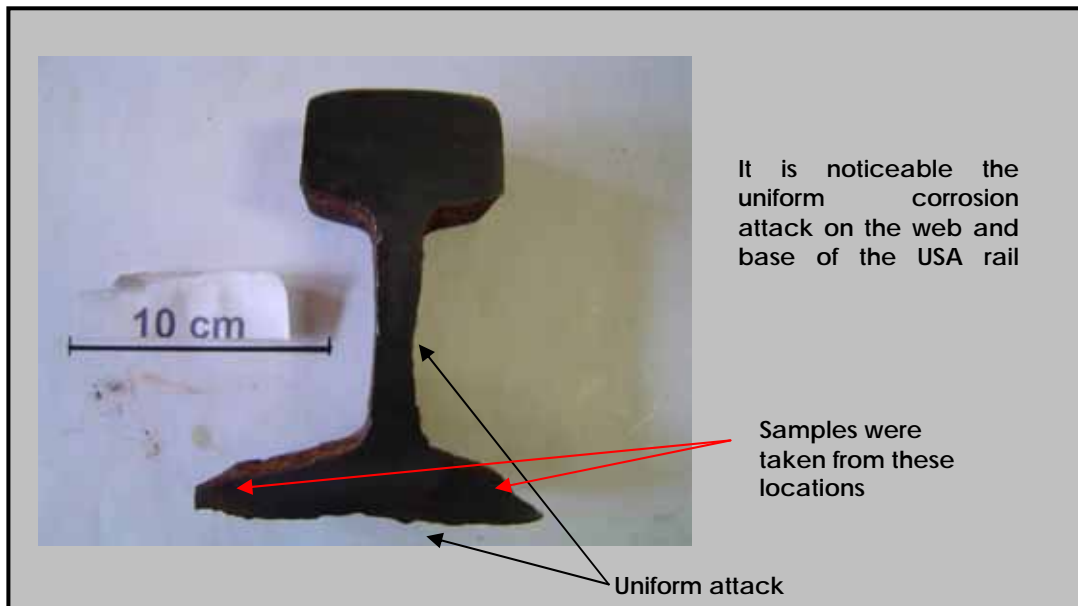
Figure D4.   USA rail sample in the as received condition.

From the first two rails, two slices with 1 cm of thickness were taken. From the first slice 5 samples were cut to evaluate them metallographically; whereas from the second slice a sample was taken for corrosion tests. In the case of the USA rail sample, due to its condition, 2 samples were taken from its base, both samples were prepared for metallographic evaluation. After completing its structural characterization, one of the samples of this rail was used for the corrosion evaluation of this sample.
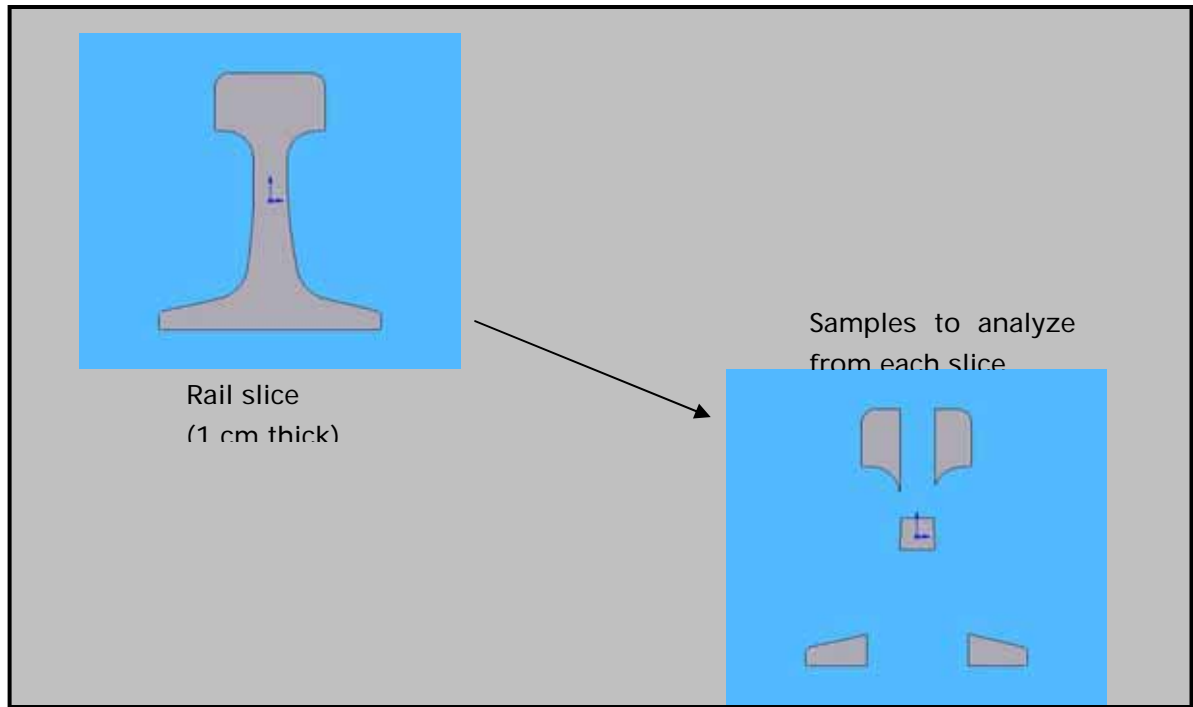
Figure D5.   Actual samples from each rail to analyze.

Metallographic Evaluation

As mentioned in the previous section, 5 samples from each the SW and SU rails were evaluated, while only two samples from the USA rail was analysed. Every sample was prepared for metallographic examination firstly by girding them with sand paper (grades 80 to 1000) and then by polishing them with alumina emulsions (10, 5, and 1 μm).

Once polished, the samples were analysed under an optical microscope to verify the size and level of non metallic inclusions. Figure D6 shows the latter.

Using the NMX-B-308-1987 [1] and ASTM-E-45-1985 [2] standards the microstructures were evaluated to determine their microcleanlines As noticed in Figure D6, the SW sample shows grouped globular oxides type D2, whereas the SU sample shows discontinuous alumina inclusions type B4. The USA sample presents globular oxides type D1. It is likely that the globular oxides reported for both the SW and the USA sample actually are mainly alumina, which indicates that these three rails are made from killed steel. Now a days all rails are manufactured under vacuum treated casting conditions.

After this initial inspection, the samples were etched with Nital 4 solution to verify their micro-structure. The microstructure of these materials is shown in Figure D7. It is clear from Figure D7 that the three samples exhibit the same microstructural features. All the samples have a homogeneous pearlitic matrix. Therefore is expected that both, the steel used in the USA or that used in Mexico would behave in the same manner under similar working and environmental conditions.

Figure D6.   *Non-metallic inclusions in the different rail samples:*
                 (a) SW, (b) SU and (c) USA

D-9
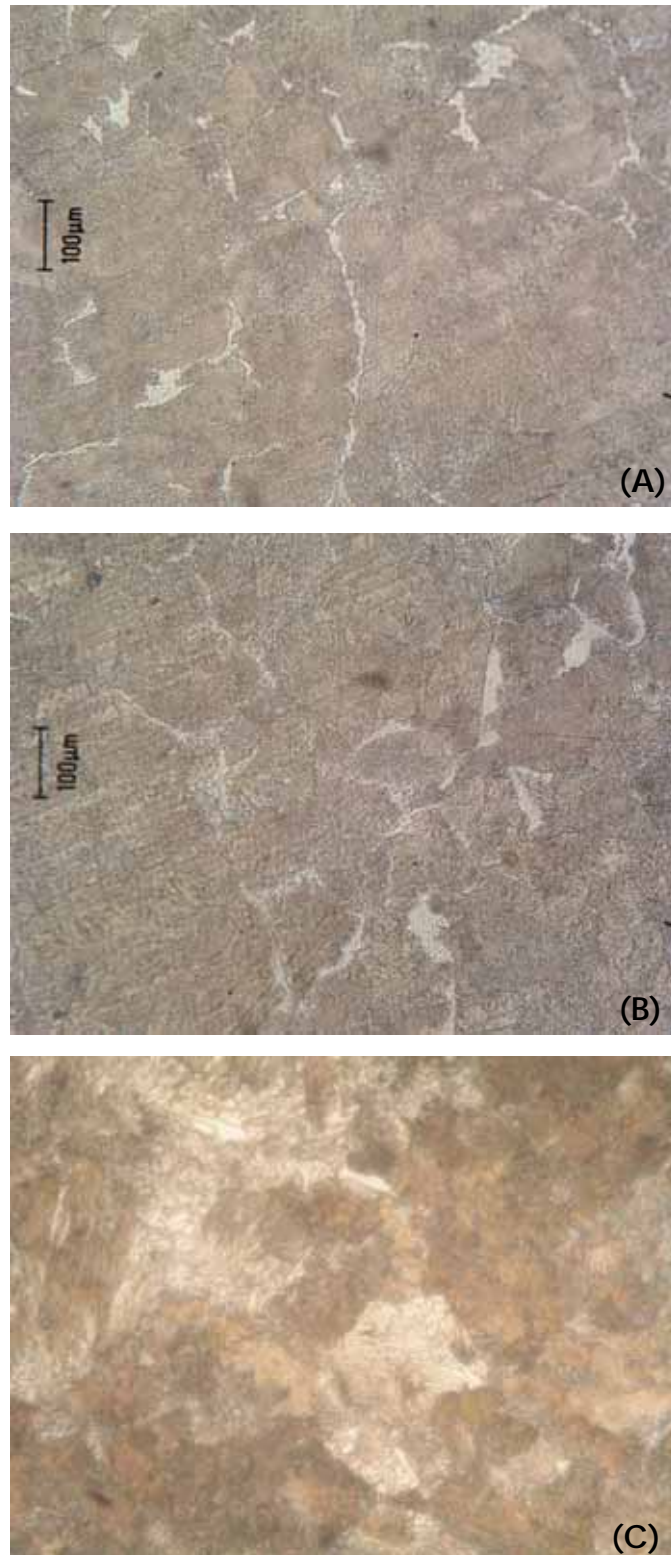
Figure D7.   *Metallographic examination of the different rails samples: (A) SW, (B) SU, (C) USA.*

The average grain sizes for these materials are within 5 & 6 according to ASTM-E-45-1985 [3] standard. The micrographs shown above were taken randomly since for every sample it was found the same type of microstructure in each of the 5 pieces evaluated (2 pieces for the USA rail).

It must be mentioned that although the micrographs shown in Figures D6 and D7 are not at 100 X, the determination of the microstructure and the level of non-metallic inclusions were conducted under 100 X as required by the ASTM standards [2,3].

The metallographic examination confirmed that the porosity in the bottom of the base of the Mexican samples corresponded to the rolling stages in manufacturing them. No cracks attributed to the pores were detected nor any corrosion product deposited into the pores. After the initial polishing of the rail samples, all the rust from weathering disappeared, leaving the surfaces free of any residue or imperfection.

Corrosion Tests

The corrosion resistance of the steel used in the rails used in St. Louis, Missouri, Metro system was measured and compared to those installed in Mexico City's subway facilities. The corrosion resistances of such steels were measured by means of the linear polarization technique. Again the three rails (SW, SU and USA) were tested.

The linear polarization technique was chosen to measure the rate of corrosion because it is easily conducted while it allows for continuous data collection under different conditions. Since it takes only a few minutes to carry out one of these tests, the potential of the corroding metal is sufficiently stable during the test to act as a reference [4].

In our particular case, we carried out our corrosion tests by applying ± 20 mV than the corrosion potential of our reference electrode. In these tests we used a silver-silver chloride electrode as the reference one. The corrosion potential of such electrode is + 799 mV respect to the normal Hydrogen electrode at 25 °C.

The corrosion tests were conducted using different electrolytes (1M KCl, 0.1M KCl, 1M Na_2SO_4, 0.1M Na_2SO_4), such electrolytes were chosen after reviewing the analysis of the soils in which US subway systems are installed. It should be mentioned that the aim of the corrosion tests was to evaluate the effect of ions such as SO_4^{2-} and Cl^- on the corrosion resistance of the rails.

The effect of such ions on the corrosion resistance of the rails are of importance due to the fact that soils across North America contain considerable amounts of sulfates, and in the other hand, the effect of the Cl⁻ ion becomes also important for Subway systems located nearby the ocean. Figure D8, shows a picture of corrosion products in New York subway system. This system needless to say is installed in the shore of the Atlantic Ocean and the soil found there present considerable amounts of sulfate salts.

Rust from rails in New York's subway system

Corrosion

Figure D8.   Corrosion products found in New York's subway system.

As evident from Figure D8, the environment in which the rails are installed plays a very important role in terms of the corrosion resistance of the rails. In view of this, we conducted several tests in 4 different electrolytes.

The experimental set up for the corrosion tests consisted of an electrolytic cell attached to a potentiostat – galvanostat apparatus, which in turn was connected to a CPU through a data acquisition system. The potentiostat used in our tests was an EG & G Princeton Applied Research apparatus model 273. This equipment has a built in corrosion software M352 which enables to automatically run the corrosion experiments while it collects data and sends it to a CPU. Figure D9, shows the experimental assembly.
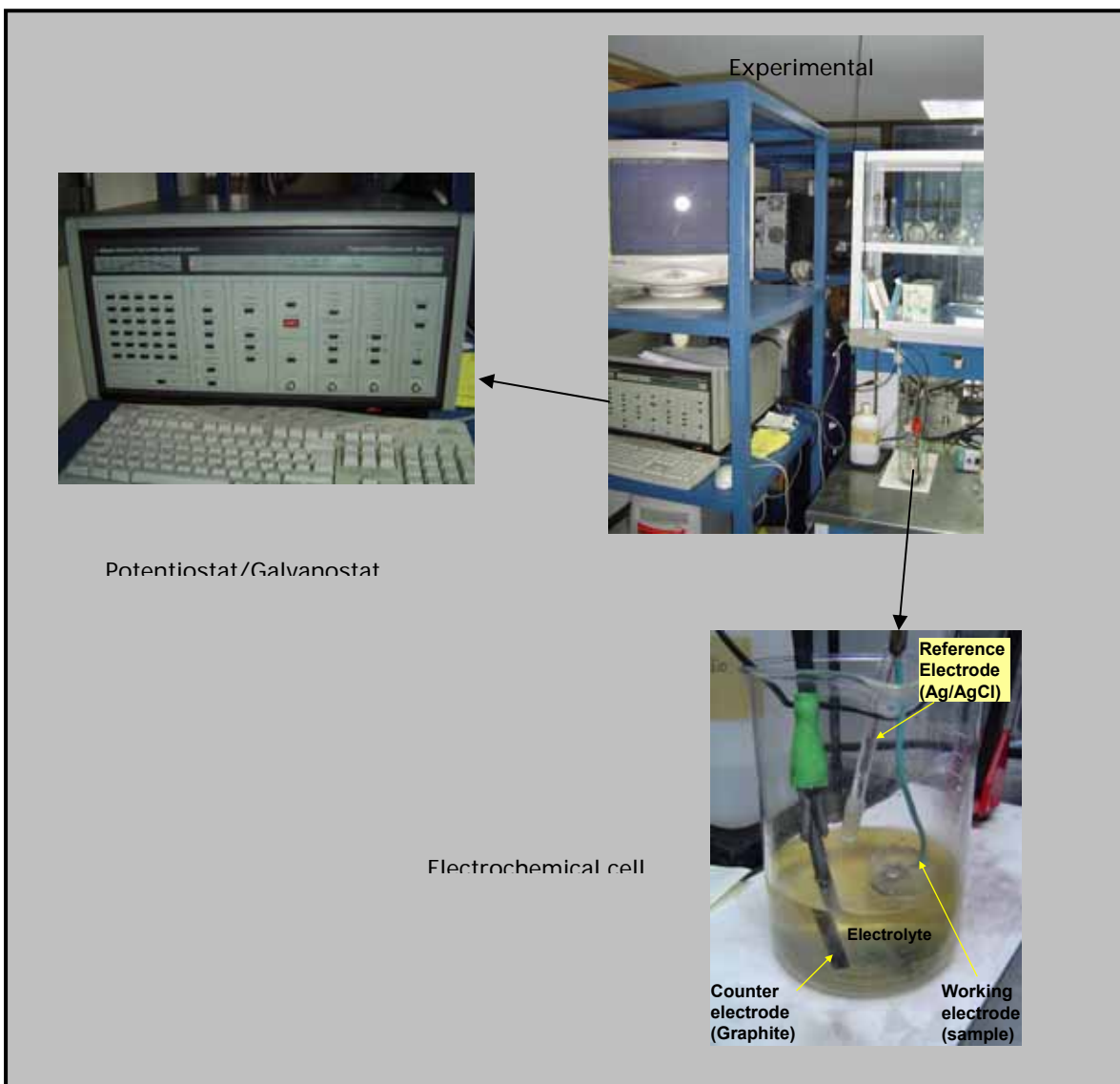
Figure D9.   Experimental set up for corrosion tests.
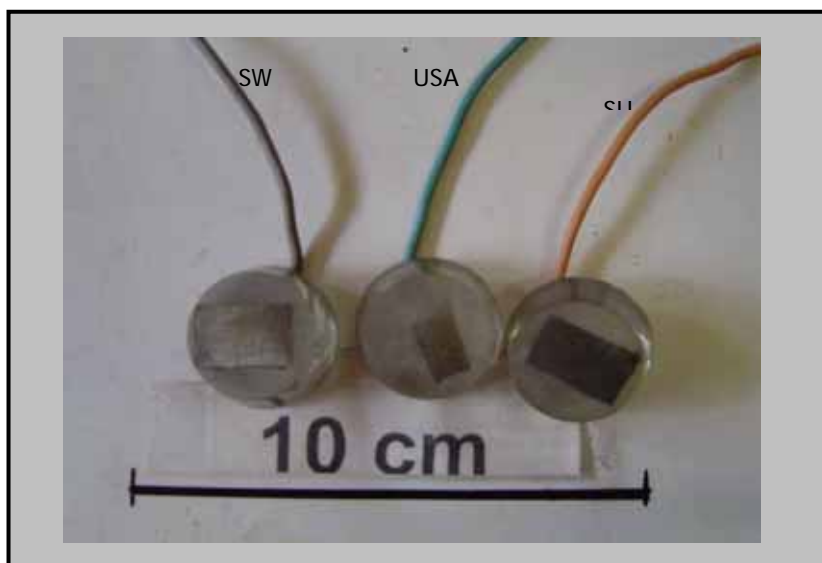
Figure D10.   Probes used for corrosion testing. The picture shows the probes after being corroded in 0.1 M KCl electrolyte.

As seen in Figure D9, every corrosion test consisted in immersing the sample to be evaluated into the different electrolytes. Once immersed, the voltage and current were applied during 20 minutes. Recording of the voltage drop and current density were taken at a scan rate of 20 readings/minute. At the end, for every single test, a total of 400 data set was obtained. At the same time every probe was tested 5 times in each electrolyte, so in total 60 experiments were conducted. The corrosion rate values reported for each sample in every electrolyte, corresponds to the average value of the different experiments. Figures D11 and D12 present such average values for tests in both KCl and Na_2SO_4.
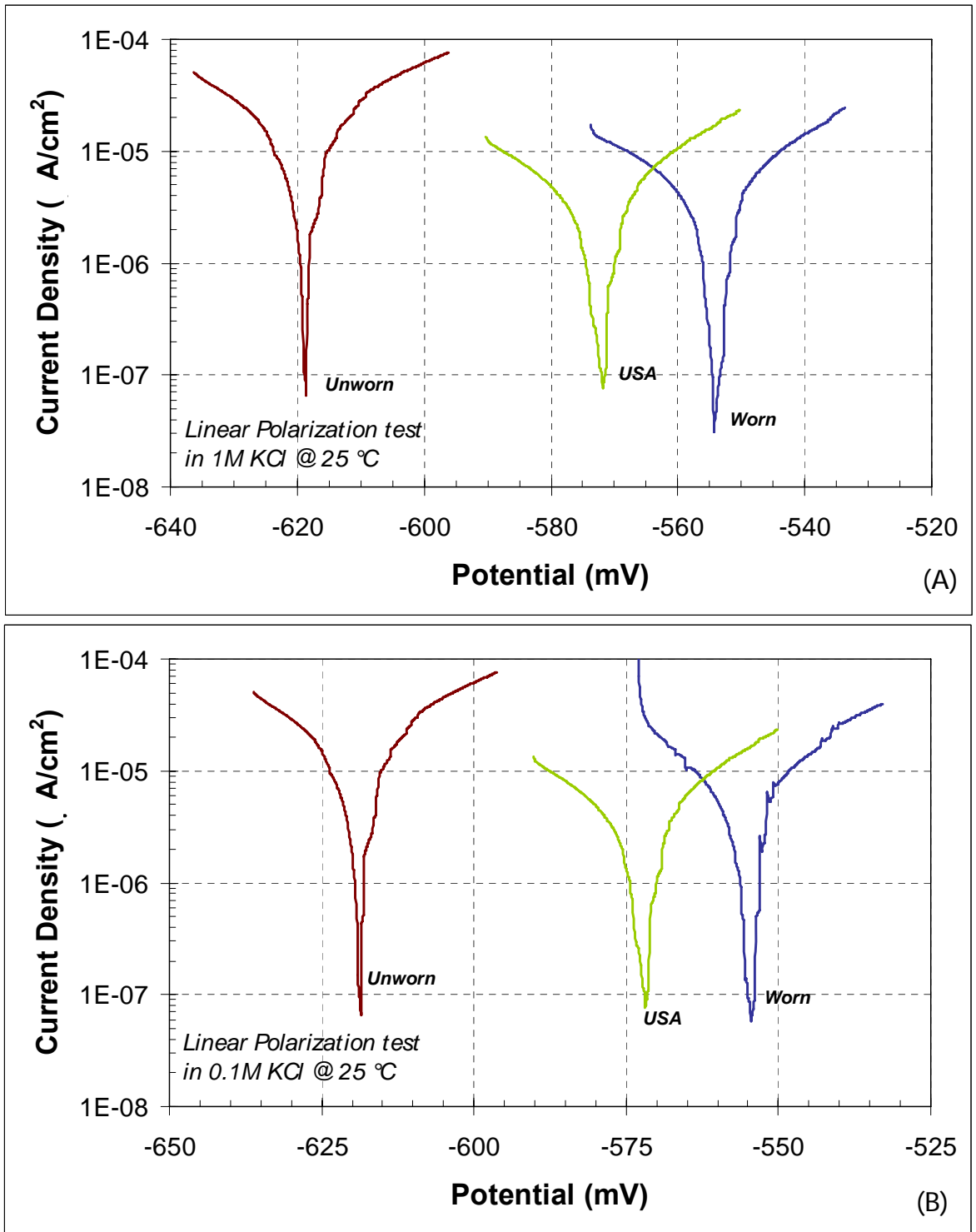
Figure D11. Corrosion resistance of the different rails in KCl.
(A) 1M KCl electrolyte, (B) 0.1 M KCl electrolyte.
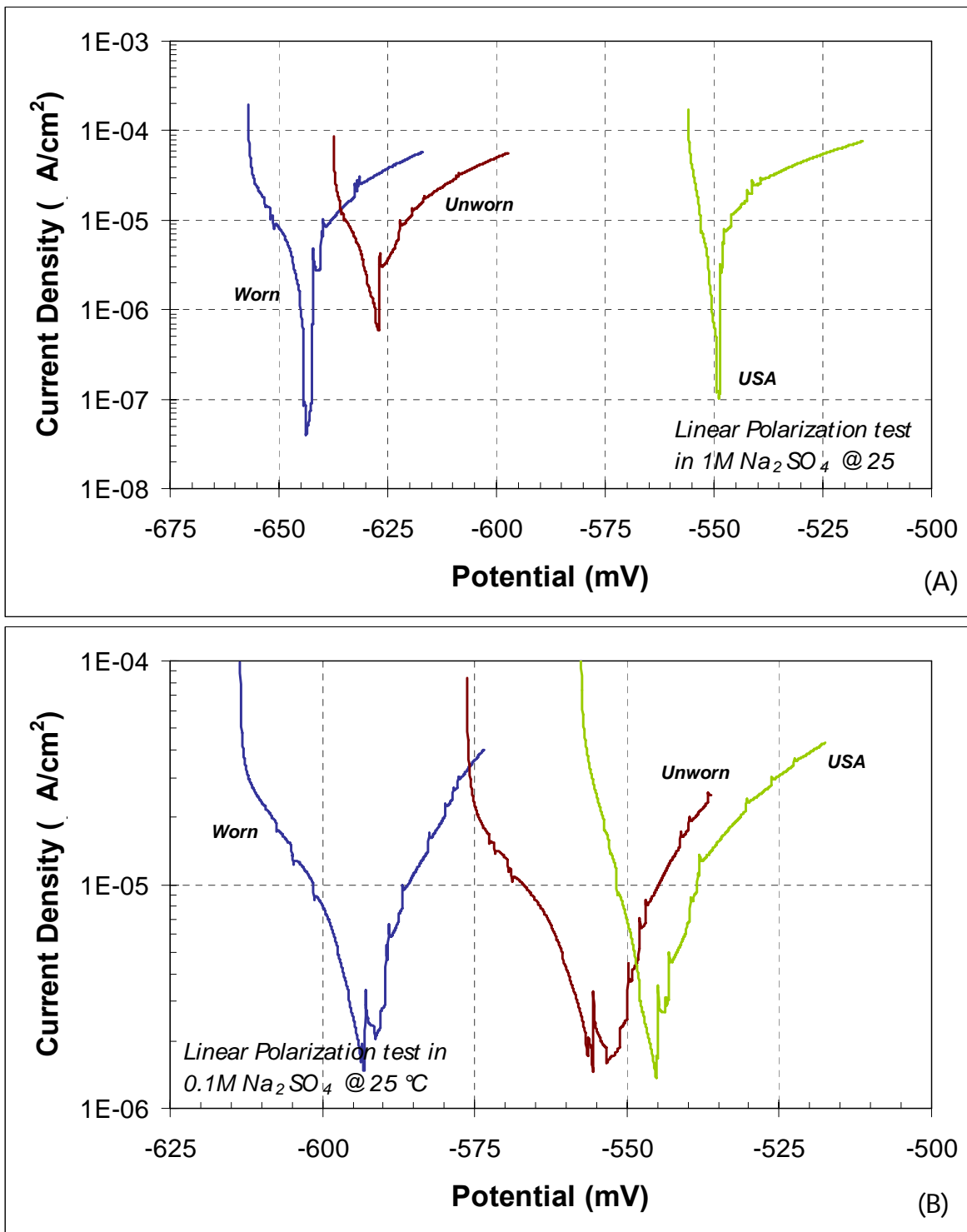
Figure D12.   Corrosion resistance of the different rails in Na_2SO_4.
(A) 1M Na_2SO_4 electrolyte, (B) 0.1 M Na_2SO_4 electrolyte.

On the other hand, it can be seen in Figure D10 that the different samples are uniformly corroded by the different media tested. This also indicates that the steel used in the different rails behave quite similarly in every case.

After reviewing the plots shown in Figures D11 and D12, it becomes more evident that the different specimens corroded at a very similar rate, there is only a slight deviation in terms of the voltage drop for every sample, however, the current density required for the corrosion of each specimen is in the same order of magnitude. The latter indicates that the materials tested present a similar corrosion resistance regardless of the medium in which they are evaluated.

With the information from the plots in Figures D11 and D12, we were able to determine the current density for corrosion. Such current density is found by intercepting the slopes of the anodic and cathodic portions of each plot. Since the current density is directly proportional to the rate of corrosion, we were able to estimate such rate by means of the following equation [4]:

$$r_{corr} = -\frac{j_0}{nF} \tag{1}$$

Where j_0 is the current density for corrosion, n is the number of electrons transferred during the oxidation of the metal and F is Faraday's constant (96500 C/mole). It must be noticed that equation 1 expresses the corrosion current as current density. Since there is no net reaction, since the rate of oxidation and reduction within the electrochemical cell are equal. Therefore the exchange reaction is equivalent to either the rate of corrosion or the rate of reduction, thus the corrosion rate can be conveniently expressed in terms of the current density [4].

Since we experimentally know the current density for corrosion, we can estimate the rate of corrosion in terms of mm/year, which is a more used expression to estimate the material losses due to corrosion. Table 1 shows such values.

According to Table 1, it is clear that since the corrosion rate of the different samples is between 0.002 and 0.07 mm/year, thus it can be said that these materials exhibit excellent corrosion resistance except for the USA sample tested under 1M Na_2SO_4 solution, whose corrosion resistance value suggests that in sulfate media this sample only posses fair corrosion resistance [4].

The data obtained in Table 1, clearly shows that the steel used for this application is able to withstand the attack of different chemicals under normal conditions. If an over voltage is applied to the corroding system, then the rate of corrosion of the steel will increase quite significantly.

Table D1.   Rate of corrosion of the different samples in every tested electrolyte.

Electrolyte	Sample	i corr (A/cm^2)	Corrosion rate (mol/cm^2/s)	Corrosion rate (g/cm^2/hr)	Corrosion rate (mm/year)
KCl 1M	Worn	2.5×10^{-6}	$- 8.6 \times 10^{-12}$	$- 1.7 \times 10^{-7}$	$- 1.8 \times 10^{-3}$
	Unworn	9.5×10^{-6}	$- 3.3 \times 10^{-11}$	$- 6.6 \times 10^{-6}$	$- 0.07$
	USA	2.5×10^{-6}	$- 8.6 \times 10^{-12}$	$- 1.7 \times 10^{-7}$	$- 1.8 \times 10^{-3}$
KCl 0.1M	Worn	4×10^{-6}	$- 1.4 \times 10^{-11}$	$- 2.8 \times 10^{-6}$	$- 0.03$
	Unworn	6×10^{-6}	$- 2.1 \times 10^{-11}$	$- 4.2 \times 10^{-6}$	$- 0.04$
	USA	3×10^{-6}	$- 1.0 \times 10^{-11}$	$- 2.1 \times 10^{-6}$	$- 0.02$
Na$_2$SO$_4$ 1M	Worn	3.5×10^{-6}	$- 1.2 \times 10^{-11}$	$- 2.4 \times 10^{-6}$	$- 0.03$
	Unworn	5.5×10^{-6}	$- 1.9 \times 10^{-11}$	$- 3.8 \times 10^{-6}$	$- 0.04$
	USA	9×10^{-5}	$- 3.1 \times 10^{-10}$	$- 6.2 \times 10^{-5}$	$- 0.64$
Na$_2$SO$_4$ 0.1M	Worn	2×10^{-6}	$- 7.0 \times 10^{-12}$	$- 1.4 \times 10^{-6}$	$- 0.01$
	Unworn	2.5×10^{-6}	$- 8.6 \times 10^{-12}$	$- 1.7 \times 10^{-7}$	$- 1.8 \times 10^{-3}$
	USA	3×10^{-6}	$- 1.0 \times 10^{-11}$	$- 2.1 \times 10^{-6}$	-0.02

D-18

Numerical Simulation

The estimation of the stresses generated in the rails with and without severe corrosion damage was done. Such estimations were conducted by means of the finite element method, using COMSOL Multiphysics™ software. The magnitude of the stresses estimated reveals that it is likely that the rails with severe corrosion attack will drastically fail under current subway traffic conditions if they develop very sharp edge cracks. This means that localized corrosion attack must be avoided. The calculations show that even in the event of uniform corrosion damage, the rails are still able to withstand the stresses developed under normal traffic conditions; therefore, replacing the damaged rails becomes a critical issue in terms of subway safety and maintenance programs. Results from these calculations are shown in the following figures.

To solve the stresses equations, the mesh generated contained at least 15000 elements. To prove the accuracy of the method, mesh tests were conducted by doubling the number of elements. In that case, the results from the solver were identical to those with the initial mesh (it should be noticed that computer time ~ nodal points^2). So in order to save computational time, we ran the simulations with a minimum of 15000 elements. More details on the simulations are shown in following.
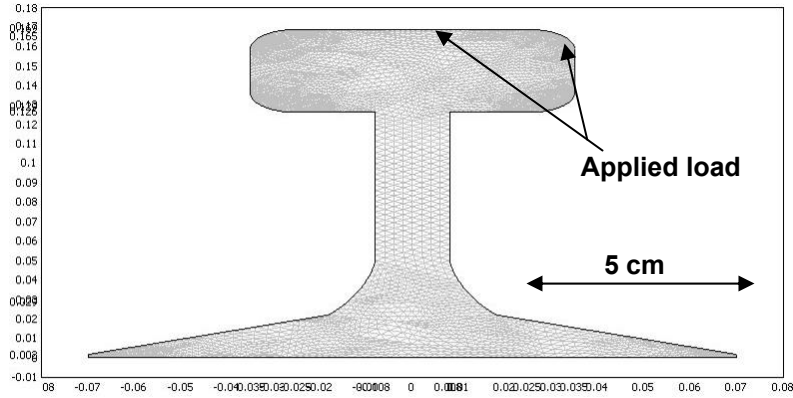
(A)
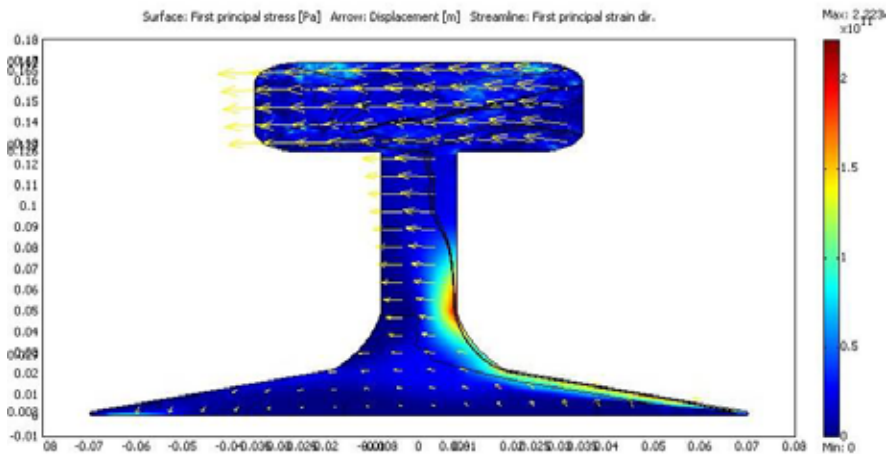
(B)
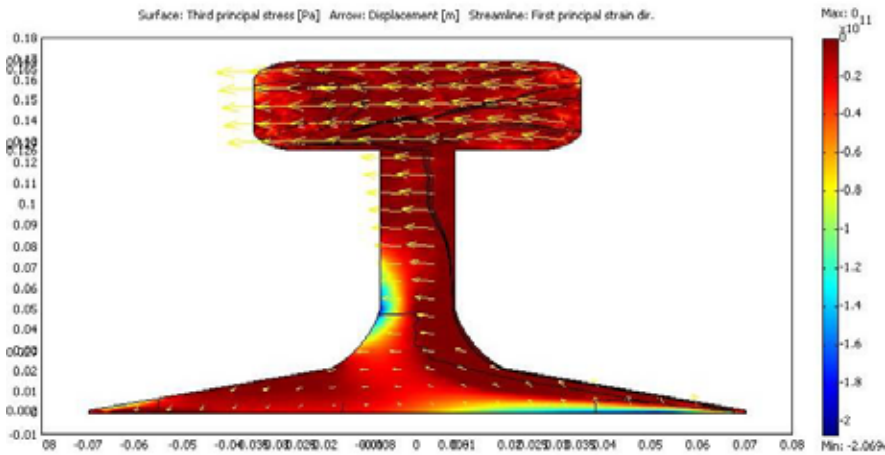
(C)

Figure D13. (A) Geometry and grid used in the calculation of mechanical stresses in a normal rail. (B) Tensile stresses developed in the rail when the load is applied. (C) Compression stresses in the rail when the load is applied. Along with the stresses, the figure shows flow lines along with the direction of the possible displacement.

D-20
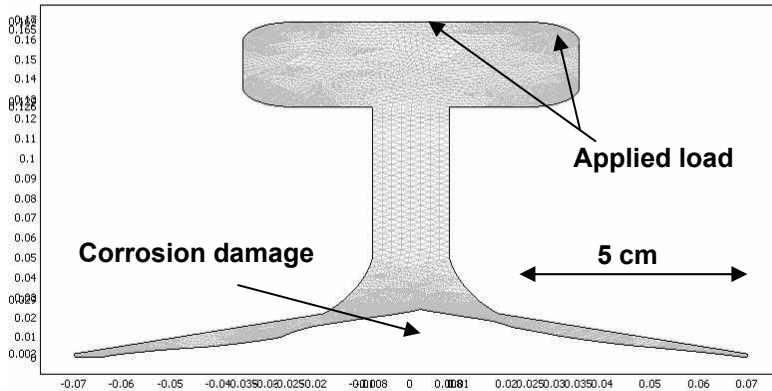
(A)
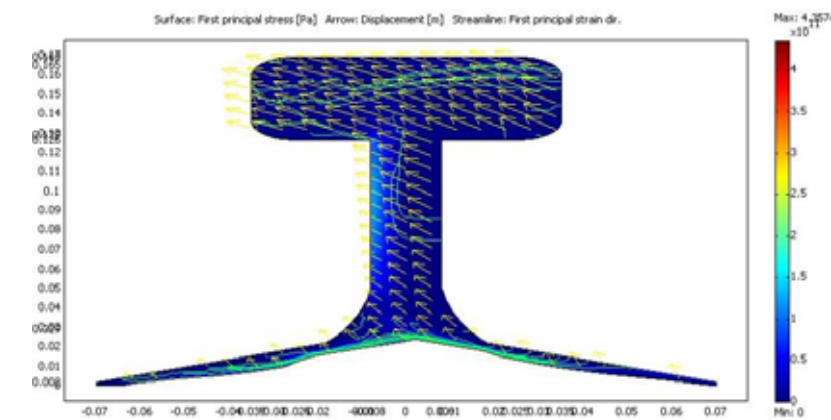
(B)
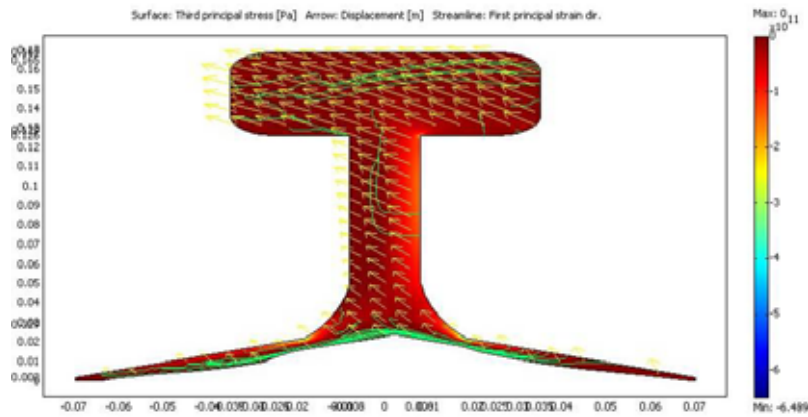
(C)

Figure D14. *(A) Geometry and grid used in the calculation of mechanical stresses in a corroded rail. (B) Tensile stresses developed in the rail when the load is applied. (C) Compression stresses in the rail when the load is applied. Along with the stresses, the figure shows flow lines along with the direction of the possible displacement.*

D-21

As seen from Figures D13 and D14, the effect of corrosion on the mechanical behaviour of the rails may have severe consequences. The stress components (tension and compression) in the stresses generated in the normal rail when the subway passes, show that they are under equilibrium and no mechanical failure is expected. On the other hand, the stresses developed in the corroded rail seem to create zones of compression and tension nearby the corroded area, such zones of tension or compression tend to accelerate or induce a catastrophic failure along the railway.

The presence of cracks, especially those with sharp edge, result in a non uniform distribution of stresses in the vicinity of the crack. If high tensile stresses are developed in these cracks (stress concentrators), then it is likely that the cracks will propagate a faster rate. On the other hand if shear stresses develop alongside the cracks, then slip will occur [5, 6]. In either case, any stress system in which large tensile stress components combines with small shear stress components develops, will favour cleavage. Such stress state consideration is important when considering any possible fracture.

On a different set of calculations, with a lateral view of the geometry, the statements above are more evident. Even with a uniform attack the material is able to withstand the loads applied, whereas the formation of sharp cracks encourages the failure of the rail when a load is applied.
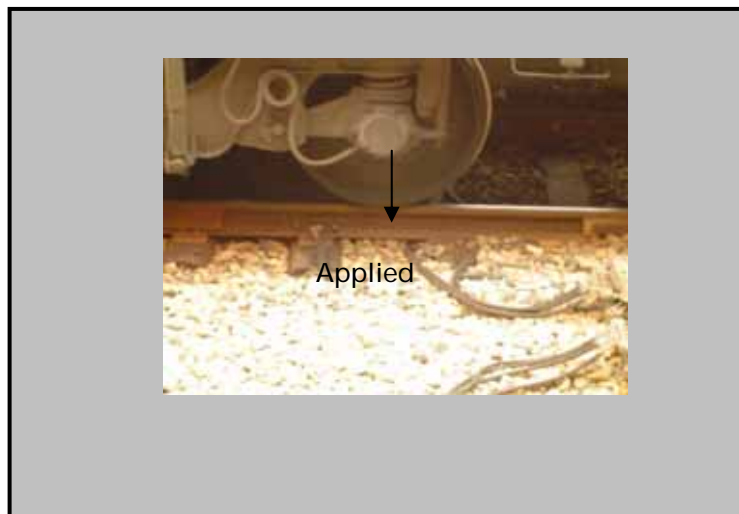
Figure D15.   Actual situation to model.

As seen in Figure D15, the new set of calculations was conducted taking in consideration the physical situation shown in the picture above. In this case 3 points of applied load will be considered. From the data of Mexico City's survey, the load used in our calculations was in the order of 45000 N.

(A)

(B)

(C)
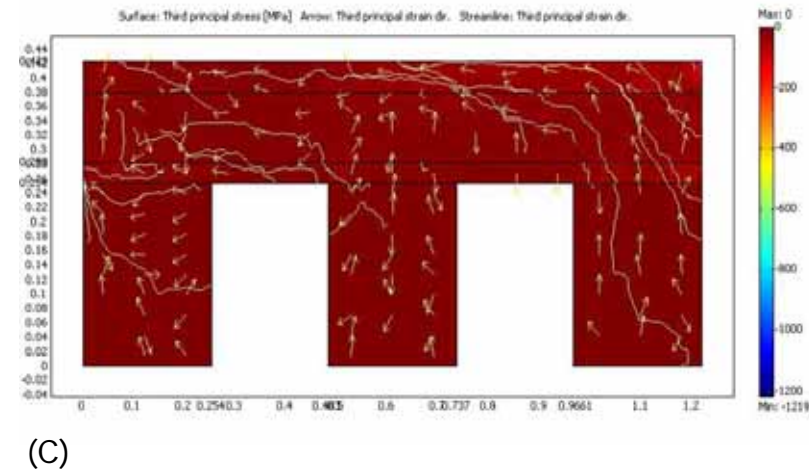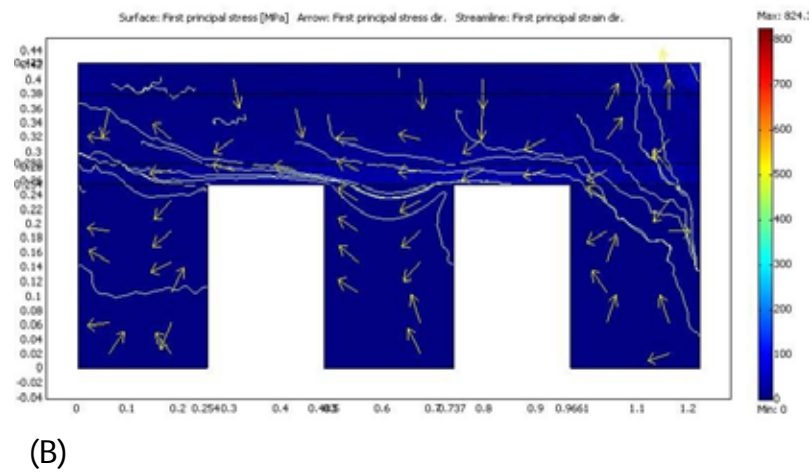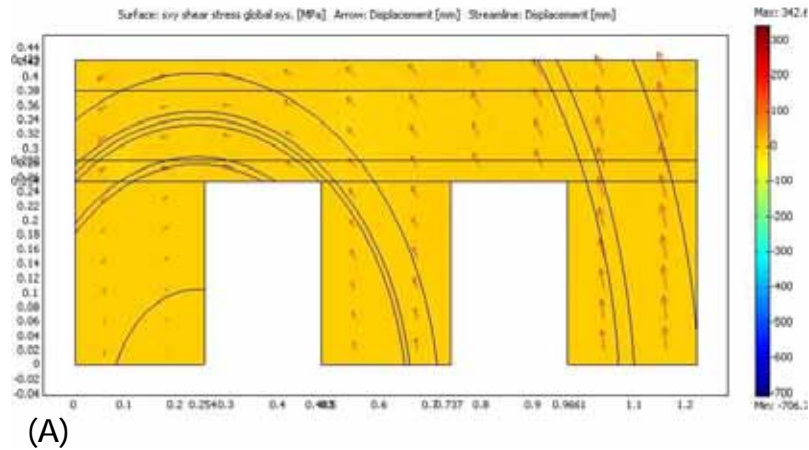
Figure D16.   Numerical results for a load applied to an un-attacked rail, the loads are applied on top of every beam. (A) Shear stresses developed along with the deformation of the rail, (B) Tensile stresses developed along with the tensile strain. (C) Compression stresses developed along with the path of strain.

D-23

(A)

(B)

(C)
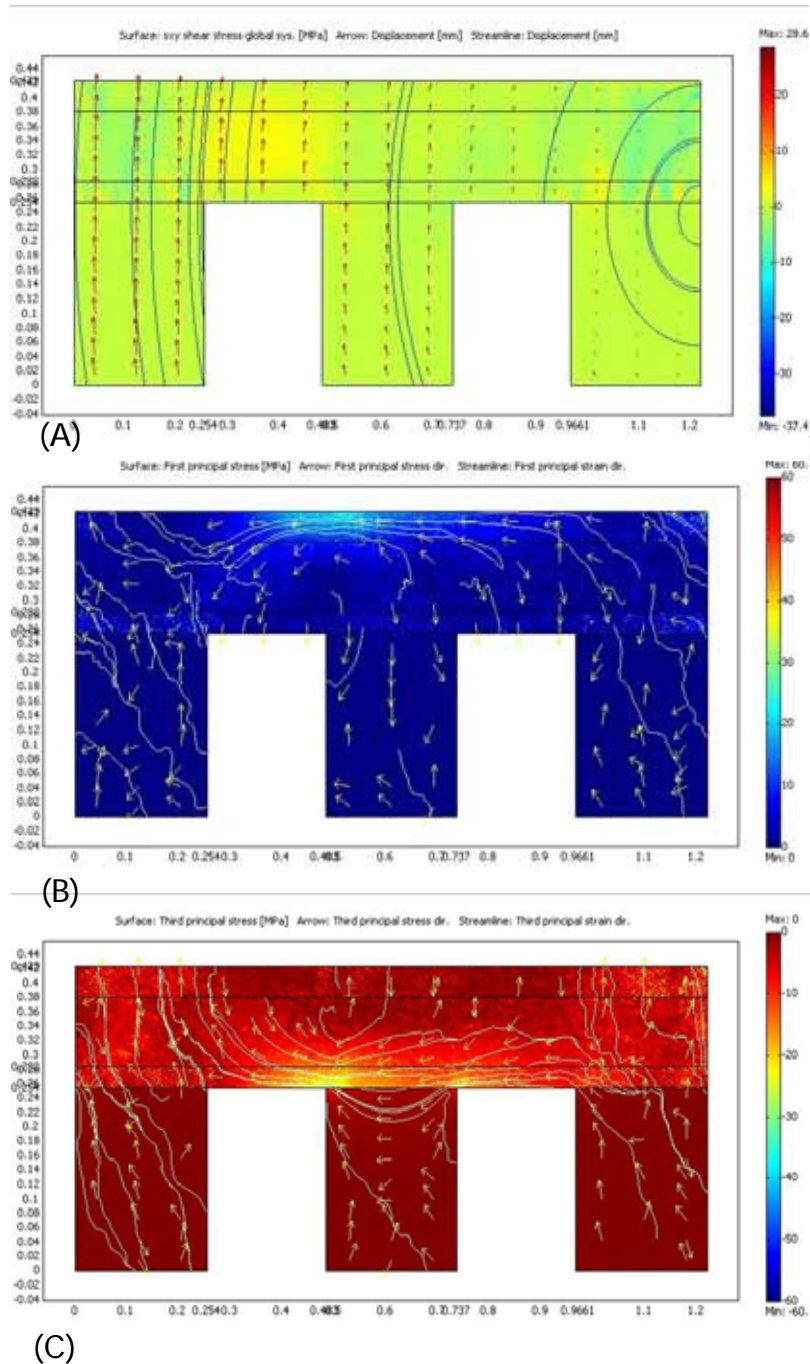
Figure D17.   Numerical results for a load applied to an un-attacked rail, the loads are applied on top of every beam except from that in the middle. (A) Shear stresses developed along with the deformation of the rail, (B) Tensile stresses developed along with the tensile strain. (C) Compression stresses developed along with the path of strain.

D-24

(A)

(B)

(C)
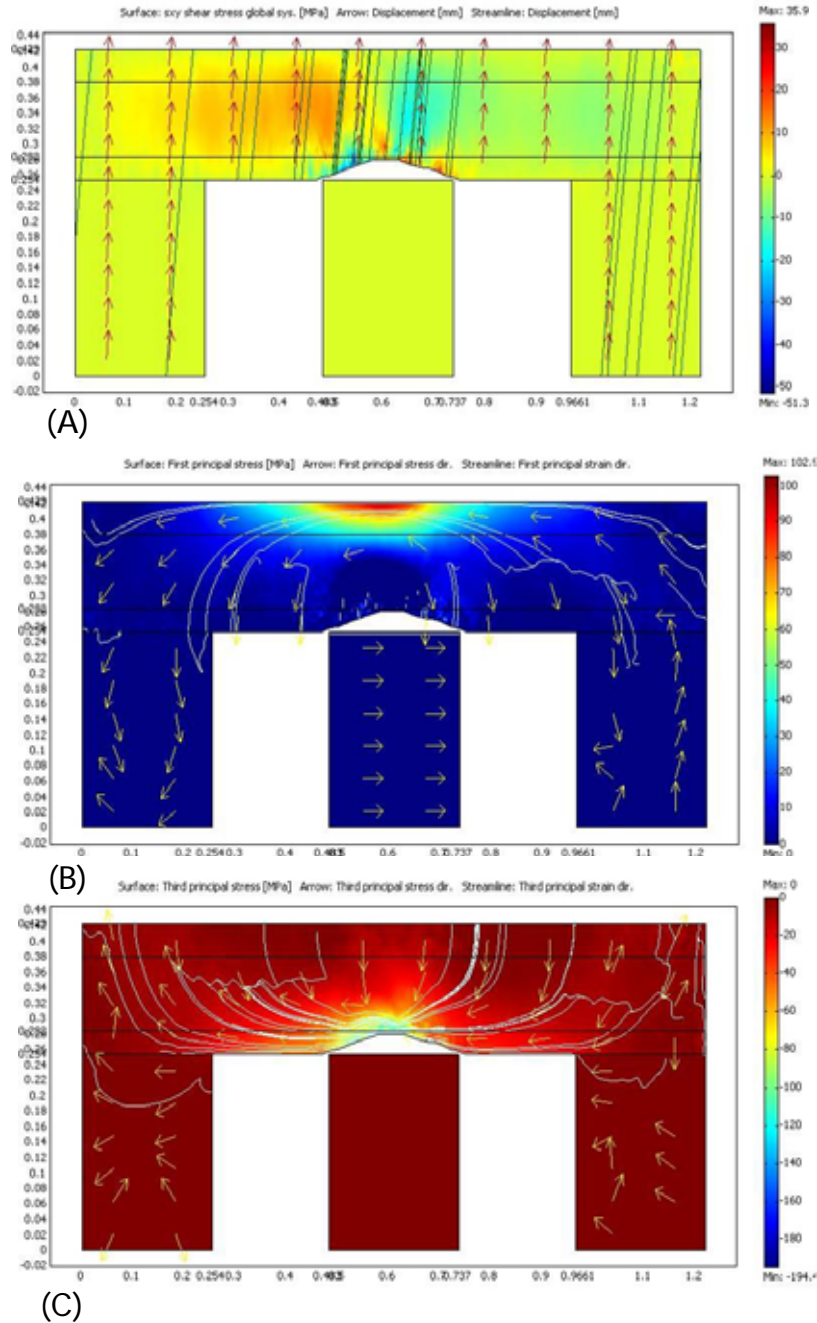
Figure D18. Numerical results for a load applied to a rail with uniform attack, the loads are applied on top of every beam. (A) Shear stresses developed along with the deformation of the rail, (B) Tensile stresses developed along with the tensile strain. (C) Compression stresses developed along with the path of strain. As seen in this figure high compressive stresses develops along the crack formed, however these stresses do not affect drastically the mechanical behavior of the rails.

D-25

(A)

(B)

(C)
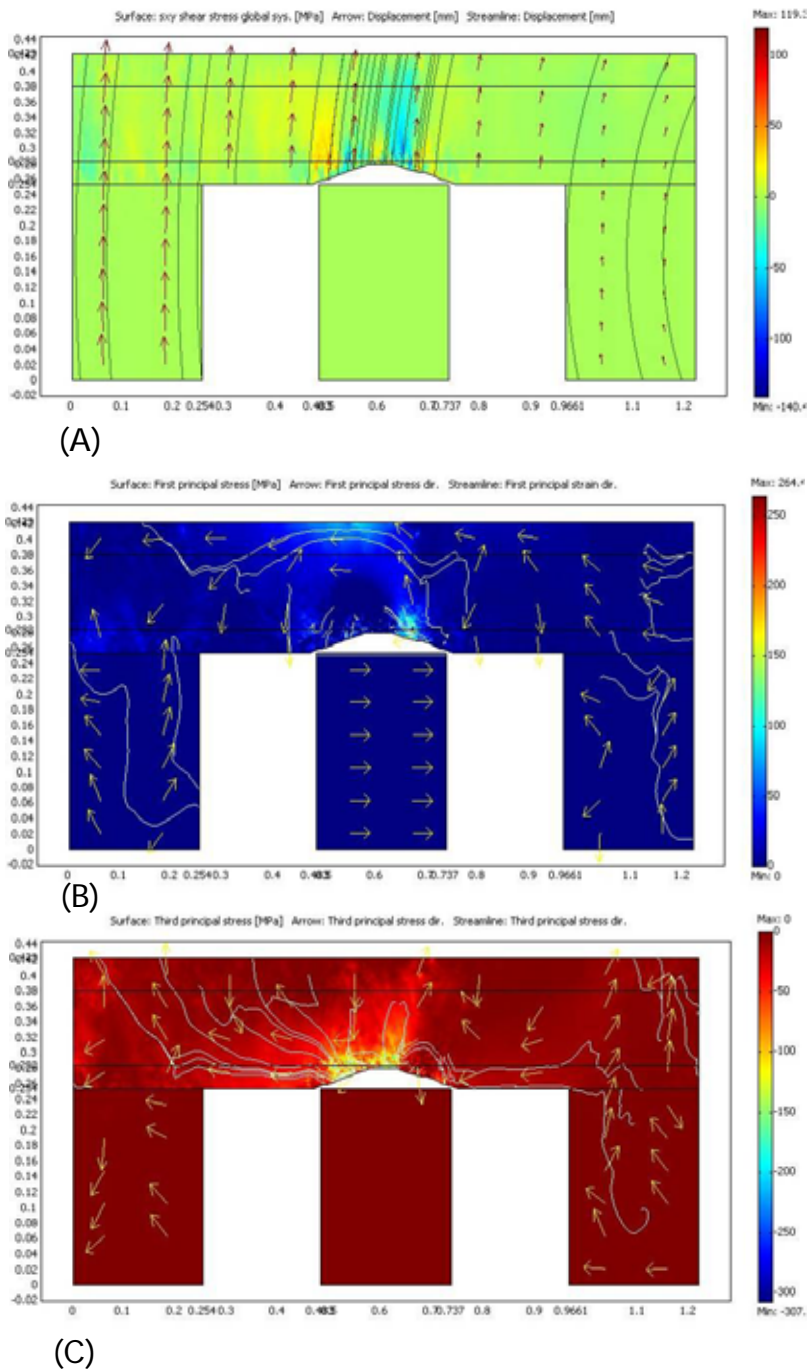
Figure D19.   Numerical results for a load applied to a rail with uniform attack, the loads are applied on top of every beam except from that in the middle. (A) Shear stresses developed along with the deformation of the rail, (B) Tensile stresses developed along with the tensile strain. (C) Compression stresses developed along with the path of strain.
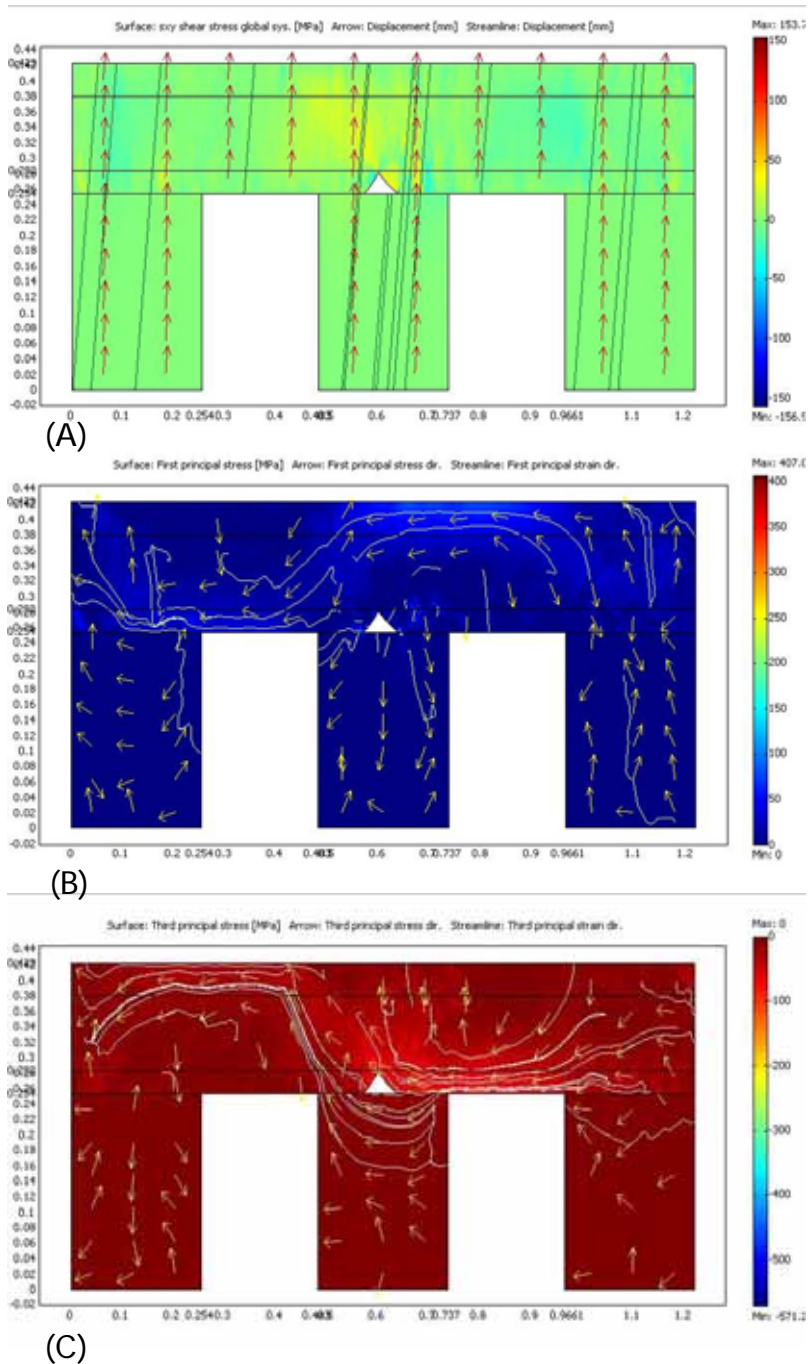
Figure D20.   Numerical results for a load applied to a rail with a sharp crack, the loads are applied on top of every beam. (A) Shear stresses developed along with the deformation of the rail, (B) Tensile stresses developed along with the tensile strain. (C) Compression stresses developed along with the path of strain.

As seen in the previous figures, it is evident that the nature of the cracks developed on the rail change the state of stresses generated. Although the tensile and compressive stresses developed in the rail are below the yield point of the material, the shear components of the stresses are in the vicinity to cause a catastrophic failure in the rails. As the crack become sharper, the magnitude of such shear stresses increase quite drastically along side the crack, thus it is expected a major failure in such type of cracks. Regarding to the uniform attack, it is clear that some shear stresses develops, however their magnitude is less than that observed in the sharp cracks, so this type of attack may not induce a severe failure as the sharp crack may, however, due to the material mass lost, it is necessary to remove the attacked rail and install a new one.

As expected, the un-attacked rail is able to comply with the mechanical demands imposed by the loads under normal operating conditions.

Summary

This investigation examined the variables that may affect the service life of rails in transit systems. Since the actual problem that these transportation systems are facing is related to severe corrosion damage, an analysis of the microstructural features of rails installed in different transit systems was conducted. In addition were conducted the measurement of the corrosion rates in different media. Parallel to these activities, the numerical estimation of the stresses generated into the rails with and without corrosion damage was conducted.

Results reveal that besides being used in different transit systems and also apart from having different geometry, the rails analyzed in this work show similar microstructural features, which lead to the conclusion that they must perform similarly under the investigated conditions. In terms of the mechanical properties it is expected that both rails will behave similarly.

Regarding to their corrosion resistance, the tests conducted in similar media shows that the materials tested exhibited an excellent corrosion resistance, except for one sample; it was also found that the corrosion resistance slightly decreased in the electrolytes with chlorine ions as expected, however, such ions did not corroded significantly the different samples.

Numerical results show that unless corrosion cracks with sharp edge form, the rails would be able to withstand the mechanical stresses associated with the rail traffic. Even in the case that uniform corrosion takes place, the rails are able to perform well under normal load conditions.

Conclusions

The present investigation lead to conclude that under normal conditions, the steel used in the fabrication of rails would withstand the effect of the environmental conditions. However, the use of direct currents significantly affects the corrosion rate, which makes the rail less corrosion resistant. It means that when the rail is subjected solely to environmental corrosion in the absence of direct currents it can sustain the effect of the environment.

In the presence of localized corrosion attacks combined with cyclic stresses creates proper conditions to induce fatigue-corrosion failures. Furthermore, the return current from the train to the rail and the improper insulation of the rails to the ground may form galvanic cells. This affects considerably the service characteristics of the rails as well as its integrity, increasing the susceptibility of the rail to fatigue corrosion.

Acknowledgements

References

[1]   Norma Oficial Mexicana NMX-B-308-1987. Steel making industry-Methods for determining the inclusion content of steel. SECOFI, México, D.F., 1987.

[2]   ASTM-E-45-1985. Standard practice for determining the inclusion content of steel. ASTM, USA, 1985.

[3]   ASTM-E-112-2004. Standard test methods for determining average grain size. ASTM, USA, 2004.

[4]   Fontna M.G., "Corrosion Engineering 3rd Edition", McGraw-Hill, New York, USA, 1987.

[5]   Dieter G.E., "Mechanical Metallurgy 2nd Edition", McGraw-Hill, New York, USA, 1976.

[6]   Reed-Hill R.E., "Physical Metallurgy Principles 2nd Edition", Brookes/Cole, New York, USA, 1973.

APPENDIX E

Data on numerical simulations
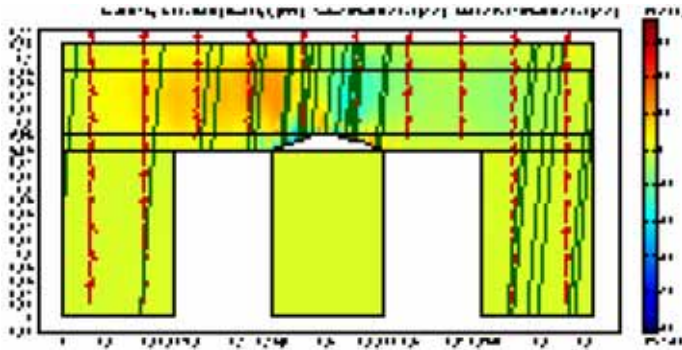
COMSOL Model Report

1. Table of Contents

- Title - COMSOL Model Report
- Table of Contents
- Model Properties
- Geometry
- Geom1
- Materials/Coefficients Library
- Solver Settings
- Postprocessing
- Variables

2. Model Properties

Property	Value
Model name	
Author	
Company	
Department	
Reference	
URL	
Saved date	Aug 3, 2006 7:35:11 PM
Creation date	Aug 3, 2006 3:11:10 PM
COMSOL version	COMSOL 3.2.0.222

File name: C:\Documents and Settings\rperez\Mis documentos\PACO\Modelos\paca 6\paca6.mph

Application modes and modules used in this model:

- Geom1 (2D)
  - Plane Stress

3. Geometry

Number of geometries: 1

3.1. Geom1
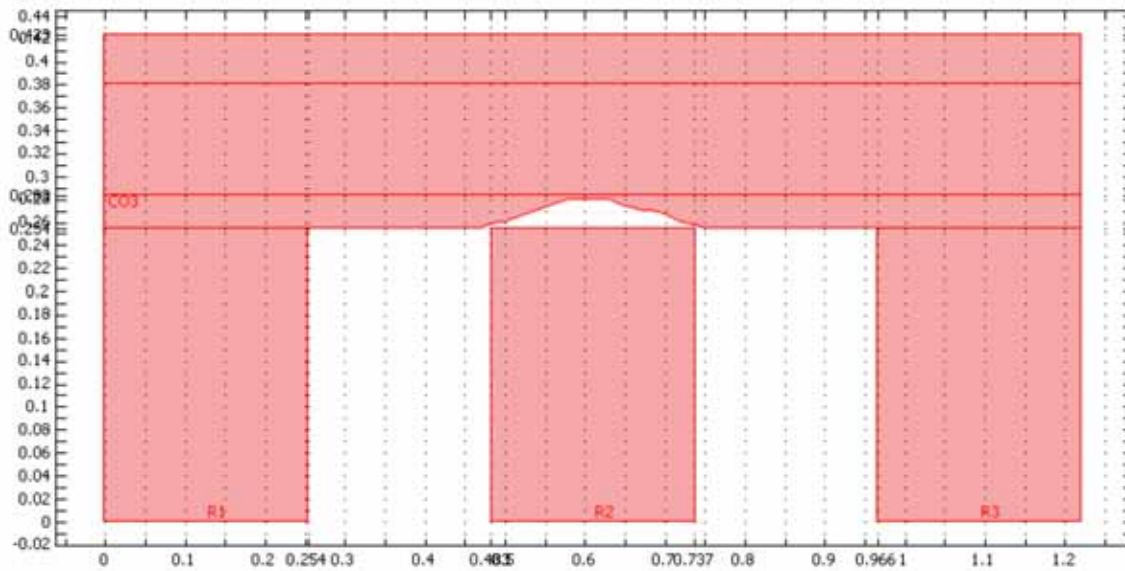
3.1.1. Subdomain mode
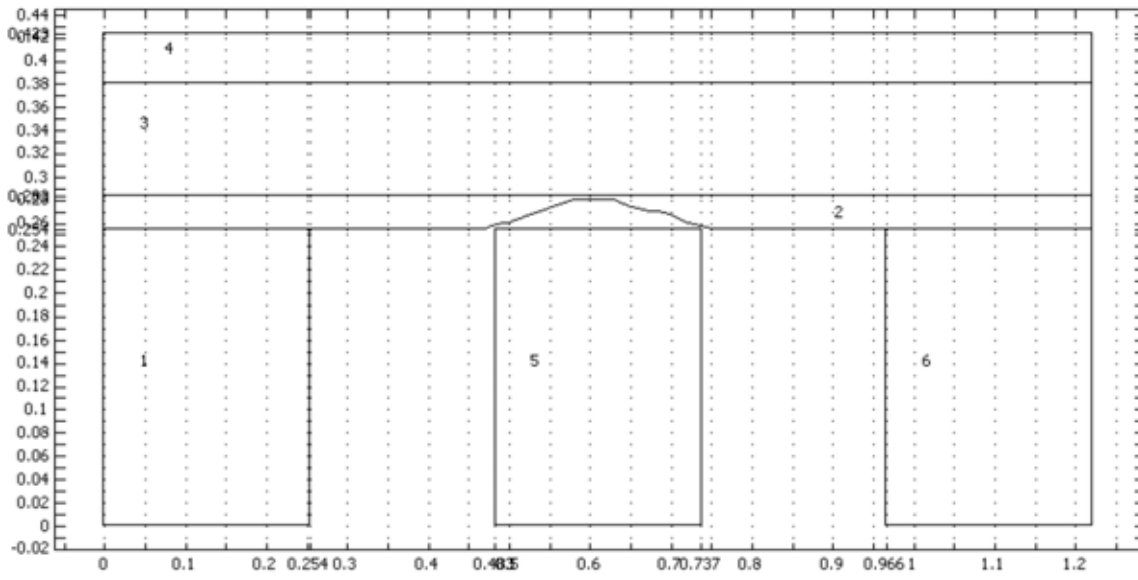
4. Geom1

Space dimensions: 2D

Independent variables: x, y, z

4.1. Mesh

4.1.1. Mesh Parameters

Parameter	Value
Maximum element size	
Maximum element size scaling factor	1
Element growth rate	1.3
Mesh curvature factor	0.3
Mesh curvature cut off	0.001
Resolution of narrow regions	1
Resolution of geometry	10
x-direction scale factor	1.0
y-direction scale factor	1.0
Mesh geometry to level	Subdomain

Subdomain	1-6
Maximum element size	
Element growth rate	

Boundary	1-36
Maximum element size	
Element growth rate	
Mesh curvature factor	
Mesh curvature cut off	

Point	1-32
Maximum element size	
Element growth rate	

4.1.2. Mesh Statistics

Number of degrees of freedom	65454
Number of boundary elements	952
Number of elements	16129
Minimum element quality	0.4382

E-4
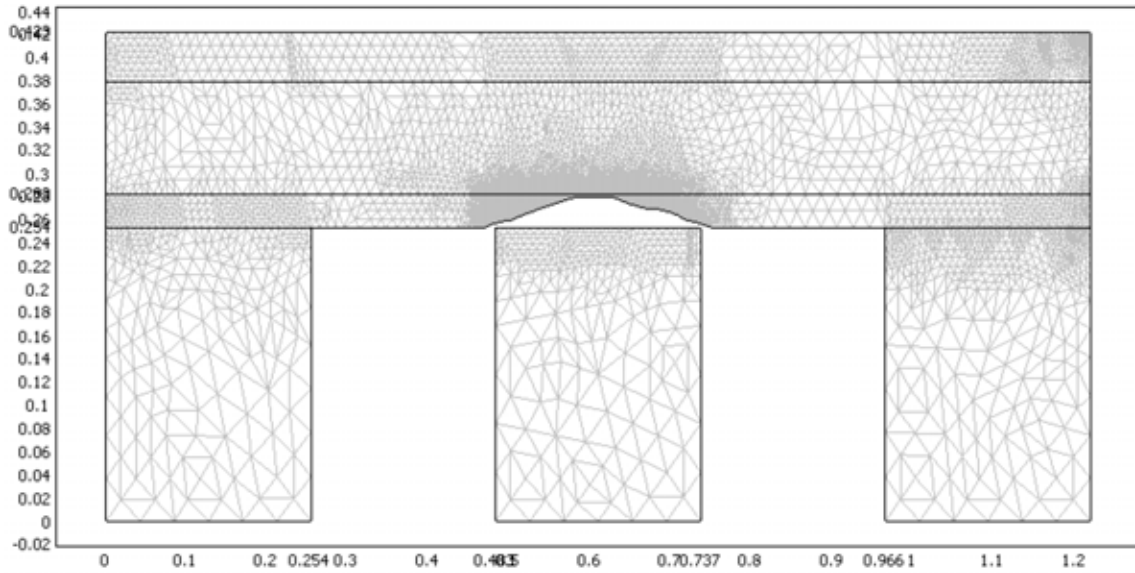
4.2. Application Mode: Plane Stress (ps)

Application mode type: Plane Stress

Application mode name: ps

4.2.1. Application Mode Properties

Property	Value
Default element type	Lagrange - Quadratic
Analysis type	Static linear
Specify eigenvalues using	Eigenfrequency
Frame	Reference frame
Weak constraints	Off

4.2.2. Variables

Dependent variables: u, v

Shape functions: shlag(2,'u'), shlag(2,'v')

Interior boundaries not active

E-5

4.2.3. Point Settings

Point		1-32
name		''
Point load (force) x-dir. (Fx)	N	0
Amp. factor point load x-dir. (FxAmp)	1	1
Phase angle point load x-dir. (FxPh)	1	0
Point load (force) y-dir. (Fy)	N	0
Amp. factor point load y-dir. (FyAmp)	1	1
Phase angle point load y-dir. (FyPh)	1	0
loadcoord		'global'
constrcoord		'global'
constrtype		'standard'
H Matrix (H)	1	{0,0;0,0}
R Vector (R)	m	{0;0}
Constraint x-dir. (Rx)	m	0
Hx	1	0
Constraint y-dir. (Ry)	m	0
Hy	1	0
weakconstr		1
Shape functions (wcshape)		[]
Initial value (wcinit)		{0;0}
style		{0,{0,0,0}}

E-6

4.2.4. Boundary Settings

Boundary		1-3, 5, 7, 9, 11-16, 18-22, 25-36	10, 17, 24
name			
Edge load x-dir. (Fx)	1	0	0
Amp. factor edge load x-dir. (FxAmp)	1	1	1
Phase angle edge load x-dir. (FxPh)	1	0	0
Edge load y-dir. (Fy)	1	0	**-45000**
Amp. factor edge load y-dir. (FyAmp)	1	1	1
Phase angle edge load y-dir. (FyPh)	1	0	0
loadcoord		global	global
loadtype		length	length
constrcoord		global	global
constrtype		standard	standard
H Matrix (H)	1	{0,0;0,0}	{0,0;0,0}
R Vector (R)	m	{0;0}	{0;0}
Constraint x-dir. (Rx)	m	0	0
Hx	1	0	0
Constraint y-dir. (Ry)	m	0	0
Hy	1	0	0
weakconstr		1	1
Integration order (wcgporder)		2	2
Initial value (wcinit)		{0;0}	{0;0}

E-7

4.2.5. Subdomain Settings

Subdomain		1, 5-6	2-4
Shape functions (shape)		shlag(2,'u') shlag(2,'v')	shlag(2,'u') shlag(2,'v')
Integration order (gporder)		4 4	4 4
Constraint order (cporder)		2 2	2 2
name			
Young's modulus (E)	Pa	**25e9 (Concrete)**	**200e9 (High-strength alloy steel)**
Density (rho)	kg/m^3	**2300 (Concrete)**	**7850 (High-strength alloy steel)**
Mass damping parameter (alphadM)	1/s	1	1
Stiffness damping parameter (betadK)	s	0.001	0.001
Initial value (dinit)		{0;0}	{0;0}
materialcoord		global	global
materialmodel		iso	iso
mixedform		0	0
hypertype		neo_hookean	neo_hookean
Initial shear modulus (mu)	Pa	8e5	8e5
Model parameter (C10)	Pa	2e5	2e5
Model parameter (C01)	Pa	2e5	2e5
Initial bulk modulus (kappa)	Pa	1e10	1e10
hardeningmodel		iso	iso
yieldtype		mises	mises
isodata		tangent	tangent
Kinematic tangent modulus (ETkin)	Pa	2.0e10	2.0e10
Isotropic tangent modulus (ETiso)	Pa	2.0e10	2.0e10
Yield stress level (Sys)	Pa	2.0e8	2.0e8
Yield function	Pa	mises_ps	mises_ps

E-8

(Syfunc)			
Yield function (Syfunc_kin)	Pa	misesKin_ps	misesKin_ps
Hardening function (Shard)	Pa	2.0e10/(1-2.0e10/2.0e11)*epe_ps	2.0e10/(1-2.0e10/2.0e11)*epe_ps
ini_stress		0	0
ini_strain		0	0
Initial shear stress sxy (sxyi)	Pa	0	0
Initial shear strain exy (exyi)	1	0	0
Initial normal stress sx (sxi)	Pa	0	0
Initial normal strain ex (exi)	1	0	0
Initial normal stress sy (syi)	Pa	0	0
Initial normal strain ey (eyi)	1	0	0
Initial normal stress sz (szi)	Pa	0	0
Initial normal strain ez (ezi)	1	0	0
Thermal expansion coeff. (alpha)	1/K	1.2e-5	1.2e-5
Poisson's ratio (nu)	1	**0.33 (Concrete)**	**0.33 (High-strength alloy steel)**
Shear_modulus xy plane (Gxy)	Pa	7.52e10	7.52e10
Poisson's ratio xy plane (nuxy)	1	0.33	0.33
Thermal expansion coeff. x-dir. (alphax)	1/K	1.2e-5	1.2e-5
Young's modulus x-dir. (Ex)	Pa	2.0e11	2.0e11
Poisson's ratio yz plane (nuyz)	1	0.33	0.33
Thermal expansion coeff. y-dir. (alphay)	1/K	1.2e-5	1.2e-5
Young's modulus y-dir. (Ey)	Pa	2.0e11	2.0e11
Poisson's ratio xz plane (nuxz)	1	0.33	0.33

E-9

Thermal expansion coeff. z-dir. (alphaz)	1/K	1.2e-5	1.2e-5
Young's modulus z-dir. (Ez)	Pa	2.0e11	2.0e11
Elasticity matrix (D)	Pa	{'2.0e11/((1+0.33)*(1-2*0.33))*(1-0.33)','2.0e11/((1+0.33)*(1-2*0.33))*0.33','2.0e11/((1+0.33)*(1-2*0.33))*0.33',0;'2.0e11/((1+0.33)*(1-2*0.33))*0.33','2.0e11/((1+0.33)*(1-2*0.33))*(1-0.33)','2.0e11/((1+0.33)*(1-2*0.33))*0.33',0;'2.0e11/((1+0.33)*(1-2*0.33))*0.33','2.0e11/((1+0.33)*(1-2*0.33))*0.33','2.0e11/((1+0.33)*(1-2*0.33))*(1-0.33)',0;0,0,0,'2.0e11/((1+0.33)*2)'}	{'2.0e11/((1+0.33)*(1-2*0.33))*(1-0.33)','2.0e11/((1+0.33)*(1-2*0.33))*0.33','2.0e11/((1+0.33)*(1-2*0.33))*0.33',0;'2.0e11/((1+0.33)*(1-2*0.33))*0.33','2.0e11/((1+0.33)*(1-2*0.33))*(1-0.33)','2.0e11/((1+0.33)*(1-2*0.33))*0.33',0;'2.0e11/((1+0.33)*(1-2*0.33))*0.33','2.0e11/((1+0.33)*(1-2*0.33))*0.33','2.0e11/((1+0.33)*(1-2*0.33))*(1-0.33)',0;0,0,0,'2.0e11/((1+0.33)*2)'}
Thermal expansion vector (alphavector)	1/K	{1.2e-5;1.2e-5;1.2e-5;0}	{1.2e-5;1.2e-5;1.2e-5;0}
Thickness (thickness)	m	0.01	0.01
Body load x-dir. (Fx)	1	0	0
Amp. factor body load x-dir. (FxAmp)	1	1	1
Phase angle body load x-dir. (FxPh)	1	0	0
Body load y-dir. (Fy)	1	0	0
Amp. factor body load y-dir. (FyAmp)	1	1	1
Phase angle body load y-dir. (FyPh)	1	0	0
loadcoord		global	global
Tflag		0	0
Strain temperature (Temp)	K	0	0
Strain ref. temperature (Tempref)	K	0	0
loadtype		area	area
constrcoord		global	global
constrtype		standard	standard
H Matrix (H)	1	{0,0;0,0}	{0,0;0,0}

E-10

R Vector (R)	m	{0;0}	{0;0}
Constraint x-dir. (Rx)	m	0	0
Hx	1	0	0
Constraint y-dir. (Ry)	m	0	0
Hy	1	0	0
weakconstr		1	1

Subdomain initial value		1, 5-6	2-4
x-displacement (u)	m	0	0
y-displacement (v)	m	0	0

E-11

5. Materials/Coefficients Library

5.1. Concrete

Parameter	Value
Young's modulus (E)	25e9
Thermal expansion coeff. (alpha)	10e-6
Thermal conductivity (k)	1.8
Poisson's ratio (nu)	0.33
Density (rho)	2300

5.2. High-strength alloy steel

Parameter	Value
Heat capacity (C)	475
Young's modulus (E)	200e9
Thermal expansion coeff. (alpha)	12.3e-6
Relative permittivity (epsilonr)	1
Thermal conductivity (k)	44.5
Relative permeability (mur)	1
Poisson's ratio (nu)	0.33
Density (rho)	7850
Electrical conductivity (sigma)	4.032e6

6. Solver Settings

Solve using a script: off

Analysis type	Static_linear
Auto select solver	On
Solver	Stationary linear
Solution form	Automatic
Symmetric	Off
Adaption	Off

6.1. Direct (UMFPACK)

Solver type: Linear system solver

Parameter	Value
Pivot threshold	0.1
Memory allocation factor	0.7

6.2. Advanced

Parameter	Value
Constraint handling method	Elimination
Null-space function	Automatic
Assembly block size	5000
Use Hermitian transpose of constraint matrix	Off
Use complex functions with real input	Off
Type of scaling	Automatic
Manual scaling	
Row equilibration	On
Manual control of reassembly	Off
Load constant	On
Constraint constant	On
Mass constant	On
Damping (mass) constant	On
Jacobian constant	On
Constraint Jacobian constant	On

E-13

7. Postprocessing

Surface: sxy shear stress global sys. [MPa]   Arrow: Displacement [mm]   Streamline: Displacement [mm]

E-14
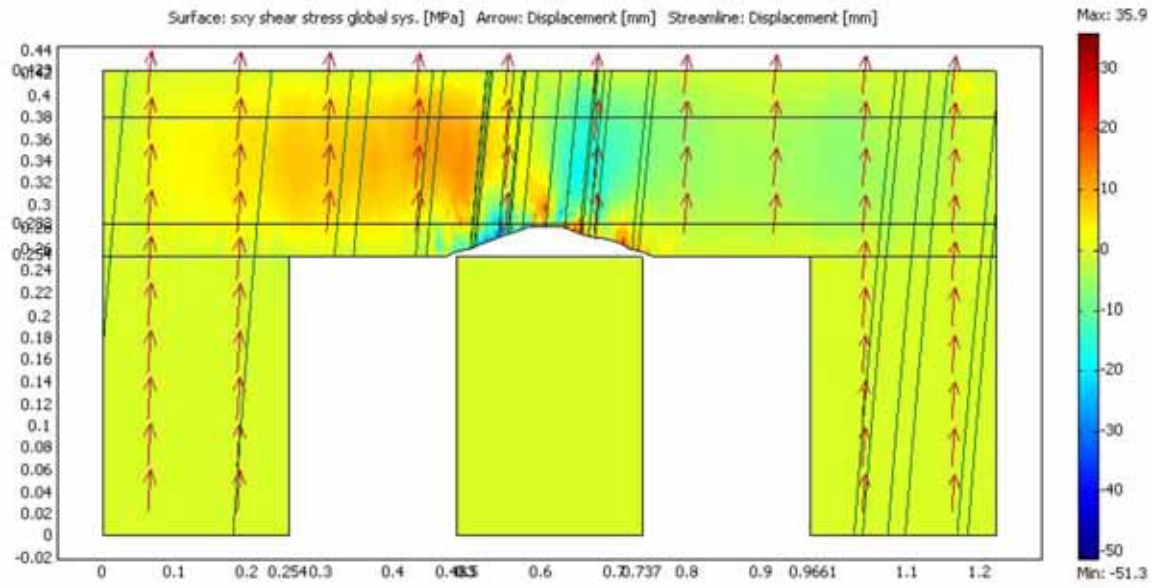
8. Variables

8.1. Point

Name	Description	Expression
Fxg_ps	Point load in global x-dir.	0
Fyg_ps	Point load in global y-dir.	0
disp_ps	Total displacement	sqrt(real(u)^2+real(v)^2)

8.2. Boundary

Name	Description	Expression
Fxg_ps	Edge load in global x-dir.	0
Fyg_ps	Edge load in global y-dir.	0
disp_ps	Total displacement	sqrt(real(u)^2+real(v)^2)
Tax_ps	Surface traction (force/area) in x-dir.	sx_ps * nx_ps+sxy_ps * ny_ps
Tay_ps	Surface traction (force/area) in y-dir.	sxy_ps * nx_ps+sy_ps * ny_ps

8.3. Subdomain

Name	Description	Expression
Fxg_ps	Body load in global x-dir.	0
Fyg_ps	Body load in global y-dir.	0
disp_ps	Total displacement	sqrt(real(u)^2+real(v)^2)
sx_ps	sx normal stress global sys.	E_ps/((1+nu_ps) * (1-2 * nu_ps)) * (1-nu_ps) * ex_ps+E_ps/((1+nu_ps) * (1-2 * nu_ps)) * nu_ps * ey_ps+E_ps/((1+nu_ps) * (1-2 * nu_ps)) * nu_ps * ez_ps
sy_ps	sy normal stress global sys.	E_ps/((1+nu_ps) * (1-2 * nu_ps)) * nu_ps * ex_ps+E_ps/((1+nu_ps) * (1-2 * nu_ps)) * (1-nu_ps) * ey_ps+E_ps/((1+nu_ps) * (1-2 * nu_ps)) * nu_ps * ez_ps
sxy_ps	sxy shear stress global sys.	E_ps/(1+nu_ps) * exy_ps
ex_ps	ex normal strain global sys.	ux
ey_ps	ey normal strain global sys.	vy
ez_ps	ez normal strain	-(E_ps/((1+nu_ps) * (1-2 * nu_ps)) * nu_ps * ex_ps+E_ps/((1+nu_ps) * (1-2 * nu_ps)) * nu_ps * ey_ps)/(E_ps/((1+nu_ps) * (1-2 * nu_ps)) * (1-nu_ps))
exy_ps	exy shear strain global sys.	0.5 * (uy+vx)
K_ps	Bulk modulus	E_ps/(3 * (1-2 * nu_ps))
G_ps	Shear modulus	E_ps/(2 * (1+nu_ps))
mises_ps	von Mises stress	sqrt(sx_ps^2+sy_ps^2-sx_ps * sy_ps+3 * sxy_ps^2)
Ws_ps	Strain energy density	0.5 * thickness_ps * (ex_ps * sx_ps+ey_ps * sy_ps+2 * exy_ps * sxy_ps)
evol_ps	Volumetric strain	ex_ps+ey_ps+ez_ps
sz_ps	sz normal stress global sys.	0
tresca_ps	Tresca stress	max(max(abs(s1_ps-s2_ps),abs(s2_ps-s3_ps)),abs(s1_ps-s3_ps))

E-15

APPENDIX F

"Chemical Analysis of Soils Provided by the Edmonton Transit"

NORWEST LABS

Analytical Report

Norwest Labs
7217 Roper Road NW
Edmonton, AB. T6B 3J4
Phone: (780) 438-5522
Fax: (780) 438-0396

Bill to: Corrpro Canada Inc.
Report to: Corrpro Canada Inc.
10848 - 214 Street
Edmonton, AB, Canada
T5S 2A7
Attn: Grant Firth
Sampled By:
Company:

Project
ID:
Name: ELRT Project Samples
Location: Phase 1
LSD:
P.O.:
Acct. Code:

NWL Lot ID: 380251

Control Number:
Date Received: May 05, 2005
Date Reported: May 10, 2005
Report Number: 696515

Page: 1 of 3

		NWL Number	380251-1	380251-2	380251-3	
		Sample Description	95 St. Outside the X-ing	Field Site / 95 St. Crossing	Gauge Site / 95 St. Street Crossing	
		Matrix	Soil - general	Soil - general	Soil - general	
Analyte		Units	Results	Results	Results	Detection Limit
Salinity						
pH	Saturated Paste	pH	8.3	8.2	8.2	
Electrical Conductivity	Saturated Paste	dS/m at 25 C	7.19	13.4	20.1	0.01
SAR	Saturated Paste		96	99	120	
% Saturation		%	36	34	33	
Calcium	Saturated Paste	meq/L	1.0	3.7	5.2	0.01
Calcium	Saturated Paste	mg/kg	7.3	26	34	
Magnesium	Saturated Paste	meq/L	0.2	0.8	0.9	0.02
Magnesium	Saturated Paste	mg/kg	0.8	3	3	
Sodium	Saturated Paste	meq/L	73.5	149	217	0.04
Sodium	Saturated Paste	mg/kg	614	1180	1650	
Potassium	Saturated Paste	meq/L	0.7	1	2	0.03
Potassium	Saturated Paste	mg/kg	10	20	20	
Chloride	Saturated Paste	meq/L	65.4	129	224	0.03
Chloride	Saturated Paste	mg/kg	842	1580	2630	
Sulfate-S	Saturated Paste	meq/L	3	5	4	0.06
Sulfate-S	Saturated Paste	mg/kg	20	30	20	
GR	Saturated Paste	T/ac	11.0	>20.0	>20.0	

		NWL Number	380251-3	380251-4		
		Sample Description	Gauge Site / 95 St. Street Crossing	Gauge Site / 112 St. Crossing		
		Matrix	Soil - general	Soil - general		
Analyte		Units	Results	Results	Results	Detection Limit
Metals Strong Acid Digestion						
Iron	Strong Acid Extractable	ug/g	95100	55200		50

F-2